Dissertation zur Erlangung des Doktorgrades

der Fakultät für Chemie und Pharmazie

der Ludwig-Maximilians-Universität München

Mechanical communication of endothelial cells and its influence on the organization of cellular structures

Daniel Rüdiger

aus Jena, Deutschland

2020

Erklärung

Diese Dissertation wurde im Sinne von §7 der Promotionsordnung vom 28. November 2011 von Herrn Prof. Dr. Stefan Zahler betreut.

Eidesstattliche Versicherung

Diese Dissertation wurde eigenständig und ohne unerlaubte Hilfe erarbeitet.

München, 26.08.2020

Daniel Rüdiger

Dissertation eingereicht am	29.06.2020
1. Gutachter:	Prof. Dr. Stefan Zahler
2. Gutachterin:	Prof. Dr. Angelika M. Vollmar
Mündliche Prüfung am	30.07.2020

Meiner Familie

Table of contents

Abbreviations

2D	Two-dimensional
3D	Three-dimensional
AFM	Atomic force microscopy
ANOVA	Analysis of variance
BSA	Bovine serum albumin
$CaCl_2$	Calcium chloride
CAM	Chick chorioallantoic membrane
CO_2	Carbon dioxide
Ctrl	Control
Dll4	Delta-like ligand 4
DMEM	Dulbecco’s modified eagle medium
DMSO	Dimethyl sulfoxide
DPSS	Diode pumped solid state
ECGM	Endothelial cell growth medium
ECM	Extracellular matrix
e.g.	For example
EGF	Epidermal growth factor
EHS	Engelbreth-Holm-Swarm
FDA	Food and Drug Administration
FCS	Fetal calf serum
FGF	Fibroblast growth factor
Fig.	Figure
FoxC2	Forkhead-Box-Protein C2
FRET	Fluorescence resonance energy transfer
GTPase	Guanosine triphosphatase

H_2O	Water
HGF	Hepatocyte growth factor
HIF	Hypoxia-inducible factor
HUVEC	Human umbilical vein endothelial cell
HyD	Hybrid detector
IgG	Immunoglobulin G
KCl	Potassium chloride
KH_2PO_4	Potassium dihydrogen phosphate
LINC	Linker of nucleoskeleton and cytoskeleton complex
LMU	Ludwig-Maximilians-Universität
LOX	Lysyl oxidase
LOXL2	Lysyl oxidase homolog 2
$MgCl_2$	Magnesium chloride
MMP	Matrix metalloprotease
MRTF-A	Myocardin-related transcription factor A
NaCl	Sodium chloride
Na_2EDTA	Ethylendiamine tetraacetic acid disodium salt
Na_2HPO_4	Disodium phosphate
NaOH	Sodium hydroxide
Nrarp	Notch-regulated ankyrin repeat protein
NRP-1	Neuropilin 1
PAA	Polyacrylamide
PBS	Phosphate buffered saline
PDGF	Platelet-derived growth factor
PDMS	Polydimethylsiloxane
PEG	Polyethylene glycol
PFA	Paraformaldehyde

PI3K	Phosphoinositid-3-kinase
PIGF	Placental growth factor
PLA	Polylactic acid
PMT	Photomultiplier
ROCK	Rho-associated protein kinase
SAM	Scanning acoustic microscopy
SEM	Standard error of the mean
SPECT	single photon emission computed tomography
Tab.	Table
TGFβ	Transforming growth factor beta
TKI	Tyrosine kinase inhibitor
TPP	Techno Plastic Products
VEGF	Vascular endothelial growth factor
VEGFR	vascular endothelial growth factor receptor

Symbols and units

°C	Degree Celsius
%	Percent
C [-]	Correlation
cm^2	Cubic centimeter
δ [m]	Indentation depth in meter
E [Pa]	Young’s modulus in pascal
F [N]	Force in newton
h	Hours
kPa	Kilopascal
mbar	Millibar
mg	Milligram
min	Minutes
ml	Milliliter
mM	Millimolar
mm	Millimeter
v [-]	Poisson’s ratio
nM	Nanomolar
nm	Nanometer
nN	Nanonewton
pH	Potentia Hydrogenii
R [m]	Bead radius in meter
r [m]	Separation distance in meter
$\hat{\boldsymbol{r}}$	Radial unit vector
rpm	Rotations per minute
s	Seconds

t [min]	Time in minutes
Δt [min]	Time interval in minutes
τ [min]	Typical timescale of tube formation in minutes
θ [°]	Angle in cylindrical coordinates in degree
$\boldsymbol{u}$	Displacement field
$\boldsymbol{\nabla \cdot u}$	Compression field
µl	Microliter
µm	Micrometer
$\boldsymbol{v}$ [m/s]	Velocity in meter per second
w/v	Weight per volume
$\boldsymbol{x}$	Cell position in coordinates

1 Abstract

The formation of new blood vessels from existing ones is called angiogenesis and plays an important role in tissue development, healing and homeostasis as well as in pathological processes, such as tumor growth. During this process, coordinated cell movement is essential for which endothelial cells use a chemical communication via the vascular endothelial growth factor (VEGF). The extracellular matrix (ECM) regulates many tissue processes and influences cell behavior. The dynamic cell-ECM interaction enables a mechanical communication between cells. This thesis aims to validate, whether endothelial cells also use a mechanical communication for coordinated cell behavior.

For the investigation of the endothelial cell behavior, tube formation assays on Matrigel were performed. Cell communication was examined with a focus on the initial “finding phase” of the cells. It was shown that cells sense each other to align and cluster over a distance of at least 106 µm. However, the finding phase was not dependent on chemical communication via growth factors, neither soluble nor matrix-bound. This led to the hypothesis that endothelial cells use a mechanical communication pathway for initial cell connection during tube formation assay.

For further analysis, Matrigel or collagen I printing on polydimethylsiloxane (PDMS) with different stiffness values was applied. This could show that stiffness had an influence on tube formation but was not a key factor, revealing the high mechanical homogeneity of Matrigel compared to collagen I to be a crucial factor. The destruction of the laminin network in Matrigel by netrin-4 or the blocking of integrins for laminin led to an inhibition of tube formation, whereas the presence of laminin supported tube formation. Thus, laminin was found to be a master regulator. Furthermore, the process of mechanical interaction was shown to be dependent on cell contraction and independent of proteolytic processes or protein secretion. Cell forces due to cellular contraction ranges in the same radius as the maximum distance of cell communication, as shown by traction force microscopy, and led to a plastic irreversible remodeling of the Matrigel matrix. Atomic force microscopy (AFM) measurements proved that the remodeling results in a stiffness gradient, a process called strain stiffening, and the interaction of the cells occurred via the remodeled stiffened fibers. In conclusion, it was shown that endothelial cells use a mechanical as well as a chemical interaction for communication and coordination.

2 Introduction

2.1 Endothelial cell communication

2.1.1 Neovascularization

The blood vessel system is responsible for the transport and distribution of respiratory gases, nutrients, metabolites, electrolytes, signal substances such as hormones and immune cells. In addition, it is also responsible for pH and temperature regulation and homeostasis [1-4]. The formation of new blood vessels is classified into vasculogenesis and angiogenesis [1, 3-5]. Vasculogenesis describes the formation of new blood vessels from precursor cells, the angioblasts, and plays a role particularly in embryonic development [3, 6, 7]. Vascular endothelial growth factor (VEGF) upregulates endothelial cell markers in angioblasts leading to the formation of endothelial cells [6]. Angiogenesis is the formation of new blood vessels from pre-existing ones and plays a role in physiological processes such as tissue regeneration, wound healing, embryonic development and morphogenesis, as well as in pathological processes such as tumor growth and metastasis [3, 4, 8-10]. Gerhardt and coworkers have done important work in the field of angiogenesis [3, 9, 11-13]. Since this work focuses on the communication of endothelial cells, only angiogenesis will be discussed in more detail.

Angiogenesis is a multicellular process that is split into different steps [3, 4, 9, 14] and is regulated by pro-angiogenic and anti-angiogenic factors [15]. A schematic overview of the process is presented in Figure 2-1 [9]. Local tissue hypoxia leads to production of growth factors (especially VEGF) and cytokines. Besides VEGF, which activates quiescent endothelial cells the fibroblast growth factor (FGF) also has an activating effect on endothelial cells [15, 16]. On a cellular level, the pro-angiogenic signal causes the surrounding basal membrane to be degraded by matrix metalloproteases (MMPs) [16]. First cells begin to migrate into the tissue, while remaining cells connect to the original vascular network. The cellular behavior is in balance between proteolysis and migration [17]. Endothelial cells subsequently differentiate into tip and stalk cells, which will be discussed in chapter 2.1.2. Filopodia-rich tip cells determine the direction of the sprout by migration along the VEGF gradient [18]. Meanwhile, stalk cells follow the tip cells and support the elongation of the sprout by proliferation. The migration of tip cells is a coordinated process and during fusion of tip cells the sprouts join to form a

functional vascular loop [1]. Once the VEGF source is reached, the migration phenotype is restored [18]. Vascular lumen formation initiates blood flow, increases tissue oxygenation and reduces VEGF levels. The maturation and stabilization of the vessels is achieved by the recruitment of pericytes and the deposition of the basement membrane. The communication between endothelial cells and pericytes is also mediated by VEGF [19].

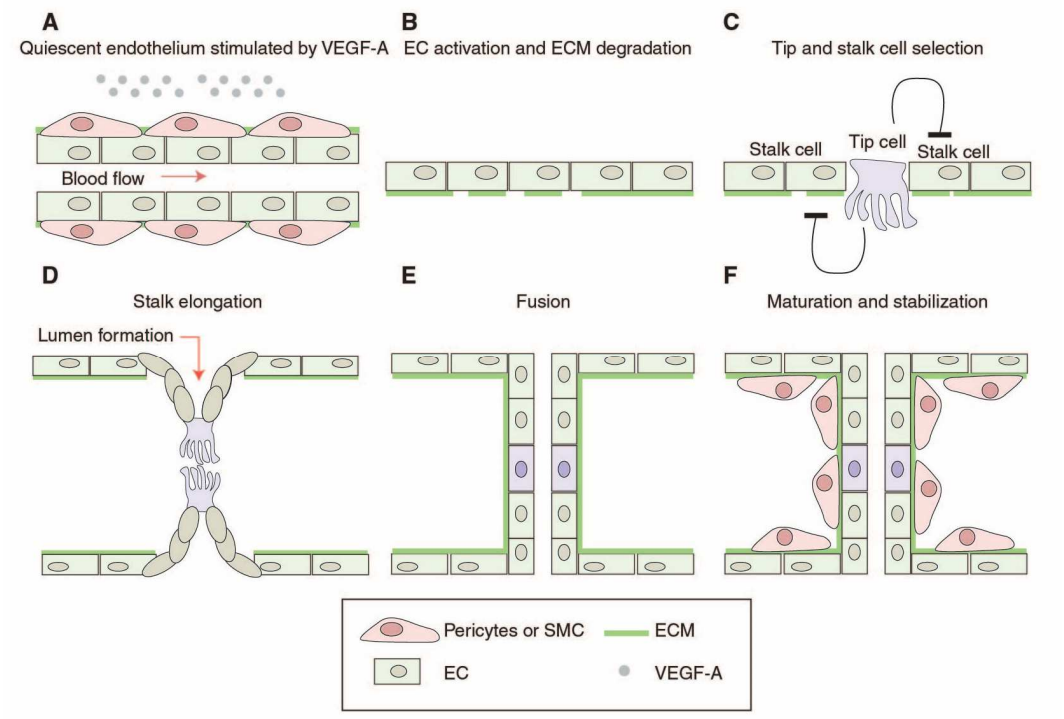

Figure 2-1: Schematic overview of the angiogenesis process (adapted from [9]).

(A) Hypoxia triggers a VEGF signal (VEGF-A) and activates the endothelial cells (EC). **(B)** This leads to a detachment of the mural cells and a degradation of the basal membrane. **(C)** The first cell starts to migrate along the VEGF gradient into the tissue and is called the tip cell. Tip cells also stimulate their neighboring cells. **(D)** These become stalk cells and follow the tip cell. The proliferation of the stalk cells supports the elongation of the sprout and forms a lumen. **(E)** The whole process is a coordinated cell movement and leads to the fusion of tip cells. Formation of the vascular lumen initiates the blood flow, whereas oxygen levels increase and VEGF is reduced. **(F)** The maturation and stabilization of the blood vessel is achieved by recruitment of mural cells and synthesis of the basal membrane.

2.1.2 Endothelial cell differentiation in tip and stalk cells

The differentiation between tip and stalk cells is an important step in angiogenesis [12]. Precise cellular communication and interaction is crucial for such a coordinated process. The differentiation and communication between cells is achieved by the Dll4/Notch signaling pathway [3, 4, 6, 9], which is shown schematically in Figure 2-2 [9]. Hypoxia-inducible factor (HIF), epidermal growth factor (EGF), and platelet-derived

growth factor (PDGF) are among many other hypoxia/ischemia-induced genes that regulate VEGF expression [4]. The VEGF protein family includes five types of VEGF (VEGF-A, VEGF-B, VEGF-C, VEGF-D, VEGF-E) and the placental growth factor (PIGF). VEGF-A and VEGFR2 are involved in angiogenesis. There are three different VEGF receptors (VEGFR1, VEGFR2, VEGFR3), which regulate the activities of several kinases and ultimately control cell proliferation, migration, survival and vascular permeability during vasculogenesis and angiogenesis [4].

The cell differentiation during Notch signaling starts by binding of VEGF-A to neuropilin 1 (NRP-1) to increase its binding affinity to VEGFR2 [4, 9]. Binding induces the expression of delta-like ligand 4 (Dll4) in tip cells. The Dll4 ligand acts on the neighboring stalk cells and activates the Notch signal pathway. This suppresses the tip cell phenotype in the stalk cells, and also reduces the expression of VEGFR2 and increases the expression of Notch target genes (e.g. Notch-regulated ankyrin repeat protein (Nrarp)). Nrarp and the Wnt pathway increase the proliferation of stalk cells [3]. The tip cell receives a low notch signal from the stalk cell and VEGFR2 and NRP-1 remain upregulated [6]. Jagged1 ligand, expressed by the stalk cells, antagonizes Dll4-Notch signaling in the sprouting front when the Notch receptor is modified by the glycosyltranferase Fringe and enhances the differential Notch activity between tip and stalk cells [9], resulting in a positive feedback loop for the conservation of both endothelial cell phenotypes. The duration and amplitude of the Notch signal are modulated by the histone deacetylase SIRT1 [9]. During the process of angiogenesis there may also be a change between tip and stalk cells [3]. In pathological angiogenesis the Dll4/Notch signaling pathway is hyperactive. Tumor cells also secrete VEGF and induce an increased angiogenesis [9]. Notch has, along with VEGF and MMPs, previously been shown to play an important role in angiogenesis [16].

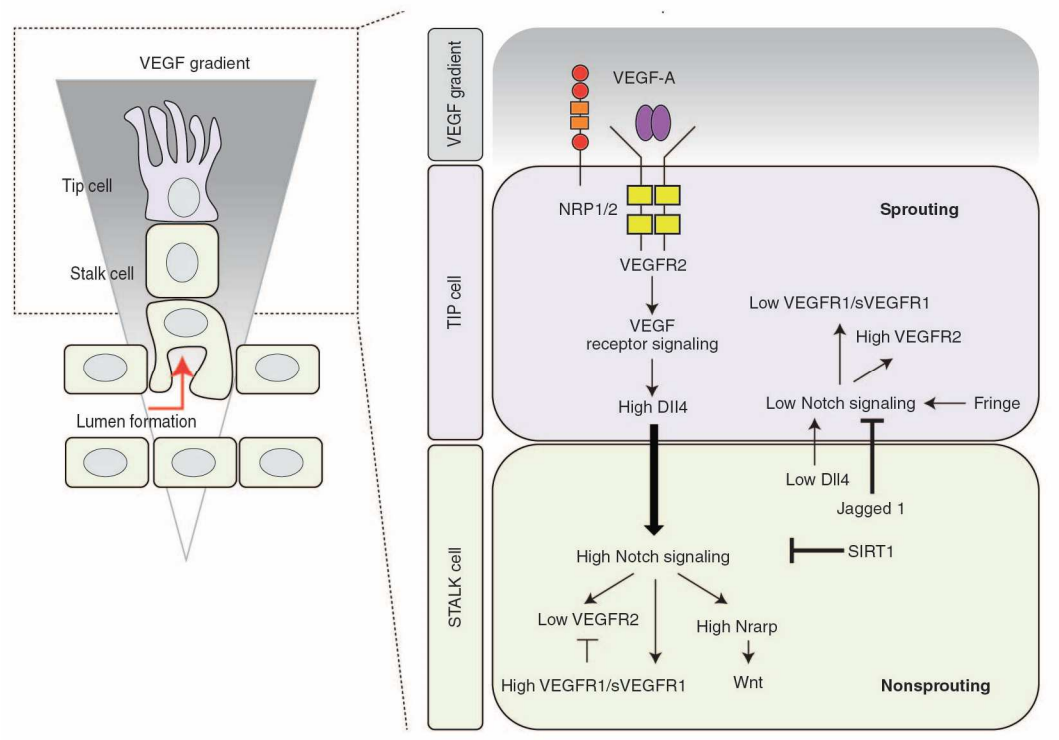

Figure 2-2: Tip and stalk cell selection via Dll4/Notch signal pathway (adapted from [9]).

A VEGF gradient provides differentiation of endothelial cells into tip cells. VEGF-A binds to VEGFR2; the binding affinity of which can be increased by NRP-1. Binding induces the expression of Dll4 and provides an increased Notch signal in neighboring stalk cells, which reduces the phenotype of the tip cells in the stalk cells. VEGFR2 is downregulated and Notch target genes, such as Nrarp, are upregulated and proliferation is stimulated via Wnt. The tip cell receives a low Notch signal from the stalk cell and VEGFR2 and NRP-1 remain upregulated in the tip cell. Jagged1 expressed by the stalk cells acts as an antagonist to the Dll4/Notch signal when the Notch receptor is modified by the glycosyltranferase fringe. This leads to an amplification of the different Notch activity between tip and stalk cells. The duration and amplitude of the Notch signal can be modified by SIRT1.

2.1.3 Endothelial cell communication with other cell types

Endothelial cells are highly heterogeneous since they have to adapt to the local requirements in different tissues [20]. The different properties of endothelial cells are also associated with the corresponding organ function. The endothelial cells are therefore organ-specific. Depending on the tissue, there are also different arrangements for endothelial cells [6]. The endothelial cells interact with different cell types of different organs and tissues [21]. The communication with the tissue cells mainly occurs via exchange of chemical signal molecules [1]. The organ development, homeostasis, tissue function, tissue regeneration and the molecular microarchitecture are controlled via multicellular crosstalk [6, 22]. Endothelial cells can induce growth and differentiation processes in a paracrine manner [21] and act as gatekeeper for their

environment [6]. To state two examples: Endothelial cells express MMP14, which leads to release of epidermal growth factor (EGF) like ligands and further to differentiation of alveolar epithelial cells in lung regeneration [21]. In liver regeneration, endothelial cells upregulate hepatocyte growth factor (HGF) and Wnt2 and downregulate transforming growth factor beta (TGFβ) to support hepatocyte proliferation [3, 6].

2.2 Cell-ECM interaction

2.2.1 Dynamic interplay between cells and ECM

Tissues are composed of cells and the surrounding ECM. The ECM determines the mechanical properties of the tissue [2]. Besides the cell-cell interaction, the cell-ECM interaction plays an important role in tissue morphogenesis, growth and healing [14, 23]. This interaction influences cell behavior, the structural and functional organization of cells and controls many tissue processes [24, 25]. The ECM can trigger cell migration, which is an important step especially during angiogenesis [26]. Because of this important relevance of the ECM, it has moved over the last 15 years more and more into the focus of the research. [23, 24]. ECM modifications are also associated with diseases such as tumor formation, fibrosis and cardiovascular diseases [25, 27].

The ECM forms a tissue-specific structure whose architecture and composition varies according to function and environment [28-31]. In general, the ECM is composed of proteoglycans, fibrous proteins and adhesion molecules that are cross-linked with each other. Proteoglycans are macromolecules consisting of a core protein (protein part) with different glycosaminoglycans (glycan part) as side chains. The side chains are differentiated into hyaluronic acid, chondroitin sulfate, dermatan sulfate, keratan sulfate and heparan sulfate. Proteoglycans are mainly used as fill material and, due to their ability to bind water, they are important for pressure resistance and viscoelastic properties of the tissue. Furthermore, they play a role in the storage of growth factors [31-34]. The most important fibrous protein is collagen, a triple helical molecule. There are 16 different types and depending on the tissue, certain types are present. Besides ensuring a stable structure, the possibility of crosslinking (by crosslinking enzymes e.g. lysyl oxidase homolog 2 (LOXL2) [29]) render the tissue resistant to tension and stress [10, 28, 29, 31, 34-36]. Figure 2-3A shows the structure and connection to other proteins of collagen IV. Another important fibrous protein is elastin. Elastin is a glycoprotein in which hydrophilic and hydrophobic areas alternate and also ensure the elasticity of the tissue through crosslinking [2, 24, 29, 31, 35]. Among the adhesion molecules are the glycoproteins laminin and nectin (fibronectin, vitronectin, osteonectin), whose main function is to mediate cell adhesion to the ECM. Laminin is a heterotrimeric molecule consisting of crossed α, β and γ chains and a globular end structure. Through the combination of different forms of the chains (α has five forms, β and γ have three forms) there are 15 different existing laminin isoforms

[2, 10, 29-31, 34, 37]. Figure 2-3B represents the structure and connection to other proteins of laminin.

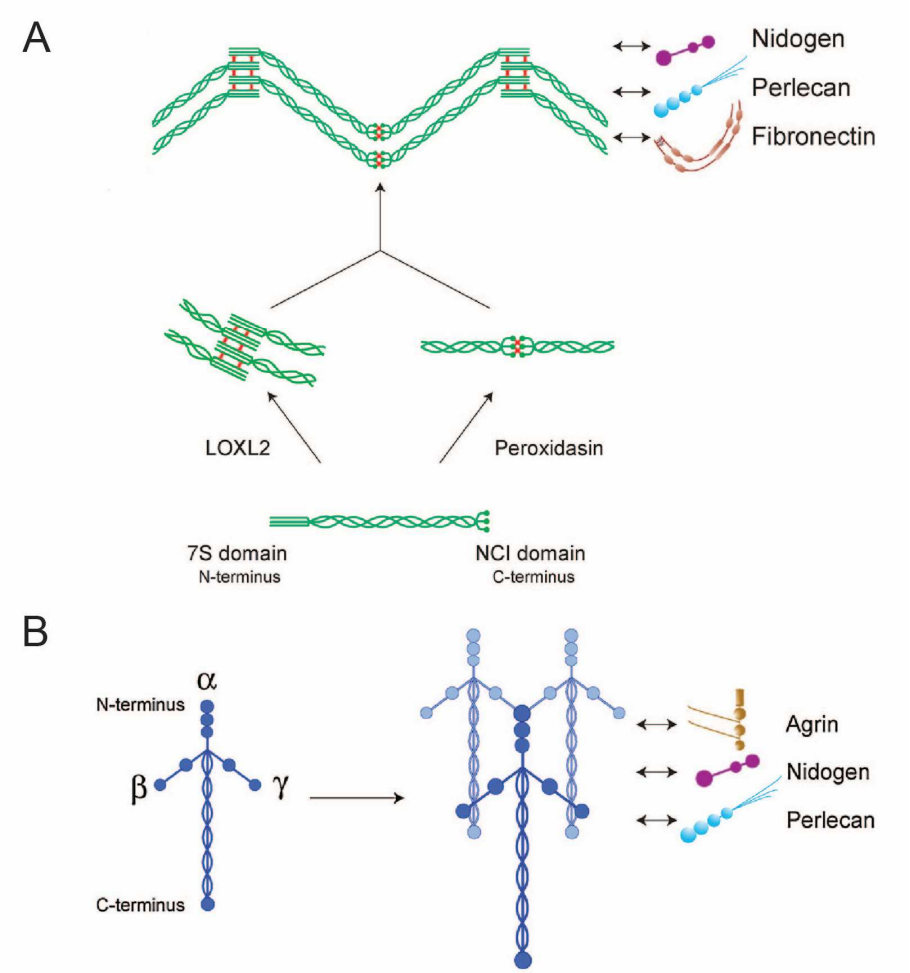

Figure 2-3: Structure of collagen and laminin (adapted from [29]).

(A) The collagen IV mesh network is constituted of α chain heterotrimers. Peroxidasin enzymes can connect the C-terminal ends and the enzyme LOXL2 provides cross-linking. Further interaction partners are nidogen, perlecan and fibronectin. **(B)** The laminin molecule consists of the arrangement of the heterotrimer of α, β and γ chains, with a globular end structure at the C-terminal. Laminin can bind together and to agrin, nidogen and perlecan.

The ECM can be divided into two types: interstitial and basement membrane. The interstitial matrix surrounds the cells and provides the structural framework for the tissue. The basement membrane is a special form of the ECM and separates cell layers from the surrounding tissue (e.g. epithelial cells from the interstitial matrix [31]) [29, 31, 35]. In the same way, the endothelial cells are separated from the surrounding tissue by the basal membrane. Thus, the basal membrane has a special significance for endothelial cell behavior [29]. The main components are laminin, collagen IV, nidogen (also called entactin) and the heparan sulfate proteoglycan perlecan. Additionally, the basal membrane contains proteases, growth factors, fibronectin and agrin [29, 31, 38]. The two networks of laminin and collagen IV are connected by the adapter molecule nidogen. The space between the two networks is filled with perlecan, which also ensures a connection between laminin and collagen IV [29, 31, 33-35]. Figure 2-4 shows a schematic view of the structure of the basement membrane [34].

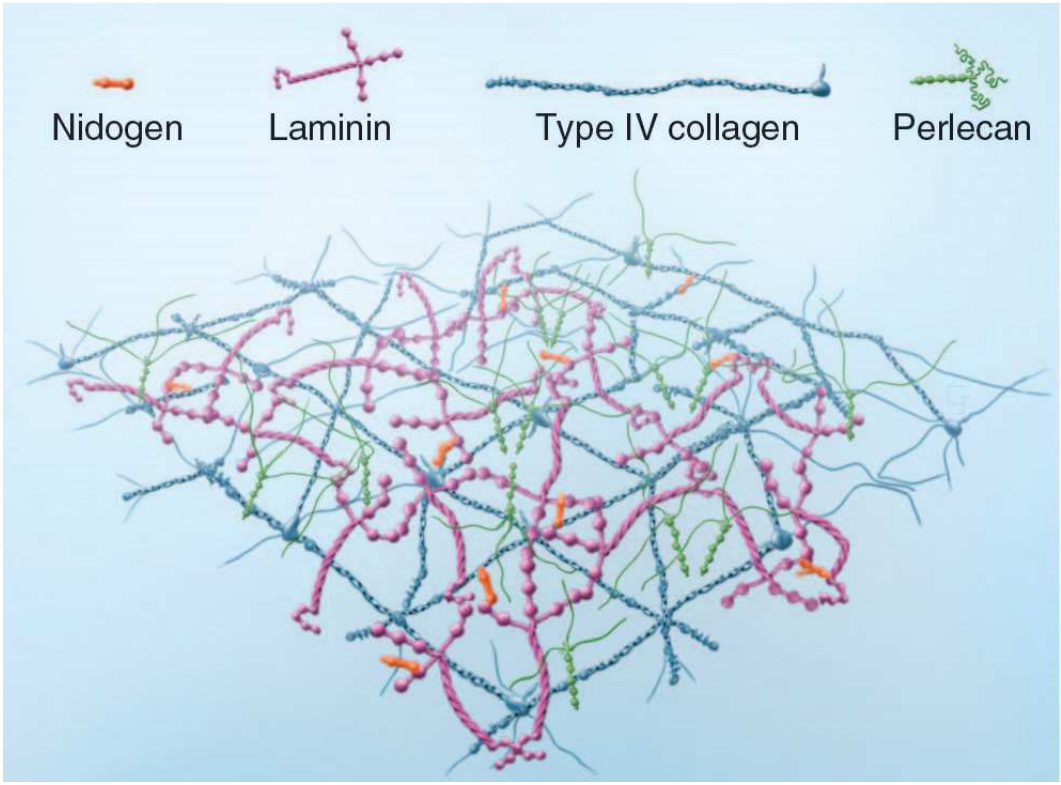

Figure 2-4: Structure of the basement membrane (adapted from [34]).

The basement membrane contains mainly laminin, collagen IV, nidogen and the heparan sulfate proteoglycan perlecan. Laminin and collagen IV form a network, which are connected to each other via the adapter molecule nidogen. However, laminin and collagen IV can also bind directly together. The interspace in between the networks is filled with perlecan, but can also mediate the connection between laminin and collagen IV.

However, the ECM is not a fixed scaffold. It undergoes constant dynamic changes through the cells [22, 25, 33, 39, 40]. A controlled remodeling provides a temporal and spatial structuring of the cell environment [15, 31, 39]. This controlled change is crucial for organ function, morphogenesis, wound healing and homeostasis [28, 31, 35, 39]. The remodeling is achieved by the synthesis of proteins [31], the secretion of crosslinking enzymes [28], the degradation of ECM proteins by MMPs [15], the rearrangement of ECM proteins as a consequence of cellular traction [31] and by a cell-induced chemical modification [31]. Dysregulation of the remodeling process can also lead to various diseases like fibrosis and inflammation [28, 35, 39]. An unregulated stiffening of the ECM particular is associated with tumor formation [31, 35, 39]. Angiogenesis and neovascular branching also increase with increased matrix crosslinking [41]. The effect of the ECM on cell behavior such as survival, migration and proliferation [28] and the alteration of the ECM by the cells results in a bidirectional complex interaction between cells and their environment [40]. Figure 2-5 from Thorne et al. shows the interaction schematically [40].

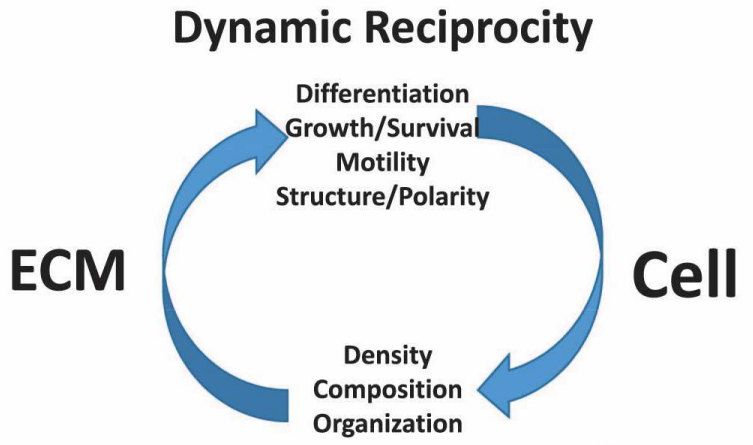

Figure 2-5: Dynamic bidirectional cell-ECM interaction (adapted from [40]).

The schematic overview shows the dynamic bidirectional connection between ECM and cells. The cells influence the composition, structure and density of the ECM by synthesis, degradation and production of crosslinking enzymes. This in turn affects various cellular processes such as differentiation, growth, survival and mobility. The changed cell behavior also affects the modification of the ECM by the cells, resulting in a dynamic, constant interaction between the ECM and the cells.

2.2.2 Mechanosensing

Cells respond to biophysical confinement [16], matrix stiffness [8, 23, 28, 41, 42] and the topography [17, 43] of the ECM. For endothelial cells, a further mechanical factor is added to the mechanical properties of the basement membrane. They are permanently exposed to the shear stress caused by the blood flow. This also influences the vascular development [6, 28]. The translation of the ECM mechanics into a specific cell response is called mechanosensing and is essential for every cell type [44, 45]. A mechanical signal is translated into a chemical signal (mechanotransduction) [23, 27] by changing the gene expression [28, 46] and leads to an adapted cell behavior. It is clear that cell behavior is determined by an interplay of biochemical (signal molecules and the composition of the ECM) and biomechanical cues (mechanical properties of the ECM) [23, 27-29, 35]. By dynamically changing the ECM and thus the mechanical properties, a cell-cell interaction can also be controlled. This is known as mechanical cell communication [22, 47]. This form of cell communication also plays an important role in coordinated collective cell behavior such as in morphogenesis and angiogenesis or in pathological process like cancer cell invasion [26, 28, 47, 48].

Adhesive cells are connected to ECM proteins via integrins. Integrins are Ca^{2+}-dependent heterodimers consisting of α and β subunits. Different integrins are known (24 types) varying in 18 different α-units and eight different β-units [49]. Integrins are intracellularly connected to the actin cytoskeleton via various adapter molecules (e.g. zyxin, vinculin, talin, α-actinin). The whole cell-ECM connecting complex is called focal adhesion [28, 50]. Force-induced integrin clustering initiates the recruitment of focal adhesion signal molecules and triggers a reorganization of the cytoskeleton via signal cascades [28, 50, 51]. Integrin acts as a bidirectional (sensor + actor) force-dependent signal transducer [28, 31].

The cells can exert a force on the ECM via contraction. Actin filaments can be moved against each other by the motor protein myosin and lead to cell contraction [28, 50]. Further, the cell can register the stiffness of the ECM by the resistance against applied cell forces [28, 50]. It remains an open question whether cells exert a constant deformation and monitor the required stress or exert constant stress and react to the degree of strain [52].

Because of the connection between the nuclear lamina and the cytoskeleton via linker of nucleoskeleton and cytoskeleton complex (LINC), the change in the cytoskeleton

has a direct influence on the nucleus. The position of the chromatin can be changed, leading to altered gene expression [53], or the activity of epigenetic regulatory molecules such as histone modifying enzymes can be adapted [28].

The gene expression can be modified via actin-dependent mechanosensitive transcription factors (e.g. myocardin-related transcription factor A (MRTF-A)) [28, 54]. The transcription factors are either bound to globular actin (G-actin) or filamentous actin (F-actin) or otherwise coupled to the actin skeleton. The factors can be released through polymerization or depolymerization of actin [54].

Further forms of mechanosensing are the connection of integrins with different signaling pathways (e.g. Rho-GTPase) [28], the stretch activation of ion channels [28] or the release of matrix-bound growth factors by cell contraction [14, 29, 31]. Many proteins involved in mechanosensing react to mechanical stress by undergoing controlled conformational changes in the molecular structure. This promotes protein-protein interactions and can trigger intracellular signals [28].

The altered gene expression, resulting from mechanosensing, also affects the expression of ECM proteins, crosslinking enzymes and proteases. This creates a dynamic feedback loop between ECM remodeling and mechanosensing [28, 29, 39].

2.3 ECM models

The ECM regulates many processes in the body. Therefore, it is also important to create different *in vitro* models to study the cell-matrix interaction [55]. ECM models are divided into natural and synthetic models [43, 56, 57]. Natural matrices are mainly hydrogels like collagen, fibrin, alginate or hyaluronic acid. Hydrogels are polymer networks that can absorb water. The advantage is that they are biodegradable, non-immunogenic and biocompatible [57], however, there are major fluctuations between different batches in terms of the matrix composition [58]. Synthetic matrices include polymers such as polydimethylsiloxanes (PDMS), polylactic acid (PLA), polyacrylamide (PAA), and polyethylene glycol (PEG) [57]. Their advantage lies in the production with controllable and reproducible properties regarding structure and mechanics [58], while their disadvantage is often the lack of biocompatibility.

The classical ECM model for angiogenesis is the tube formation assay on Matrigel [1, 16, 30, 57]. The self-organization of endothelial cells into a network serves very well as a model [1], because different steps of angiogenesis are represented, such as adhesion, migration and alignment [30, 59]. Matrigel is a non-fibrous [60], sponge-like [55] protein mixture, mainly consisting of laminin and collagen IV [38, 55, 60-62]. Its composition is very similar to the basement membrane (also known as reconstituted basement membrane) and thus very suitable for endothelial cells [60]. Matrigel is extracted from the Engelbreth-Holm-Swarm (EHS) mouse sarcoma, a tumor rich in extracellular matrix proteins [30, 38, 60]. It is not only used for endothelial cells, but also for the differentiation of serval cell lines [38].

In addition to the tube formation assay on Matrigel, there are further *in vitro* models with different endothelial cell types on different natural matrices, as well as 2D and 3D models [57, 63]. Kannan et al. [57] and Stryker et al. [63] provide a good overview of the different models. Because of its postnatal growth, the mouse retina is used, as an *in vivo* model of angiogenesis [6, 63]. Another example of an *in vivo* model is the chick chorioallantoic membrane (CAM). CAM is a highly vascularized membrane that is accessible outside the chicken embryo [20, 63].

Another widely used natural matrix is collagen I. It is the main component of many different tissue ECMs [35] and is therefore often used as tissue equivalent [64]. Collagen is also used as a matrix in a 3D model of endothelial cells [17]. In contrast to Matrigel, collagen shows a clear fiber structure [65] and the structure and mechanical

properties of a collagen gel can be easily adjusted by concentration, pH value or polymerization temperature [66].

The cell behavior in 2D and 3D is different [58, 67, 68]. To be closer to the *in vivo* conditions, ECM models and cell cultivation in general will move towards 3D. For this purpose, 3D structured scaffolds are in the focus. Synthetic materials are suitable for this purpose due to their multiple manipulation possibilities (light, heat, layer-by-layer stereolithography, two-photon polymerization) [55]. Furthermore, development focuses on the combination of natural and synthetic materials (e.g. combination PEG with the amino acid sequence for cell adhesion RGD) [56].

2.4 Aim of the study

Angiogenesis is the formation of new blood vessels from pre-existing ones and plays a role in physiological and pathological processes. An essential part of this process is a coordinated cell behavior of endothelial cells, which is mainly achieved by cell communication through the exchange of chemical signaling molecules. However, it is known that other cell types can also communicate via a mechanical way, in which the ECM acts as a mediator between cells through its direct effect on cell behavior and signaling pathways. Thus, the cell-ECM interaction plays an important role in tissue morphogenesis, growth and healing.

This study aims to validate whether the mechanical form of communication occurs between endothelial cells and focuses on the initial cell connection during the early phase of the tube formation assay on Matrigel. First of all the presence of a coordinated cell movement has to be analyzed, followed by a verification whether this movement depends on the chemical communication. As the properties of the ECM play a role for mechanical communication, it is essential to investigate its mechanical properties such as stiffness, homogeneity and structural components regarding their importance during communication of endothelial cells. Furthermore, the study examines the responsibilities of cellular processes such as proteolytic activity, protein synthesis and cell contraction for mechanical communication.

3 Materials and methods

3.1 Materials

3.1.1 Chemicals and reagents

Table 3-1: Chemicals and reagents.

Reagent	Company
Amphotericin B	PAN Biotech, Aidenbach, Germany
Blebbistatin	Sigma Aldrich, St. Louis, MO, USA
Bovine serum albumin (BSA)	Sigma Aldrich, St. Louis, MO, USA
Calcium chloride ($CaCl_2$)	AppliChem, Darmstadt, Germany
Collagen-G	Merck Millipore, Darmstadt, Germany
Dimethyl sulfoxide (DMSO)	AppliChem, Darmstadt, Germany
Disodium phosphate (Na_2HPO_4)	VWR International, Radnor, PA, USA
Distilled water (dH_2O)	From Ultra Clear® TP, Evoqua Water Technologies, Günzburg, Germany
Ethanol	Carl Roth, Karlsruhe, Germany
Ethylendiamine tetraacetic acid disodium salt dihydrate (Na_2EDTA x 2 H_2O)	Carl Roth, Karlsruhe, Germany
Fetal calf serum (FCS)	Biochrom, Berlin, Germany
FluorSave™ Reagent	Merck Millipore, Darmstadt, Germany
FluoSpheres™ sulfate microspheres, 1 µm, yellow-green fluorescent, 2% solids	Life Technologies, Carlsbad, CA, USA
Hollow glass bead 18 µm	Kisker Biotech, Steinfurt, Germany
Magnesium chloride hexahydrate ($MgCl_2$ x 6 H_2O)	AppliChem, Darmstadt, Germany
Netrin-4	Kind gift from R. Reuten (University of Copenhagen)
Paraformaldehyde (PFA)	Thermo Fisher Scientific, Waltham, MA, USA
Penicillin/streptomycin	PAN Biotech, Aidenbach, Germany

Reagent	Company
Polydimethylsiloxane (PDMS) Sylgard 184 silicone elastomer kit	Dow Corning, Midland, MI, USA
Potassium chloride (KCl)	VWR International, Radnor, PA, USA
Potassium dihydrogen phosphate (KH_2PO_4)	Merck Millipore, Darmstadt, Germany
Recombinant human vascular endothelial growth factor (VEGF) 165	PeproTech, Rocky Hill, NJ, USA
Sodium chloride (NaCl)	Sigma Aldrich, St. Louis, MO, USA
Sodium hydroxide (NaOH)	Merck Millipore, Darmstadt, Germany
Trypsin	PAN Biotech, Aidenbach, Germany
Two component glue (Power-Mix)	Henkel, Düsseldorf, Germany

3.1.2 Buffers and solutions

Table 3-2: Buffers and solutions.

Buffer / solution	Composition
Collagen-G solution	1.25 ml collagen-G in 500 ml PBS
Phosphate buffered saline (PBS) (pH 7.4)	132.2 mM NaCl 10.4 mM Na_2HPO_4 3.2 mM KH_2PO_4 in H_2O
PBS + Ca^{2+}/Mg^{2+} (PBS^{+}) (pH 7.4)	137 mM NaCl 2.68 mM KCl 8.1 mM Na_2HPO_4 1.47 mM KH_2PO_4 0.25 mM $MgCl_2$ x 6 H_2O 0.5 mM $CaCl_2$ x 2 H_2O in H_2O
TE solution	Trypsin 0.05% (w/v) Na_2EDTA x 2 H_2O 0.02% (w/v) in PBS

3.1.3 Cells and cell culture medium

Table 3-3: Cells.

Cells	Company
Human umbilical vein endothelial cells (HUVEC)	Promocell, Heidelberg, Germany

Table 3-4: Cell culture media.

Cell culture medium	Manufacturer
Endothelial cell growth medium (ECGM) kit enhanced	Pelobiotech, Matrinsried, Germany
Dulbecco's modified eagle medium (DMEM)	PAN Biotech, Aidenbach, Germany

3.1.4 Hydrogels

Table 3-5: Hydrogels.

Hydrogel	Manufacturer
Collagen I high concentration, rat tail	Corning, New York, NY, USA
Laminin I	R&D systems, Minneapolis, MN; USA
Matrigel, growth factor reduced, phenol red free	Corning, New York, NY, USA
TissueSpec® Bone ECM (TissueSpec® ECM hydrogel + component A + component B)	Xylyx Bio, New York, NY; USA
TissueSpec® Intestine ECM (TissueSpec® ECM hydrogel + component A + component B)	Xylyx Bio, New York, NY; USA
TissueSpec® Lung ECM (TissueSpec® ECM hydrogel + component A + component B)	Xylyx Bio, New York, NY; USA

3.1.5 Antibodies

Table 3-6: Primary antibodies.

Name	Species	Catalogue	Manufacturer	Dilution
Anti-collagen I	Rabbit, IgG	34710	Abcam, Cambridge, UK	1:200
Anti-collagen IV	Rabbit, IgG	AB756P	Sigma Aldrich, St. Louis, MO, USA	1:100
Anti-fibronectin	Mouse, IgG	sc-73611	Santa Cruz Biotechnology, Dallas, TX, USA	1:200
Anti-laminin	Rat, IgG	MA1-06100	Thermo Fisher Scientific, Waltham, MA, USA	1:200
Anti-mouse antibody fragment	Donkey, IgG (H+L)	715-007-003	Jackson ImmunoResearch, West Grove, PA, USA	1:30

Table 3-7: Secondary antibodies.

Name	Species	Catalogue	Manufacturer	Dilution
Alexa Fluor 488	Goat anti-Mouse IgG (H+L)	A-11001	Life Technologies, Carlsbad, CA, USA	1:200
Alexa Fluor 488	Goat anti-rabbit IgG (H+L)	A-11008	Life Technologies, Carlsbad, CA, USA	1:200
Alexa Fluor 488	Goat anti-rat IgG (H+L)	A-11006	Life Technologies, Carlsbad, CA, USA	1:200
Alexa Fluor 647	Chicken anti-rabbit IgG (H+L)	A-21443	Life Technologies, Carlsbad, CA, USA	1:200

3.1.6 Fluorescent dyes

Table 3-8: Fluorescent dyes.

Fluorescent dyes	Company
5(6)-FAM, SE (5-(6)-carboxyfluorescein, succinimidyl ester	Thermo Fisher Scientific, Waltham, MA, USA
CellTracker™ Red CMTPX	Life Technologies, Carlsbad, CA, USA
Hoechst 33342	Sigma Aldrich, St. Louis, MO, USA
Rhodamin-phalloidin	Sigma Aldrich, St. Louis, MO, USA

3.1.7 Devices

Table 3-9: Technical devices and lab equipment.

Device	Manufacturer
Axiovert 200 inverted microscope	Carl Zeiss Microscopy, Jena, Germany
Bold Line incubation system	Okolab, Pozzuoli, Italy
Climate chamber for Eclipse Ti	Ibidi, Gräfelfing, Germany
Colibri 7 (light source for Axiovert 200)	Zeiss, Oberkochen, Germany
Compartment drier	Memmert, Schwabach, Germany
Desiccator	Glaswerk Wertheim, Wertheim, Germany
Eclipse Ti inverted microscope + CCD camera (DS-Qi1Mc)	Nikon, Tokyo, Japan
EXT-440 (liquid water cooling system for Zyla camera)	Koolance, Auburn, WA, USA
HeraCell 150i incubator	Thermo Fisher Scientific, Waltham, MA, USA
Laminarflow Heraeus, Herasafe	Thermo Fisher Scientific, Waltham, MA, USA
Leica DMi1 microscope + camera Leica MC120 HD	Leica Microsystems, Wetzlar, Germany
Leica TCS SP8 confocal microscope	Leica Microsystems, Wetzlar, Germany

Device	Manufacturer
Megafuge 1.0 RS centrifuge	Thermo Fisher Scientific, Waltham, MA, USA
Modular Compact Rheometer MCR 100 + PP25 measuring plates	Physica, Stuttgart, Germany
NanoWizard® 4 + PetriDishHeater	JPK Instruments, Berlin, Germany
Plasma cleaner typ “ZEPTO”	Diener electronic, Ebhausen, Germany
Ultrasonic bath Sonorex RK 100	Bandelin electronic, Berlin, Germany
ViCell™ XR cell counter	Beckman Coulter, Brea, CA, USA
Water bath Haake W19	Thermo Fisher Scientific, Waltham, MA, USA
ZYLA-4.2P-USB3-W	Andor, Belfast, Northern Ireland

3.1.6 Consumables

Table 3-10: Consumables.

Consumables	Manufacturer
100-mm petri dish	Sarstedt, Nümbrecht, Germany
40-mm petri dish	Techno Plastic Products (TPP), Trasadingen, Switzerland
Cantilever MLCT-C	Bruker, Billerica, MA, USA
Cantilever MLCT-D tipless	Bruker, Billerica, MA, USA
Cell culture flasks 75 cm^2	Sarstedt, Nümbrecht, Germany
Cover slips 8x8 mm	H. Saur Laborbedarf, Reutlingen, Germany
Disposable pipettes: 5 ml, 10 ml, 25 ml	Sarstedt, Nümbrecht, Germany
Falcon tubes: 15 ml, 50 ml	Greiner Bio-One, Kremsmünster, Austria
Pipette tips: 10 µl, 100 µl, 1000 µl	Sarstedt, Nümbrecht, Germany
SafeSeal tube: 0.5 ml, 1.5 ml, 2 ml	Sarstedt, Nümbrecht, Germany
µ-Slide 2 well uncoated	Ibidi, Gräfelfing, Germany

Consumables	Manufacturer
µ-Slide 8 well uncoated	Ibidi, Gräfelfing, Germany
µ-Slide angiogenesis ibiTreat	Ibidi, Gräfelfing, Germany

3.1.9 Software

Table 3-11: Software.

Software	Origin
Chemotaxis Tool	Ibidi, Gräfelfing, Germany
Data processing software	JPK Instruments, Berlin, Germany
GraphPad Prism 8	GraphPad Software, San Diego, CA USA
ImageJ	National Institutes of Health, Bethesda, MD, USA
ImageJ plugin Manual Tracking	Fabrice Cordelires, Institut Curie, Orsay, France
ImageJ plugin TrackMate	[69]
ImageJ software tool “Angiogenesis Analyzer”	Gilles Carpentier, Faculte des Sciences et Technologie Universite Paris Est Creteil Val-de-Marne, Paris, France
LAS X Core Software	Leica Microsystems, Wetzlar, Germany
Microsoft Office Standard 2016	Microsoft, Redmond, WA, USA
NIS-Elements	Nikon, Tokyo, Japan
Trainable Weka Segmentation	[70]
SPM software	JPK Instruments, Berlin, Germany

3.2 Methods

3.2.1 Cell culture

HUVECs were maintained in ECGM containing 10% FCS, 1% penicillin/streptomycin and 1% amphotericin B. Cells were cultivated under constant humidity at 37 °C and a 5% CO_2 atmosphere. All experiments were performed using cells at passage #6.

For detachment of the cells, the medium was removed and the cells were washed twice with PBS. The cells were trypsinized with 2x TE for 2 min at 37 °C. The reaction was stopped by adding DMEM containing 10% FCS and 1% penicillin/streptomycin. The cells were centrifuged at 1000 rpm for 5 min and resuspended in ECGM. The cell concentration was determined with a ViCell™ XR cell counter. For sustaining and further seeding, the cell suspension was diluted, depending on the planned experiments. All cell culture flasks were coated with a collagen-G solution for 30 min at 37 °C prior to seeding.

3.2.2 Hydrogel preparation

Four different hydrogels were used: Matrigel, 2 mg/ml collagen I, 6 mg/ml laminin as well as a mixture gel of 6 mg/ml laminin and 4 mg/ml collagen I at a ratio of 6:1 (final concentration 4.8 mg/ml:0.8 mg/ml) (L:C 6:1). Matrigel and laminin were thawed on ice overnight the day before use. Collagen I was constantly stored at 4 °C. For a better handling, ice-cold tips were used. The gels were mixed thoroughly to ensure homogeneity after thawing and kept on ice.

Netrin-4 was mixed with Matrigel to manipulate the structure of Matrigel. The volume of netrin-4 was based on the amount of laminin in the Matrigel and set at ratios of 1:2, 1:1 and 1.5:1 netrin-4 to laminin. For a positive control, Matrigel was mixed with the same volume of PBS. In the lower netin-4:laminin ratios (1:1 and 1:2) PBS was added to reach the same volume as in the highest ratio (1.5:1). For gelation, Matrigel was kept at 37 °C, 5% CO_2 in a humid environment for at least 30 min.

Collagen I gels consisted of 10% 10x PBS, 1 N NaOH (0.023 times the final volume of collagen I) and dH_2O to adjust the collagen concentration. The 10x PBS, 1 N NaOH and dH_2O were mixed and kept on ice. Subsequently, the calculated volume of collagen I was added and mixed. For the L:C 6:1 gel, laminin and collagen I were mixed on ice. For gelation, collagen I, laminin and L:C 6:1 were kept at 37 °C, 5% CO_2 in a humid environment for at least 1 h.

Organ-specific ECM gels (bone, intestine and lung) were obtained from Xylyx Bio and used according to the manufacturer´s protocols. Briefly, the prescribed amount of component A and B were added to the TissueSpec® ECM hydrogel and were mixed. ECGM was mixed with the other components to yield a final hydrogel concentration of 6 mg/ml. For gelation, gels were kept at 37 °C, 5% CO_2 in a humid environment for at least 45 min.

3.2.3 Gel printing on PDMS

PDMS and the curing agent were mixed in the required ratio. Air bubbles were removed in a desiccator for 15-20 min. Afterwards, the gels were cured for 20 h in a compartment drier at 60 °C. The following table shows the different ratios of the curing agent and the resulting stiffness.

Table 3-12: PDMS stiffness for different curing agent ratios.

Curing agent ratio	**Stiffness [kPa]**
0.1	70
0.04	25
0.022	4
0.02	1.5
0.013	0.5

Two different approaches were used to combine a hydrogel with the PDMS. In the first approach, a certain volume of the hydrogel was added to a µ-Slide angiogenesis ibiTreat. The inner well was filled with PDMS. After the curing, the PDMS was hydrophilized by plasma cleaning. The plasma process lasted for 3 min at 0.3 mbar. Then the hydrogel was prepared and different volumes (1-10 µl) were added on top of the PDMS. Afterwards, the HUVECs were prepared and added to the slide.

In the other approach, a µ-Slide 2 well uncoated was used and filled with a thin PDMS layer. The PDMS was also hydrophilized by plasma cleaning and 5 µl of the hydrogel were added. A stiff PDMS stamp (70 kPa) was pressed on the hydrogel to create a thin evenly distributed hydrogel layer. After the gelation of the hydrogel, the well was filled with 1000 µl PBS. The PDMS stamp was carefully removed. Figure 3-1 shows the model of the hydrogel printing.

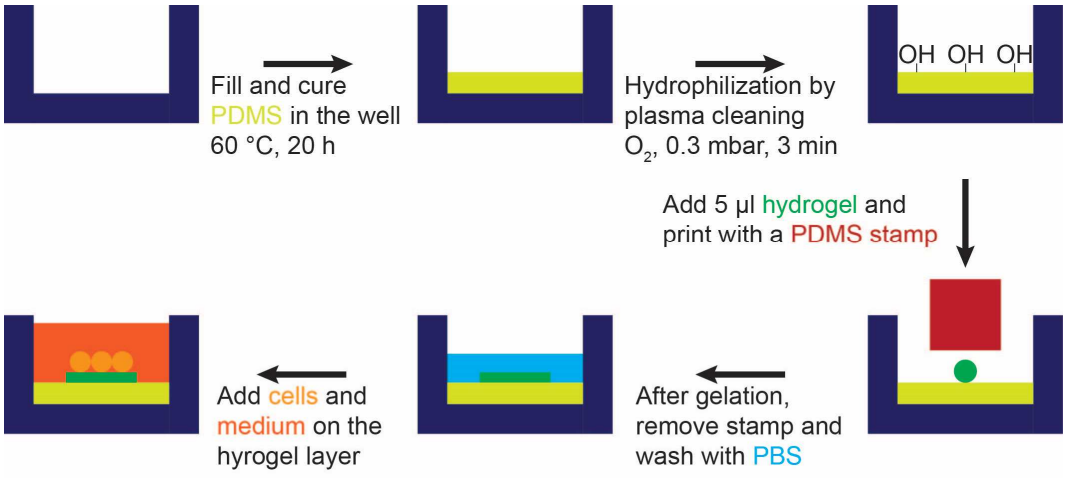

Figure 3-1: Hydrogel printing workflow.
PDMS was filled in the well and cured after the desiccator. The surface was hydrophilized with the plasma cleaner and 5 µl of the hydrogel were added. With a PDMS stamp a thin hydrogel layer was created. After the gelation, the stamp was removed and unbound hydrogel was washed out with PBS. Then, the cells were seeded on the hydrogel layer.

For a coating instead of hydrogel printing, a µ-Slide 8 well was filled with PDMS and 15 µl of the corresponding hydrogel was added after plasma activation.

Matrigel was mixed with the fluorescent dye 5(6)-FAM, SE (5-(6)-carboxyfluorescein, succinimidyl ester) at a final concentration of 0.1 mg/ml. With a z-stack (40 steps) the thickness of the Matrigel layer was measured. A Leica TCS SP8 confocal microscope with HC PL Fluotar CS2 10x/0.3 NA DRY together with the LAS X Core Software were used for imaging. The thickness was measured with ImageJ.

3.2.4 Tube formation assay

HUVEC tube formation assays were performed in a µ-Slide angiogenesis ibiTreat or a µ-Slide 8 well uncoated. The inner well of the µ-Slide angiogenesis was filled with 10 µl of the hydrogels. The µ-Slide 8 well was first hydrophilized by plasma cleaning. The plasma process lasted for 3 min at 0.3 mbar. Then, 30 µl of the hydrogels were added in the µ-Slide 8 well. After the gelation of the hydrogels, 50 µl of the cell suspension were applied to the top well of the angiogenesis slide and 250 µl of the cell suspensions were added to the 8-well slide. The cell concentration was 20 x 10^4 cells/ml for the µ-Slide angiogenesis and 10 x 10^4 cells/ml for the µ-Slide 8 well. For treatment with blebbistatin, the blebbistatin was diluted directly in the cell suspension to the indicated final concentration. DMSO was used as control. The slides were incubated at 37 °C and 5% CO_2. Images were taken on a Leica DMi1 microscope with a 4x/10x phase

contrast objective. All images were processed using ImageJ. The tube formation was analyzed using the ImageJ software tool “Angiogenesis Analyzer” to determine the number of tubes and nodes. If the tool could not distinguish the cells directly from the background, the images were previously segmented with “Trainable Weka Segmentation” plugin [70].

3.2.5 Live cell imaging

Live imaging was performed with an Eclipse Ti inverted microscope with a 4x/10x phase contrast objective and a CCD camera. The measurements were coordinated with the NIS-Elements software. The slides were inserted into a 37 °C heating and incubation system from Ibidi that was flushed with actively mixed 5% CO_2 at a rate of 10 l/h, and the humidity was kept at 80% to prevent dehydration. Time lapse sequences were processed using ImageJ.

3.2.6 Cell tracking

For cell tracking of different cell concentrations, HUVECs were stained with Hoechst 33342. A confluent cell layer was washed with PBS^+ and then stained with 5 µg/ml Hoechst in PBS^+ for 20 min. The tube formation assay was performed according to the protocol described above. The movies were analyzed by Andriy Goychuk (Arnold Sommerfeld Center for Theoretical Physics and Center for NanoScience, LMU Munich).

The positions of stained cell nuclei were detected from fluorescent channels of tube formation videos and then stitched together into sets of time-lapse cell trajectories. The following procedure was applied. First, to detect the cell cores, (i) the contrast was improved via a contrast-limited adaptive histogram equalization using OpenCV (https://github.com/opencv/opencv), (ii) all image data were normalized, and (iii) a multipass Laplace-of-Gaussian filter was applied using scikit-image [71]. Then, the individual cell core coordinates were linked into cell trajectories with Trackpy (https://doi.org/10.5281/zenodo.1226458). Additionally, the results were analyzed with the software ImageJ and its plugin TrackMate [69] for comparison (not shown). Further analysis of the obtained cell trajectories was performed, as described below.

To measure whether cell motion during tube formation could be described by a persistent random walk with a typical timescale, a metric for the correlation between

the direction of cell motion at a reference time t and a time $t + \Delta t$, the normalized velocity autocorrelation function, was introduced:

$$C(t, \Delta t) = \left\langle \frac{\boldsymbol{v}(\boldsymbol{x}, \boldsymbol{t}) \cdot \boldsymbol{v}(\boldsymbol{x}, \boldsymbol{t} + \Delta t)}{\|\boldsymbol{v}(\boldsymbol{x}, \boldsymbol{t})\| \, \|\boldsymbol{v}(\boldsymbol{x}, \boldsymbol{t} + \Delta t)\|} \right\rangle_{cell\ positions\ \boldsymbol{x}}$$

For a time-independent process, one can average over all available reference times t. Tube formation, however, is a time-dependent process that might change, if, for example, cell velocities change over time. It was averaged over reference times, which lie within a window, $C(\Delta t) \equiv \langle C(t, \Delta t) \rangle_{t \leq 50\ min}$. This time window is shorter than the timescale of tube formation (80 min) and much shorter than the overall duration of the experiments (20 h). The normalized velocity autocorrelation function decayed rapidly from $C(0) = 1$ to $A = C(10\ min) \approx 0.42$, by the first frame. For all subsequent frames, the typical timescale of tube formation, τ, was obtained from an exponential fit:

$$C(\Delta t) \approx A\ exp(-\Delta t / \tau)$$

A possible correlation between the migration of distant cells was determined as a function of separation distance between the considered cells as follows:

$$\mathrm{C(t, r)} = \left\langle \frac{\boldsymbol{v}(\boldsymbol{x}, \boldsymbol{t}) \cdot \boldsymbol{v}(\boldsymbol{x} + r\ \hat{\boldsymbol{r}}(\theta), \boldsymbol{t})}{\|\boldsymbol{v}(\boldsymbol{x}, \boldsymbol{t})\| \, \|\boldsymbol{v}(\boldsymbol{x} + r\ \hat{\boldsymbol{r}}(\theta), \boldsymbol{t})\|} \right\rangle_{cell\ positions\ \boldsymbol{x}, angle\ \theta}$$

The cosine of the angle between the velocity vector of a cell at position $\boldsymbol{x}$ and that of a cell at position $\boldsymbol{x} + r\ \boldsymbol{\theta}$ was measured, where $\hat{\boldsymbol{r}}(\theta)$ is the radial unit vector pointing in the direction of the angle θ (in cylindrical coordinates). Again, it was averaged over reference times, which lie within a window, $C(r) \equiv \langle C(t, r) \rangle_{t \leq 50\ min}$. Then, the typical length scale of a cell-cell velocity alignment, r_1, was obtained from a biexponential fit:

$C(r) \approx A\ exp(-r/r_1) + B\ exp(-r/r_2)$, where $r_1 \ll r_2$.

Finally, a correlation between the migration of a cell and the position of a distant cell that lies in the direction $\hat{\boldsymbol{r}}(\theta)$ was determined as a function of their separation distance r in a similar way:

$$\mathrm{C(t, r)} = \left\langle \frac{\boldsymbol{v}(\boldsymbol{x}, \boldsymbol{t}) \cdot \hat{\boldsymbol{r}}(\theta)}{\|\boldsymbol{v}(\boldsymbol{x}, \boldsymbol{t})\|} \right\rangle_{cell\ positions\ \boldsymbol{x}, \boldsymbol{angle\ \theta}}$$

Notably, this value does not vanish, if the cells are distributed inhomogeneously.

3.2.7 Cell migration

To observe the migration of HUVEC after seeding on collagen I (2 mg/ml) in a short time scale, the cells were stained with CellTracker™ Red. A confluent cell layer was washed twice with PBS^+ and then stained with 2 µM CellTracker™ Red for 30 min in PBS^+. The tube formation assay was performed according to the protocol described above. Live cell imaging was performed using a Leica TCS SP8 confocal microscope equipped with HC PL APO CS2 20x/0.75 NA immersion or an 63x/1.4 NA oil objective using LAS X Core Software together with the Bold Line incubation system. Movies were recorded over 3 h with a time interval of 15 min.

For the cell migration experiment over 20 h, HUVECs were prepared according to the protocol of the tube formation assay on Matrigel or 2 mg/ml collagen I in the µ-Slide angiogenesis. A low cell concentration of 1×10^4 cells/ml was used to observe the migration behavior of single cells. The live cell imaging was recorded with the Eclipse Ti inverted microscope with a 4x phase contrast objective and a time interval of 10 min.

All movies were processed and analyzed using ImageJ. Cell migration was analyzed in three different experiments and in every experiment three different wells of the µ-Slide angiogenesis were imaged. Five cells per well were tracked with the ImageJ plugin Manual Tracking; in total 45 cells for each hydrogel. The data were saved and then imported to the Chemotaxis Tool. After adding the time interval and the x/y calibration, the software tool plotted the migration and calculated the accumulated migration distance.

3.2.8 Traction force microscopy

For the traction force microscopy, HUVECs were prepared according to the protocol of the tube formation assay on Matrigel in the µ-Slide 8 well. Matrigel was mixed with yellow-green microbeads (1:200). To determine the forces of single cells, cells were seeded at a low concentration of 1×10^4 cells/ml. Time-lapse video microscopy with the Eclipse Ti inverted microscope with a 10x phase contrast objective was performed with a time interval of 1 min between images for 3 h. Furthermore, experiments with cell numbers for tube formation (10×10^4 cells/ml) were performed. The cells were stained with the CellTracker™ Red. A confluent cell layer was washed twice with PBS^+ and then stained with 2 µM CellTracker™ Red for 30 min.in PBS^+. Live cell imaging was performed with a Leica TCS SP8 confocal microscope equipped with HC PL APO CS2 20x/0.75 NA immersion or an 63x/1.4 NA oil objective using LAS X Core Software

together with the Bold Line incubation system. Movies were recorded over 3 h with a time interval of 4 min. The movies were analyzed by Andriy Goychuk.

Substrate displacement fields, $\boldsymbol{u}(\boldsymbol{x},t)$, were obtained from fluorescence channels of the videos by computing the corresponding optical flow fields using the “Two-Frame Motion Estimation Based on Polynomial Expansion” by Gunnar Farnebäck [72] implemented in OpenCV. Then, compression fields, $\boldsymbol{\nabla}\cdot\boldsymbol{u}(\boldsymbol{x},t)$, were determined and visualized in phase contrast channels of the videos. Each (round) cell generated a radially symmetric compression field. Therefore, the average radial component of the compression field, $\langle\boldsymbol{\nabla}\cdot\boldsymbol{u}(\boldsymbol{x},t)\rangle_\theta$, was determined and the radial component of the displacement field, $\langle\hat{\boldsymbol{r}}(\theta)\cdot\boldsymbol{u}(\boldsymbol{x},t)\rangle_\theta$, in the reference frame of the individual cells. To approximate the cell positions, the coordinates with maximal compression field were measured.

3.2.9 Immunostaining and confocal microscopy

Cells were washed with PBS$^+$ for 10 min and fixed with 4% PFA in PBS for 10 min, followed by three washing steps with PBS for 10 min, and blocking with 1% BSA in PBS for at least 2 h or overnight at 4 °C. In the case of murine primary antibody, an additional blocking procedure with donkey anti-mouse antibody fragment diluted 1:30 with 1% BSA in PBS was performed, avoiding nonspecific binding of the secondary antibody in the Matrigel. After the blocking step, the slide was washed with PBS for 10 min. The primary antibodies were diluted with 1% BSA in PBS and incubated overnight at 4 °C. Prior to incubation with the secondary antibody, which was also diluted with 1% BSA in PBS, the slide was washed six times with PBS for 10 min and then incubated overnight at 4 °C. Again, cells were washed three times with PBS for 20 min and stained with Hoechst 33342 at a final concentration of 5 µg/ml and rhodamine-phalloidin diluted 1:400 in 1% BSA in PBS for 1 h. Afterwards, the preparation was washed three times with PBS for 10 min. The samples were mounted with one drop of FluorSave™ reagent and the µ-Slide 8 well was additionally covered with a cover slip.

Confocal images were collected using a Leica TCS SP8 confocal microscope with HC PL APO CS2 20x/0.75 NA immersion or an 63x/1.4 NA oil objective using LAS X Core Software. Hybrid detectors (Leica HyD) and photomultipliers (PMT) were used as detectors. Pinhole size was adjusted to 1.0 airy units, the pixel size was 1024x1024, the frame rate was 0.582 per second and an average of two frames were acquired for

every channel in sequential scanning mode. Z-stacks were imaged with 40 steps. The following laser lines and excitation sources were used: 405 nm (diode), 561 nm (diode pumped solid state (DPSS)), 488 nm and 647 nm (both argon).

The structure of fibrous hydrogels can be made visible using reflection microscopy. The argon laser with a wavelength of 488 nm was used and the wavelength range of the detector was set between 480 and 530 nm. The laser light was reflected on the fibers of the hydrogel and then detected by the detector.

All images were processed and analyzed using ImageJ.

3.2.10 Rheological measurements

The stiffness of PDMS was measured after hydrophilization with a Modular Compact Rheometer MCR 100 in the amplitude sweep mode with a constant frequency of 1 Hz at 37 °C between the PP25 measuring plates. For these measurements, the gels were prepared in a 40-mm petri dish and pieces of the same size as the measuring plates were cut out. The deformation was varied from 0.01% to 10% in ramp mode. For each measurement, 30 measurement points were obtained, each for a duration of 15 s. The measurements were averaged and the Grubbs outlier test was applied.

3.2.11 Atomic force microscopy (AFM)

For the AFM measurements, 40-mm petri dishes were used. After the gelation process of the hydrogels, ECGM was filled in the petri dish and kept at 37 °C with the PetriDishHeater. The AFM measurements were performed on a NanoWizard® 4 with an integrated Axiovert 200 inverted microscope LD ACHROSTIGMAT 20x/0.3 PH1 or LD ACHROSTIGMAT 40x/0.55 PH2 in combination with a Zyla sCMOS camera from Andor, using SPM software in contact mode. To measure the gel stiffness homogeneity, an MLCT-C cantilever (silicon nitride, resonance frequency 7 kHz, spring constant 0.01 N/m) was used and calibrated with the contact-free method. The following values were set: setpoint 1 nN, z-length 8 µm, speed 2 µm/s and pixel size 16x16 on a 30x30 µm grid. For measuring the strain stiffening, a tipless MLCT-D cantilever (silicon nitride, resonance frequency 15 kHz, spring constant 0.03 N/m) glued with a hollow glass bead (by using two component glue) was used and calibrated with the contact-free method. Immediately before the measurement, the diameter of the bead was measured using ImageJ. For the setting, the following parameters were used: setpoint 2 nN, z-length 10 µm, and speed 10 µm/s. The measuring area was

adjusted to the distance between the cells. The pixel size was 10x10, and every pixel was directly measured three times. For analysis, the mean value of every pixel was used. For the control area, a 5x5 µm grid far from the cells was measured after every single cell measurement. Every single cell measurement was compared directly with the control measurement. In the end 21 pairs of measurements were analyzed.

All data were analyzed with the Data processing software. The stiffness (Young's modulus) was calculated with the Hertzian contact model, based on Hooke's law according to equation [73]:

$$E = \frac{3}{4} \cdot \frac{F \cdot (1 - v^2)}{\sqrt{\delta^3} \cdot \sqrt{R}}$$

In the software, the spring constant and sensitivity of the cantilever were put in and the baseline and contact point were determined. The tip shape of the MLCT-C was modeled as a square pyramid and the half angle of the front of the cantilever was set to 15 °. For the MLCT-D with the bead, a sphere model was used, and the radius of the bead was set. The Poisson ratio was set to 0.5.

3.2.12 Statistical analysis

The results of at least three independent experiments (biological replicates, each performed in two or three technical replicates) are expressed as the mean ± standard error of the mean (SEM). Statistical analysis was performed using GraphPad Prism 8 with either a two-tailed unpaired Student's t-test with Welch's correction or a one-way ANOVA with Dunnett's test (n.s. ≙ not significant, *P < 0.033, **P < 0.002, ***P < 0.001). Significantly different groups are indicated in the respective figures.

4 Results

4.1 Evidence for mechanical communication

4.1.1 Tube formation shows cell-cell finding at a short time scale.

The tube formation assay was performed to investigate the endothelial cell behavior. HUVECs were seeded on Matrigel and after cell adhesion, they began to form a tubular network. This process can be divided into two phases. First, there was an initial “finding phase” in which the first cell contacts were made by cell stretching and moving to a neighboring cell. Nodes with several cells and connections (tubes) with single or few cells that connected the nodes were formed. The “finding phase” was on a time scale of up to 6 h and the first cell contacts were formed in the range of 1 to 2 h (Fig. 4-1 white arrows). The second phase can be called the “maturing phase”. The structure of the network was not changed until the end of the experiment after 20 hours. Existing tubes and nodes were stabilized, while small tubes became detached over time. The work focuses on the mechanism behind cell finding in the short time scale. Figure 4-1 shows the time course of the tube formation over 20 h.

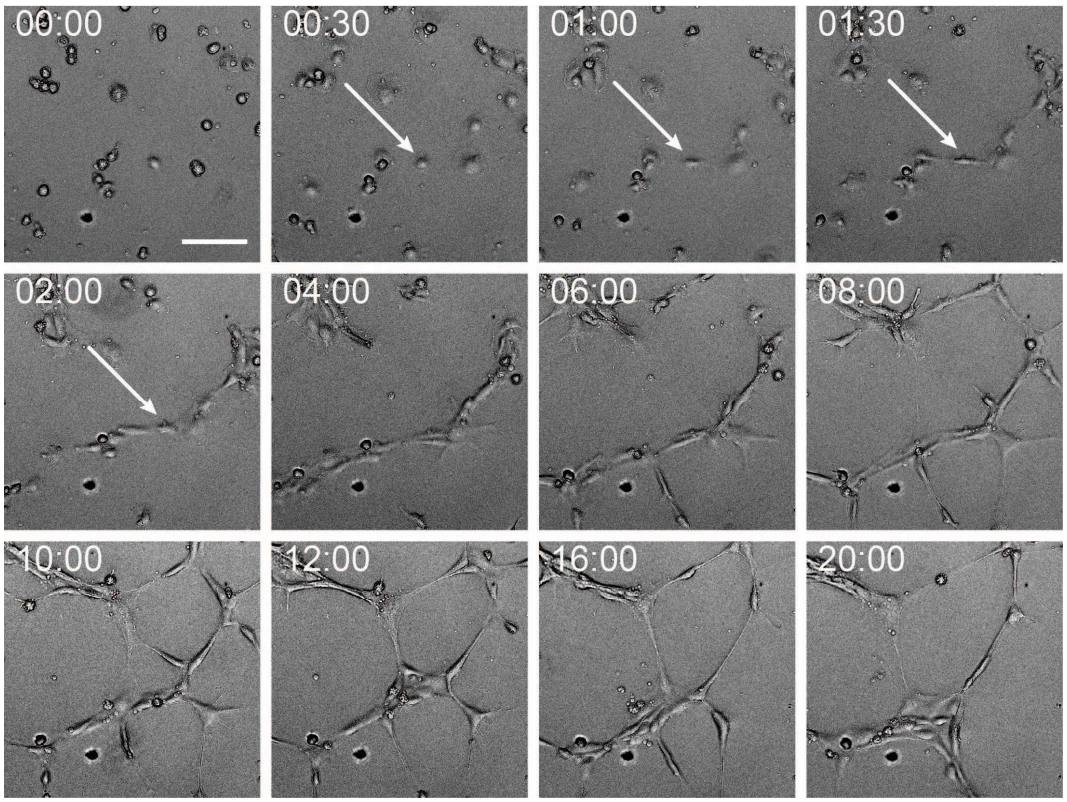

Figure 4-1: HUVEC tube formation on Matrigel.

HUVECs rapidly formed cell-cell contacts when seeded on Matrigel. White arrows indicate the initial formation of the first cell-cell contacts in a time range from 1 to 2 h. After the “finding phase” (first 6 h) the “maturing phase” followed, in which existing tubes and nodes were stabilized. Scale bar: 100 µm.

4.1.2 Cell interaction depends on cell density and has an intrinsic length scale

To investigate the impact of cell-cell distances on network formation, tube formation assays were performed with different cell densities. At low densities (up to 6×10^4 cells/ml) the cells barely moved, and no network formation occurred (Fig. 4-2A). At a cell concentration of 2×10^4 cells/ml first cell contacts were built, but no network was formed. With higher cell numbers than 10×10^4 cells/ml, tube formation was observed (Fig. 4-2A). Kerstin Kick (Pharmaceutical Biology, LMU Munich) performed the experiments for lower cell densities (0.5×10^4 cells/ml up to 6×10^4 cells/ml) [74]. Quantification of the number of tubes and nodes after 6 h are shown in the appendix Figure 7-1A. There was a significant difference between the higher cell numbers for tube formation and lower cell numbers where no network was formed. The difference between cell densities, which form a distinct network, was relatively small. To characterize cell behavior during tube formation, Andriy Goychuk analyzed a large body of individual trajectories of cells. The mean squared

displacement (Fig. 4-2B, upper left panel) shows that cells move only significantly when tube formation occurs. It can be concluded that cell motility must be a result of the macroscopic self-organization of the cells into a network and not the reverse. Therefore, the behavior of single cells are related to the behavior of the collective. The typical time scale of tube formation was found to be approximately 80 min, which was calculated by a normalized velocity autocorrelation function (Fig. 4-2B, lower left panel). Furthermore, network formation was only observable above a critical cell density, which suggests that cells cannot detect each other if they are far apart. To test whether there is an intrinsic length for intercellular signaling, the mutual velocity alignment of distant cells was measured. Here, the cells weakly aligned their motion across the whole field of view, especially within a typical radius of 106 µm (Fig. 4-2B, lower right panel). Finally, there is a directed component of cell motion so that cells sense the positions of surrounding neighbors. The cells were attracted to distant cells while being sterically repelled from nearby cells. For the range of a cell diameter, the cells show repulsive behavior because they need space for adhesion. The distance over which cells optimally sense other cells coincides well with the distance over which cells align their direction of motion (Fig. 4-2B, upper right panel). Taken together, these findings suggest that cells can sense each other to align and cluster over a typical distance of at least 106 µm. To communicate over such long distances, cells would have to employ either chemical or mechanical signaling. Therefore, it is to be determined which type of cellular signal is necessary for tube formation.

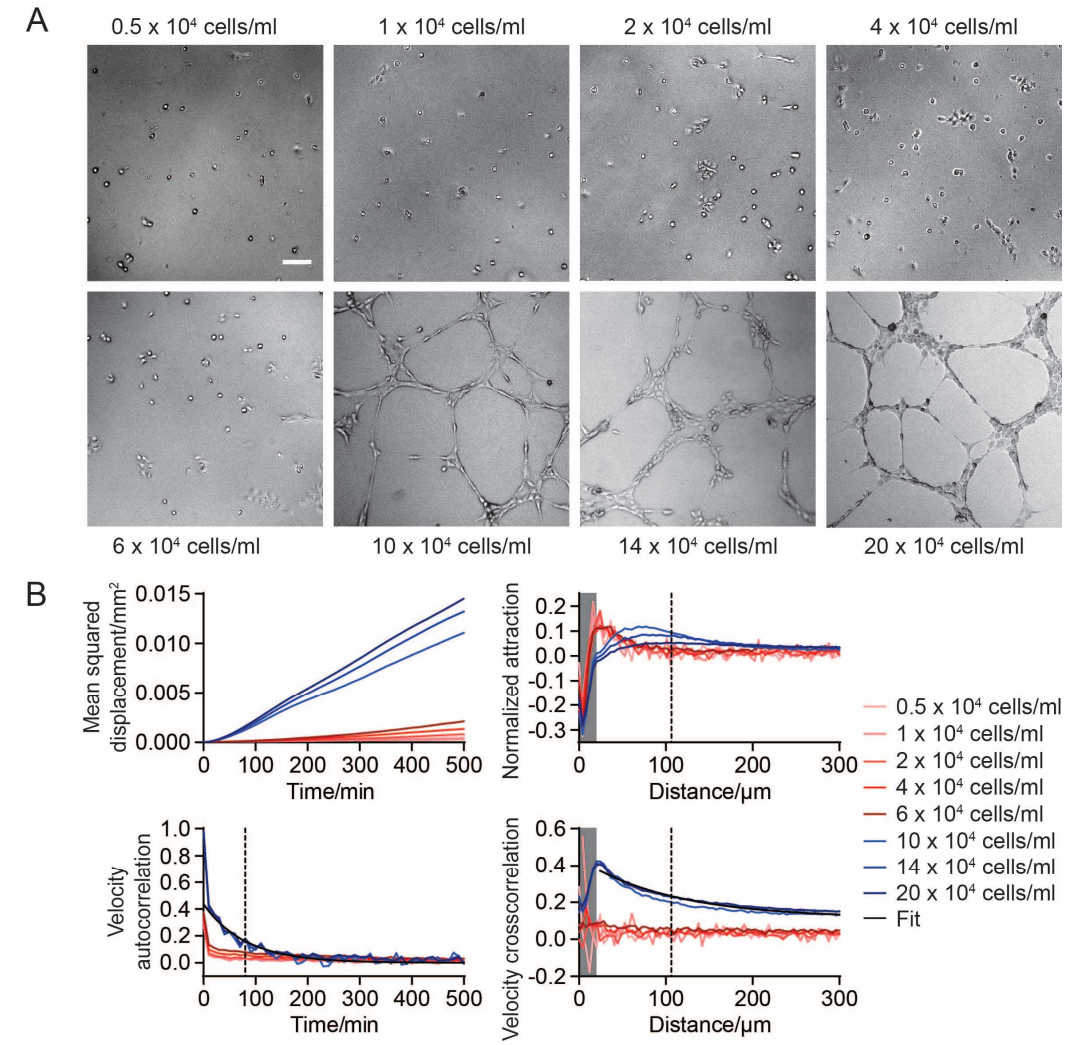

Figure 4-2: The initial finding phase depends on cell-cell distance.

(A) Tube formation after seeding cell densities from 0.5 x 10^4 cells/ml to 20 x 10^4 cells/ml. Up to a density of 6 x 10^4 cells/ml no tube formation was possible and the cells arranged in small groups. For higher densities, the cells were able to form a complete network. Images were taken after 6 h. Scale bar: 100 µm. **(B)** The cell densities inducing tube formation (blue curves) showed a higher mean squared displacement than the cell densities without tube formation (red curves). The normalized attraction and the velocity cross-correlation showed that cells can sense each other to align and cluster over a typical distance of at least 106 µm (vertical dotted line in the attraction graph). The typical interaction distance was extracted from the exponential fit with a constant offset that is indicated in black. The typical time scale for tube formation (80 min) was obtained by fitting the velocity autocorrelation with an exponential function (indicated in black). The grey shaded area indicates the typical cell size.

4.1.3 Soluble or matrix bound chemotactic gradients do not initiate the finding phase

To investigate which parameter enables cells to initially find each other and form early patterns, first the potential role of chemotactic gradients was examined. The tube formation assay was performed with three different media. As control (Ctrl) the basic ECGM was used but without the supplements, only with 1% penicillin/streptomycin. To investigate the influence of VEGF, 20 nM VEGF was added to the basic ECGM with 1% penicillin/streptomycin. Furthermore, the cells were cultivated in PBS^+. After 3 h and 6 h, no significant difference in the number of tubes and nodes was detectable (Fig. 4-3A). Even when the cells were totally deprived of nutrients or growth factors, which was the case during cultivation in PBS^+, initial tube formation took place. In further experiments the possible existence of matrix-bound gradients was investigated. Kerstin Kick [74] performed an immunostaining of VEGF (green) after cell adhesion (20 min) and after 3 h. For both time points, no matrix-bound gradient of VEGF was observed (Fig. 4-3B). After cell adhesion, the intensity profile showed a peak of VEGF only over the cell area, while an equal distribution was observed over the remaining area. After 3 h the profile looked similar, with peaks being solely above the cells. A long-range VEGF gradient could not be determined at any time point. Kerstin Kick also performed microfluidic experiments, in which the tube formation setting was constantly superfused (Fig. 4-3C left panel experimental setup) [74]. In this setting all soluble gradients were neglected and the tube formation occurred nevertheless (Fig. 4-3C right panel). Therefore, matrix bound chemotactic gradients and soluble gradients are not a critical parameter driving cell finding.

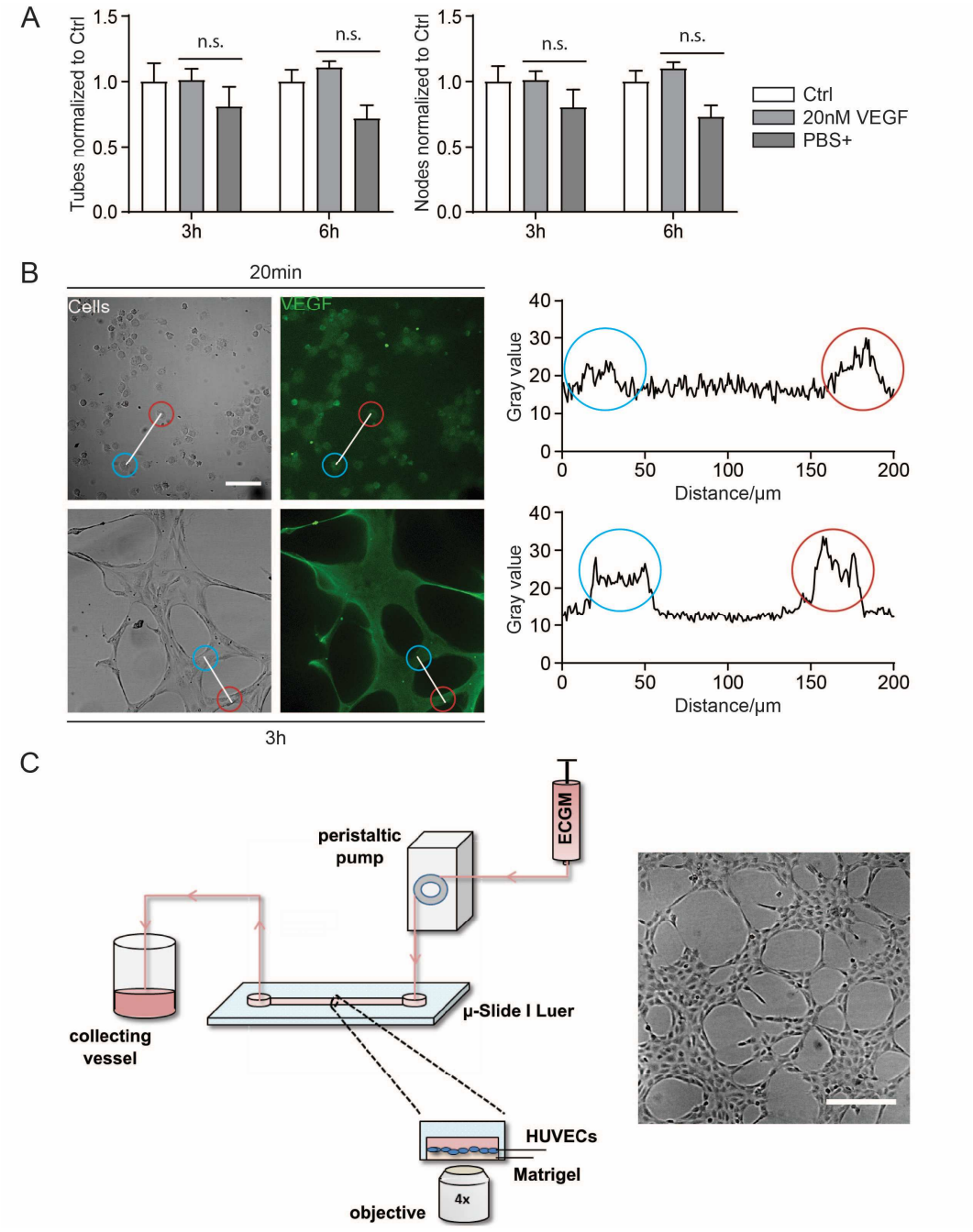

Figure 4-3: Tube formation is independent of chemotactic gradients.

(A) Quantification of the number of tubes and nodes after 3 h and 6 h. Neither a saturation of potential gradients by external addition of 20 nM VEGF nor complete deprivation of nutrients and growth factors (PBS+ instead of growth medium) significantly changed tube formation (one-way ANOVA with Dunnett's test, compared to control, n.s. ≙ not significant). **(B)** To detect potential bound gradients of VEGF, immunostaining for VEGF was performed (left panel). VEGF levels were highest around the cells, and no continuous long-range gradient between cells could be detected. Right panel: Fluorescence intensity profiles along the indicated white lines in the left panel. Scale bar: 100 µm. The red and blue circles around cells in the images correspond to the respective peaks in the intensity diagram. [74] **(C)** The tube formation setting was continuously superfused in a microfluidic device (left panel). The absence of soluble gradients did not impair HUVEC tube formation (right panel). Image was captured after 6 h. Scale bar: 100 µm. [74]

4.2 Influence of material-related parameters on cell communication

4.2.1 Stiffness influences tube formation but is not a key player

Due to the exclusion of a chemotactic form of cell communication, the hypothesis that mechanical signaling drives the tube formation is to be investigated. For a mechanical cell communication, the matrix stiffness should be an important factor. To change the matrix stiffness without affecting the structure of the Matrigel, a synthetic gel (PDMS) was combined with Matrigel. In order to avoid misinterpretations, the maximum Matrigel layer thickness had to be determined, so that the cells still sense the PDMS. A very stiff PDMS (70 kPa) was used, where no tube formation was expected and different thickness of Matrigel layers were added. In the first approach, PDMS was filled in the µ-Slide angiogenesis and after the hydrophilization different volumes of Matrigel (10 µl, 5 µl, 2.5 µl, 1 µl) were added. With this approach, the minimal possible thickness was 25 µm (Fig. 4-4A). In the tube formation assay the cells formed a tubular network in all cases and did not sense the stiffness of the underlying PDMS (Fig. 4-4B). As a control a hydrophilized PDMS surface without Matrigel was tested. Here, the cells had problems with the adhesion and formed only cell clusters with a few weak connections. To create even thinner Matrigel layers, another approach was used – the hydrogel printing. In this approach, the Matrigel was pressed on the hydrophilized PDMS with a stamp. The layer thickness was equally distributed and below 20 µm (Fig. 4-4A). The cells sensed the PDMS and were not able to form a network. HUVECs only spread on the surface and created a cell monolayer (Fig. 4-4B). In Figure 7-1B the quantification of tube formation for different layer thicknesses is shown. The number of tubes and nodes for thicknesses from 25 µm to 150 µm were similar compared to a thickness of 350 µm. However, the tube formation with a layer thickness <20 µm and on hydrophilized PDMS showed a significant decrease of the number of tubes and nodes compared to a thickness of 350 µm.

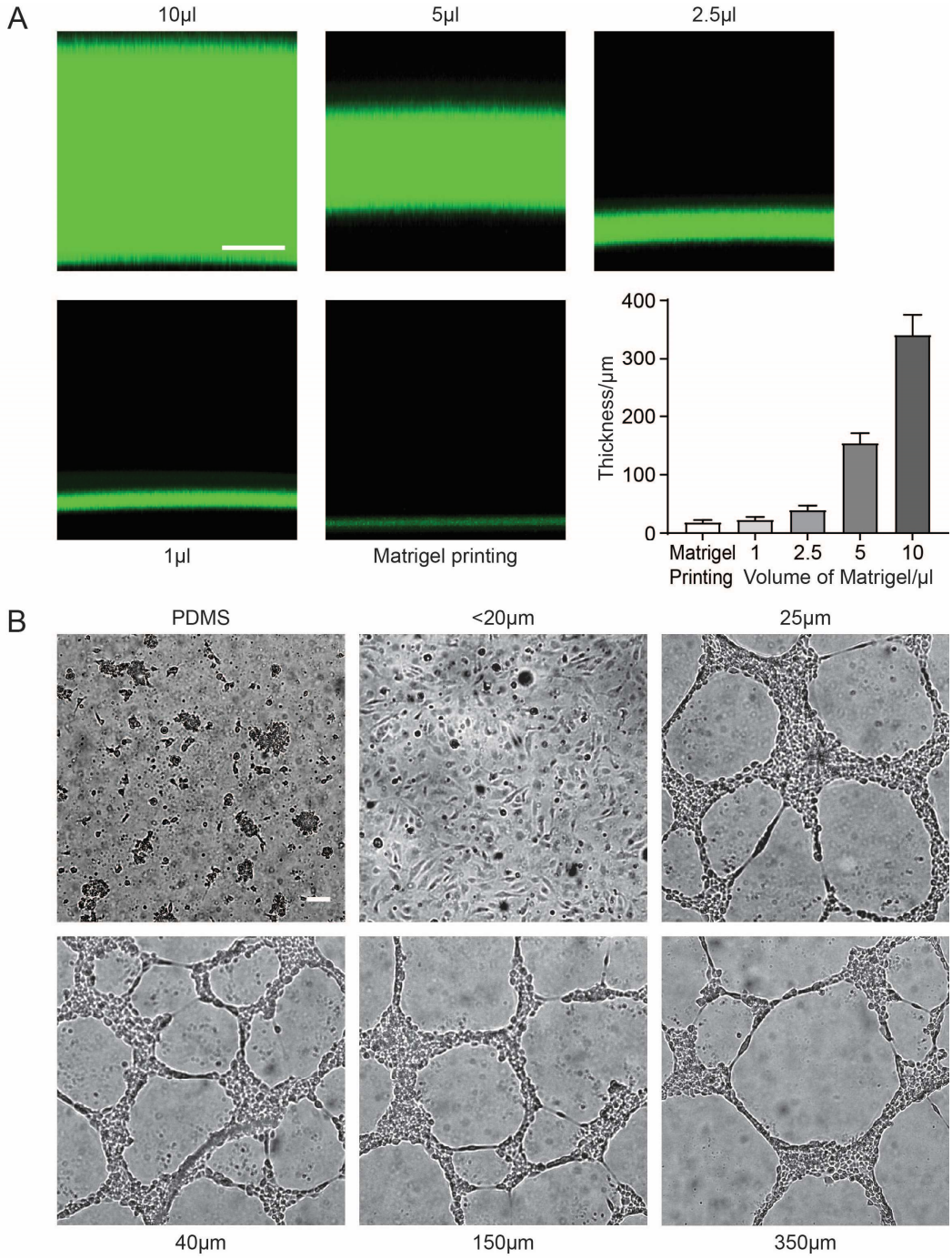

Figure 4-4: Role of Matrigel layer thickness for cell sensing of an underlying gel.

(A) Matrigel was labeled with a fluorescent dye to measure the gel thickness by confocal microscopy. Different volumes of Matrigel (from 1 to 10 µl) were added to a PDMS gel, and the thickness was measured. To achieve a thickness of less than 20 µm, Matrigel was applied by hydrogel printing. Scale bar: 100 µm. **(B)** HUVECs were seeded on a stiff PDMS gel (70 kPa) coated with layers of Matrigel with different thicknesses. On uncoated PDMS gels cells adhered only poorly and formed cell clusters. At a gel thickness below 20 µm, the cells sensed the stiffness of the underlying PDMS and formed no tubes. In all other cases, the cells did not sense the PDMS and formed a tubular network similar to that on a thick Matrigel layer. Images were captured after 20 h. Scale bar: 100 µm.

The stiffness of PDMS can be adjusted by varying the amount of curing agent (Tab. 3-12). Different stiffness values were tested and compared with a pure Matrigel (lowest stiffness) and a glass surface (highest stiffness). On gels with stiffness values between 0.5 and 1.5 kPa, the cells formed a tubular network comparable to the pure Matrigel. From a stiffness of 4 kPa and higher, as well as on glass, the cells could not form tubes (Fig 4-5A). Kerstin Kick performed similar experiments with another synthetic hydrogel. She used polyacrylamide (PAA), which showed similar results as the PDMS gel [74] (Fig. 4-5A). This was also reflected in the quantification of tubes and nodes, which showed a significant difference between Matrigel and 4 or 5 kPa or glass (Fig. 4-5B). There was no significant difference between Matrigel and 0.5, 1 and 1.5 kPa. Only the number of nodes on PDMS 0.5 kPa showed a significant increase. Therefore, it was concluded that matrix stiffness has an influence on tube formation. Nevertheless, the experiment was repeated with collagen I instead of Matrigel to verify the importance of stiffness. In all cases HUVECs only formed a monolayer and no tubes, which resulted in a significant difference to Matrigel in the number of tubes and nodes (Fig. 4-5C). It becomes clear that the stiffness has an impact, but does not seem to be the key factor.

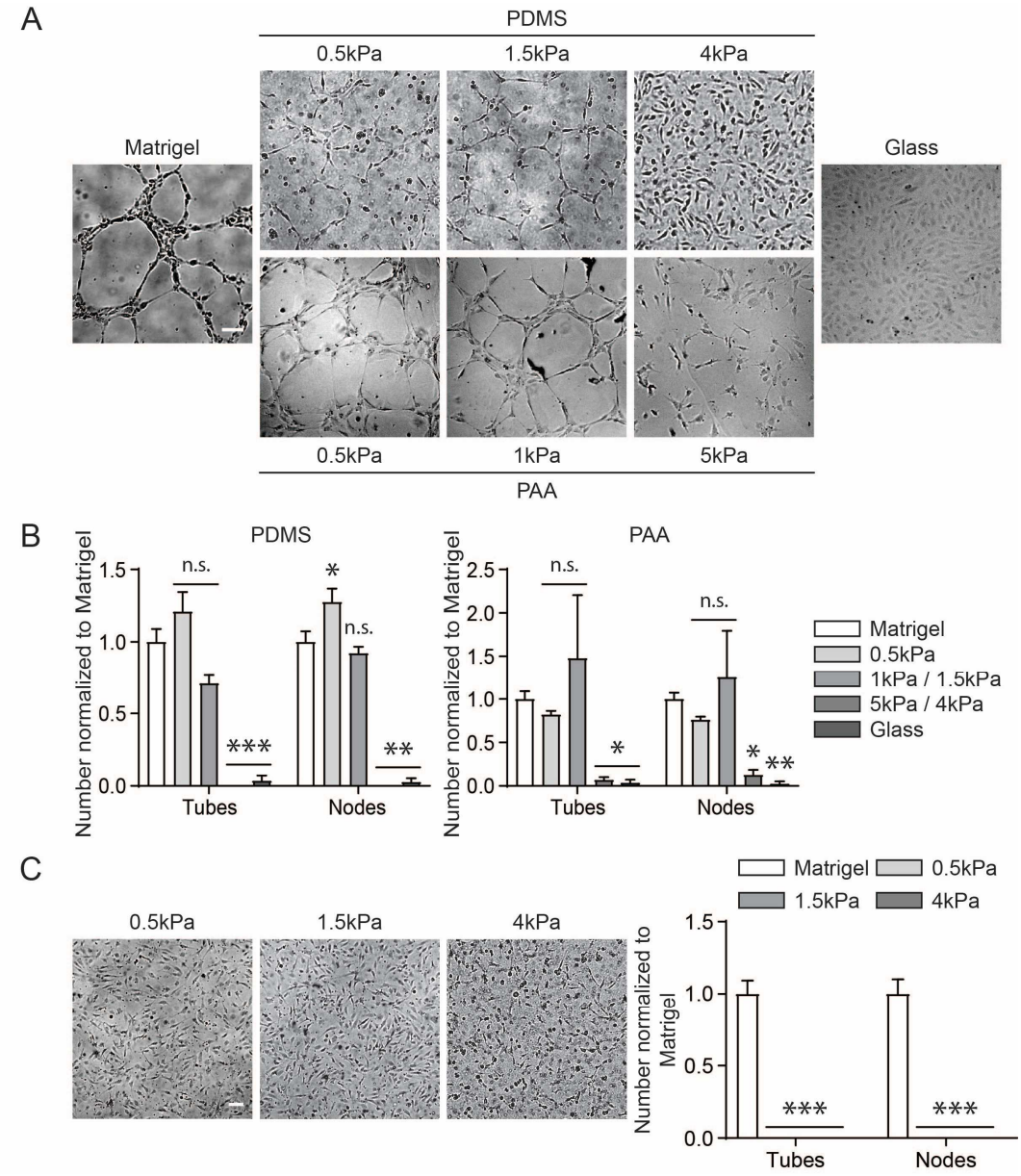

Figure 4-5: Substrate stiffness influences tube formation.

(A) HUVECs were seeded on PDMS or PAA gels with different stiffnesses from 0.5 kPa to 5 kPa that were coated with Matrigel, on Matrigel alone or on glass coated with Matrigel. At high stiffness values (4 kPa and glass), the cells formed no network. On substrates with a stiffness between 0.5 and 1.5 kPa, HUVECs formed a tubular network similar to the Matrigel control. Images were captured after 6 h. Scale bar: 100 µm. **(B)** Quantification of the number of tubes and nodes significantly decreased on 4 kPa, 5 kPa and glass compared to Matrigel. Matrigel 0.5, 1 and 1.5kPa did not differ significantly. Only the number of nodes on PDMS 0.5kPa is significantly increased (one-way ANOVA with Dunnett's test, compared to Matrigel, n.s. ≙ not significant, *P < 0.033, **P < 0.002, ***P < 0.001). **(C)** HUVECs were seeded on a collagen I gel printed on top of PDMS gels with different stiffnesses. In all cases the cells did not form tubes but formed a monolayer which displayed a significant decrease in the number of tubes and nodes compared to Matrigel (one-way ANOVA with Dunnett's test, compared to Matrigel, ***P < 0.001). Images were taken after 6 h. Scale bar: 100 µm.

4.2.2 Mechanical homogeneity is necessary for cell finding

Since stiffness is not the key factor, it was decided to investigate the impact of matrix structure. Various tissue specific ECM hydrogels (bone, intestine and lung) from Xylyx Bio were tested. The stiffness can be compared to the Matrigel, only the ECM bone is around half of the Matrigel stiffness but showed no significant difference (Fig. 4-6). On all ECMs, cells only formed a monolayer, as they do on collagen I (Fig. 4-6). As a result of the cell behavior, the tube formation was significantly reduced in terms of number of tubes and nodes, compared to Matrigel (Fig. 4-6). The commonality between the ECM hydrogels and the collagen I was the fibrous structure. The ECM hydrogels differed in fiber length (intestine long fibers) and density (bone very dense, lung less dense), but all had a basic fiber structure (Fig. 4-6).

Regarding the results showing that stiffness plays a role, the mechanical homogeneity of the substrates was analyzed without cells with the AFM. Collagen I showed a strong mechanical inhomogeneity in the stiffness landscape, with stiff regions at the fiber location alternating with soft regions in between. However, the Matrigel had a mechanically homogeneous surface (Fig. 4-7A). Cells seeded on collagen I orientated towards the collagen fibers during the migration (Fig. 4-7B, white arrows show fibers for orientation). Furthermore, the number of filopodia per cell on collagen was significantly increased, compared to Matrigel. The cell migration on Matrigel and collagen I showed a significant difference. On collagen single cells migrated over a longer distance as compared to Matrigel. On Matrigel HUVECs usually remained on the same place or only migrated a short distance (Fig. 4-7C).

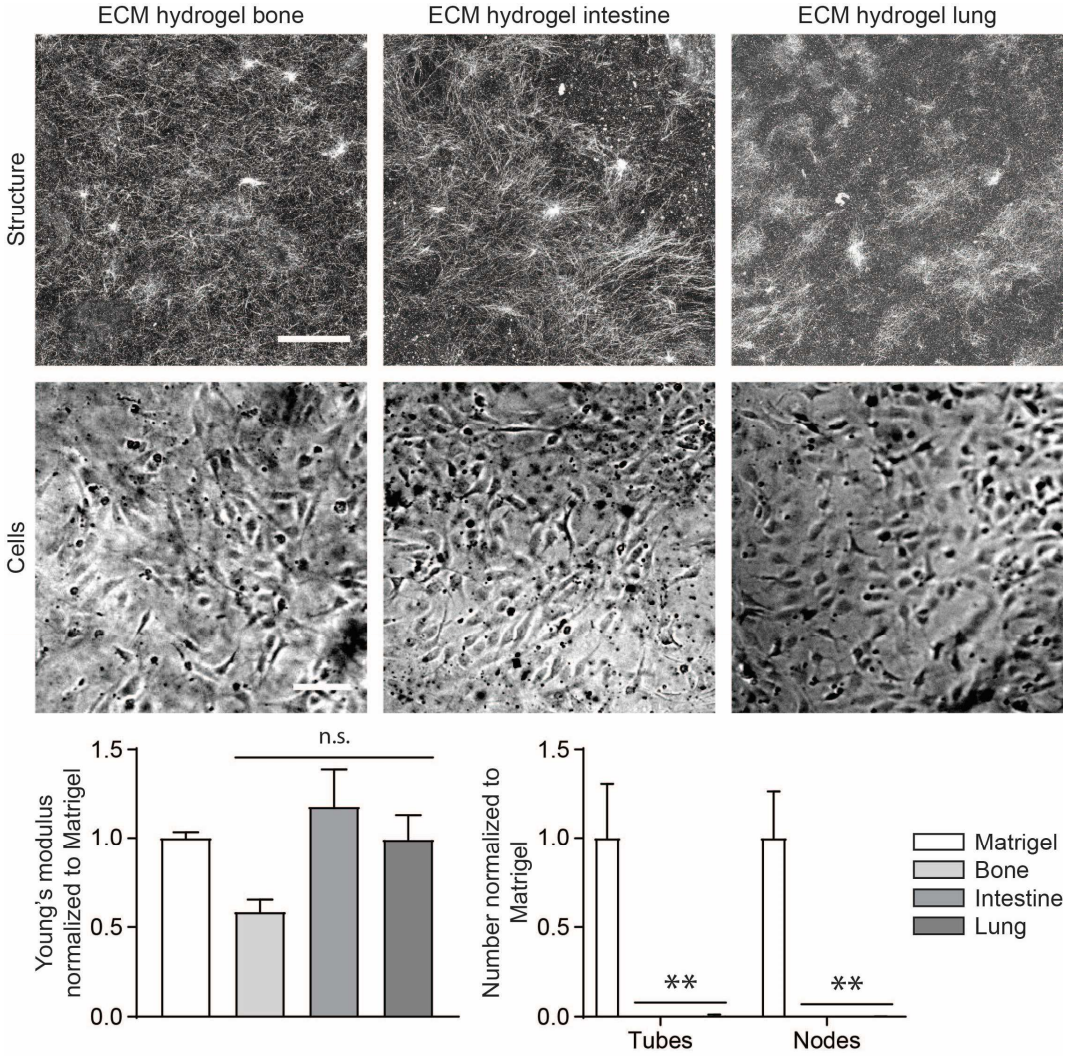

Figure 4-6: Tube formation on ECM specific hydrogels.

First row: total reflection microscopy image of different ECM hydrogels from different organs. All hydrogels showed a fiber structure. Scale bar: 100 µm. Second row: Cell behavior on different ECM hydrogels. Cells always formed a monolayer, and no tube formation was observed. Images were captured after 6 h. Scale bar: 100 µm. The ECM specific hydrogels showed no significant change in stiffness compare to Matrigel (one-way ANOVA with Dunnett's test, compared to Matrigel, n.s. ≙ not significant). However, by the tube formation on the ECM specific hydrogels the number of tubes and nodes was significantly reduced, compared to Matrigel (one-way ANOVA with Dunnett's test, compared to Matrigel, **P < 0.002)

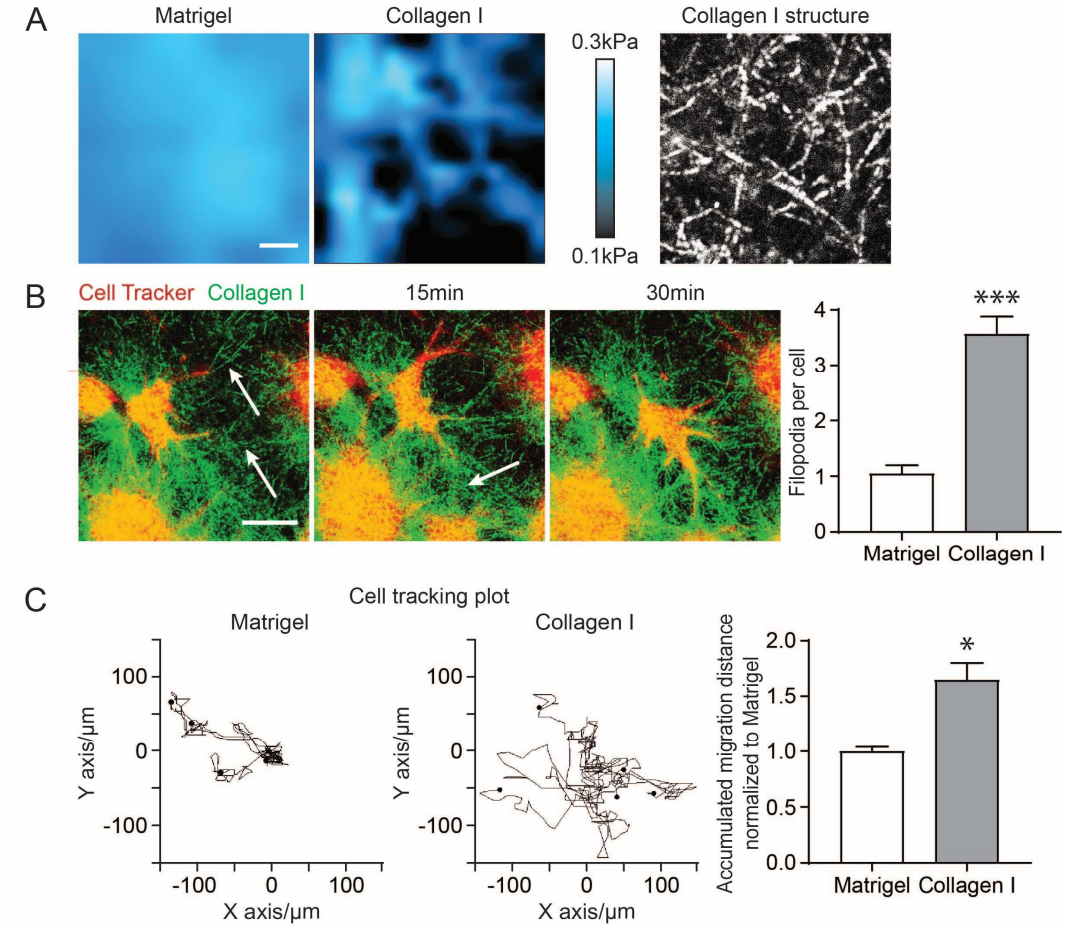

Figure 4-7: Mechanical homogeneity and migration cell behavior on Matrigel and collagen I. **(A)** Pseudocolored AFM stiffness map of Matrigel and collagen I gel: while the stiffness was evenly distributed in Matrigel, the collagen gel contained stiff fibers and soft interspaces. Right panel: Total reflection microscopy image of the collagen I gel showed the collagen fiber network. Scale bar: 5 µm. **(B)** Cells migrated along collagen fibers. White arrows mark collagen fibers to which the cell was aligned (scale bar: 25 µm). The filopodia per cell were analyzed on Matrigel (n = 59 cells) and collagen I (n = 56 cells). On collagen the number per cell was significantly increased (two-tailed unpaired Student's t test with Welch's correction, ***P < 0.001). **(C)** Exemplary cell trajectories on Matrigel and collagen I over 20 h. Single cells on collagen migrated over a longer distance in all directions than cells on Matrigel. The accumulated distance for 45 cells for each gel was normalized to the Matrigel results and showed a significant increase on collagen I (two-tailed unpaired Student's t test with Welch's correction, *P < 0.033).

4.2.3 Laminin plays a key role for cell communication

The main structural component in Matrigel is laminin. With netrin-4 it is possible to manipulate the structure of Matrigel. Netrin-4 binds to laminin-γ1 and is able to destroy the laminin network [75]. Netrin-4:laminin ratios of 1:2, 1:1 and 1.5:1 were tested (Fig 4-8A). With a laminin excess, no change in the laminin structure was observed. Both, in pure Matrigel and a gel with a netrin-4 to laminin ratio of 1:2, laminin showed a very homogeneous structure, and cells formed a tubular network. The quantification

of the number of tubes and nodes showed only a slight decrease (Fig. 7-2A). For a netrin-4 to laminin ratio of 1:1, the homogenous structure of laminin was slightly interrupted, and the cells formed clusters instead of a network. This resulted in a significant decrease of the number of tubes and nodes, compared to Matrigel (Fig. 7-2A). With a netrin-4 excess, the structure of the laminin network completely changed and became rough. HUVECs sedimented through the gel and spread on the plastic bottom of the well. Therefore the cell behavior was not analyzed with the “Angiogenesis Analyzer”. The crosslinking of laminin and the homogeneity of the substrate seem to be necessary for tube formation.

As a different approach to test the relevance of laminin for tube formation, Kerstin Kick used integrin-blocking antibodies (Fig. 4-8B) [74]. Inhibition of integrins, which mainly bind to laminin (α_1, α_2, α_3 and α_6), hindered the cells to form a tubular network and displayed a significant reduction of the number of tubes and nodes, compared to the control (Fig. 7-2B). In contrast, inhibition of integrins for the binding with fibronectin, collagen or other ECM proteins (α_4, α_5 and α_v) did not affect the tube formation and showed only small differences in tubes and nodes, compared to the control (Fig. 7-2B). A laminin gel printed on PDMS with different stiffnesses showed that the tube formation occurred in the same stiffness range as for Matrigel (Fig. 4-8C). Number of tubes and nodes showed no difference between Matrigel and 0.5 and 1.5 kPa. Only the number of nodes at 0.5 kPa showed a significant increase. On 4 kPa there was a significant decrease in the number of tubes and nodes compared to Matrigel (Fig. 7-2C). The results underscore that laminin seems to be the important matrix component for the formation of tubes on Matrigel.

A commercially available pure laminin gel was much softer than Matrigel, but supported the initial tube formation. At later time points, however, the tubular networks collapsed (Fig. 4-9A&B). The collagen I gel has the same stiffness value, but did not promote the tube formation (Fig. 4-9A&B). A mixture gel with a 6:1 ratio of laminin to collagen I (4.8 mg/ml:0.8 mg/ml) (L:C 6:1) supported tube formation over a long period of time (Fig. 4-9B), although this gel was as soft as the gel with laminin alone (Fig. 4-9A). The number of tubes and nodes after 6 h were significantly increased for the L:C 6:1 ratio, compared to the Matrigel control (Fig. 4-9C). Collagen I and laminin showed a significant reduction in tubes and nodes after 6 h. Thus, the presence of laminin seems to be of crucial importance.

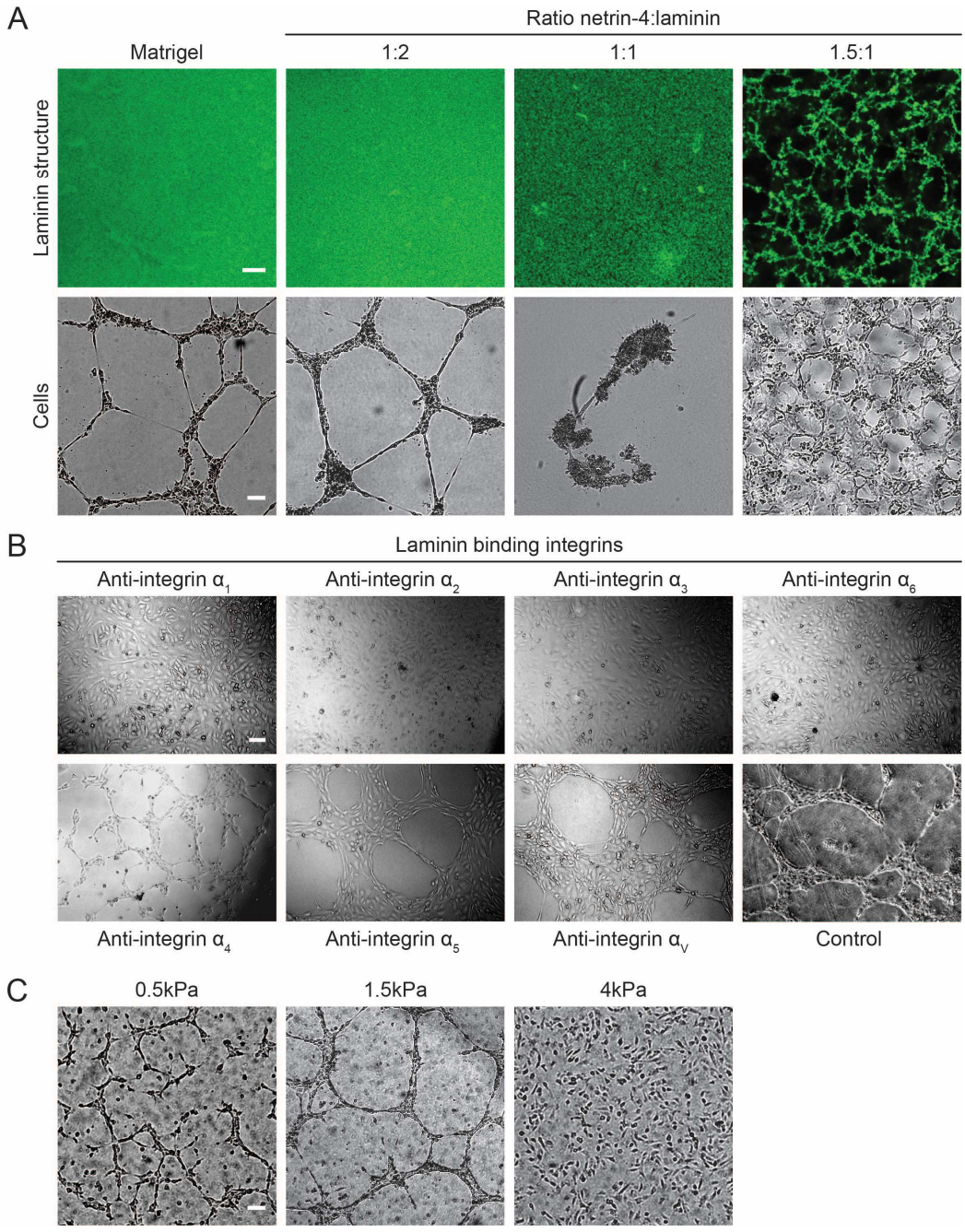

Figure 4-8: Influence of laminin on the tube formation.

(A) Upper row: immunostaining of laminin in Matrigel after treatment with netrin-4 at different ratios (Scale bar: 10 µm). Lower row: Tube formation on Matrigel with different ratios of netrin-4 to laminin. At the ratio of 1:1, netrin-4 changed the structure of the laminin network and influenced tube formation. At the ratio of 1.5:1 the laminin structure was completely destroyed and cells sedimented through the gel and spread on the plastic bottom of the well. Images were taken after 6 h. (Scale bar: 100 µm) **(B)** Antibodies that functionally block integrins α_1, α_2, α_3, α_4, α_5, α_6 and α_v were added (40 µg/ml). Inhibition of integrins associated with laminin binding (α_1, α_2, α_3 and α_6) hindered the cell to form a tubular network. In contrast, inhibition of integrins for the binding with fibronectin, collagen or other ECM proteins (α_4, α_5 and α_v) did not affect the tube formation. Images were captured after 6 h. Scale bar: 100 µm. [74] **(C)** Laminin printing on PDMS showed the same cell behavior as with Matrigel. A tubular network was formed on 0.5 and 1.5 kPa and a cell monolayer on 4 kPa. Scale bar: 100 µm.

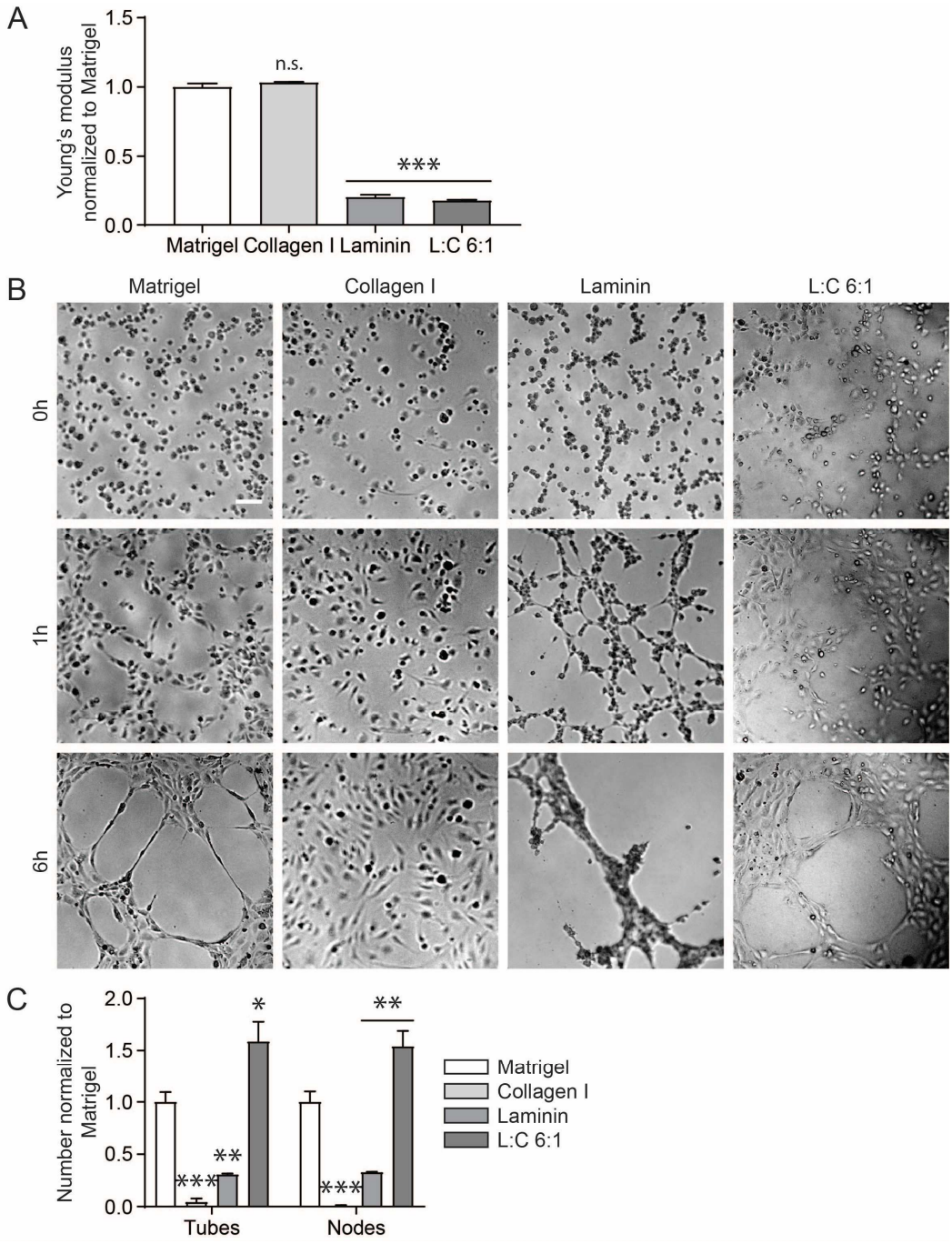

Figure 4-9: Tube formation on different hydrogels.

(A) Young's modulus of Matrigel, collagen I gel (2 mg/ml), laminin gel and a mixture of laminin and collagen I at the ratio 6:1 (L:C 6:1) (4.8 mg/ml:0.8 mg/ml). The stiffness of Matrigel was significantly higher than that of the L:C 6:1 mixture or pure laminin, while it did not differ with that of collagen (one-way ANOVA with Dunnett's test, compared to Matrigel, n.s. ≙ not significant, ***P < 0.001). **(B)** HUVECs were seeded on Matrigel, collagen I, laminin or L:C at a ratio of 6:1. Cells showed typical tube formation on Matrigel and the L:C 6:1 gel, while on collagen, endothelial cells formed only a monolayer. After a short time (1 h), the cells on the laminin gel also formed a small network which then collapsed. Scale bar: 100 µm. **(C)** Quantitative analysis of the number of tubes and nodes normalized to the Matrigel after 6 h. Numbers showed significant increase to L:C 6:1 and significant decrease to collagen I and laminin (one-way ANOVA with Dunnett's test, compared to Matrigel, n.s. ≙ not significant, *P < 0.033, **P < 0.002, ***P < 0.001).

4.3 Influence of cell biological parameters on cell communication

4.3.1 Proteolytic activity is not essential for cell communication

In addition to material parameters, it is also important to investigate, which cellular processes in relation to the matrix play a role in mechanical cell communication. It has already been shown that growth factors play a subordinate role. However, growth factors can be released from the matrix through the proteolytic activity of the cells. In order to investigate this cell process, Kerstin Kick treated the cells with 10 µM batimastat, which inhibits a variety of matrix metalloproteases (MMPs) [74]. However, there was no negative influence on tube formation (Fig. 4-10). This indicates that proteolytic processes in mechanical communication during tube formation assay can be neglected.

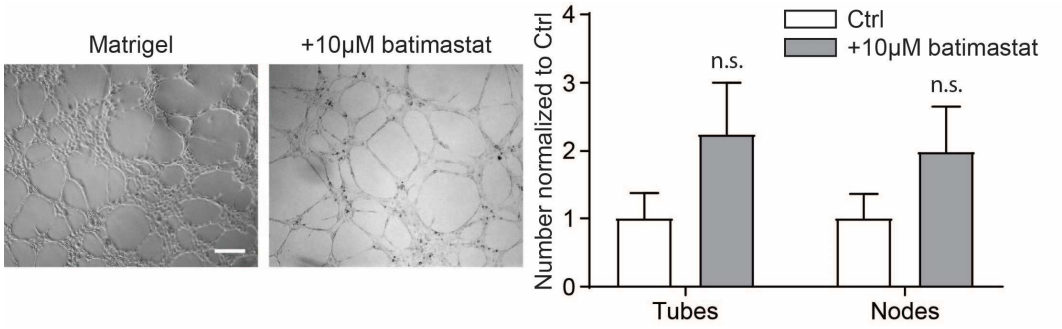

Figure 4-10: Inhibition of proteolytic activity has no negative influence on tube formation.
HUVECs were seeded on Matrigel and treated with 10 µM batimastat to inhibit a broad range of matrix metalloproteases (MMPs). Images were taken after 6 h. Quantitative analysis of the number of tubes and nodes normalized to the control (Ctrl) showed that the inhibition of MMPs has no negative effect on HUVEC tube formation. A two-tailed unpaired Student's t test with Welch's correction showed no significant differences (n.s. ≙ not significant). Scale bar: 100 µm [74]

4.3.2 Protein secretion plays no role in the finding phase

In addition to the proteolytic activity, the secretion of ECM proteins was also investigated with focus on the secretion of fibronectin. Matrigel without cells showed no signal for fibronectin. During the initial finding phase in the tube formation, the fibronectin secretion of the cells was very low. The staining showed only a very weak signal after 3 or 6 h (Fig. 4-11). The cells only released significant fibronectin amounts over a longer period of time. Since the focus is on the "finding phase", protein secretion for cell interaction can be neglected in the first hours.

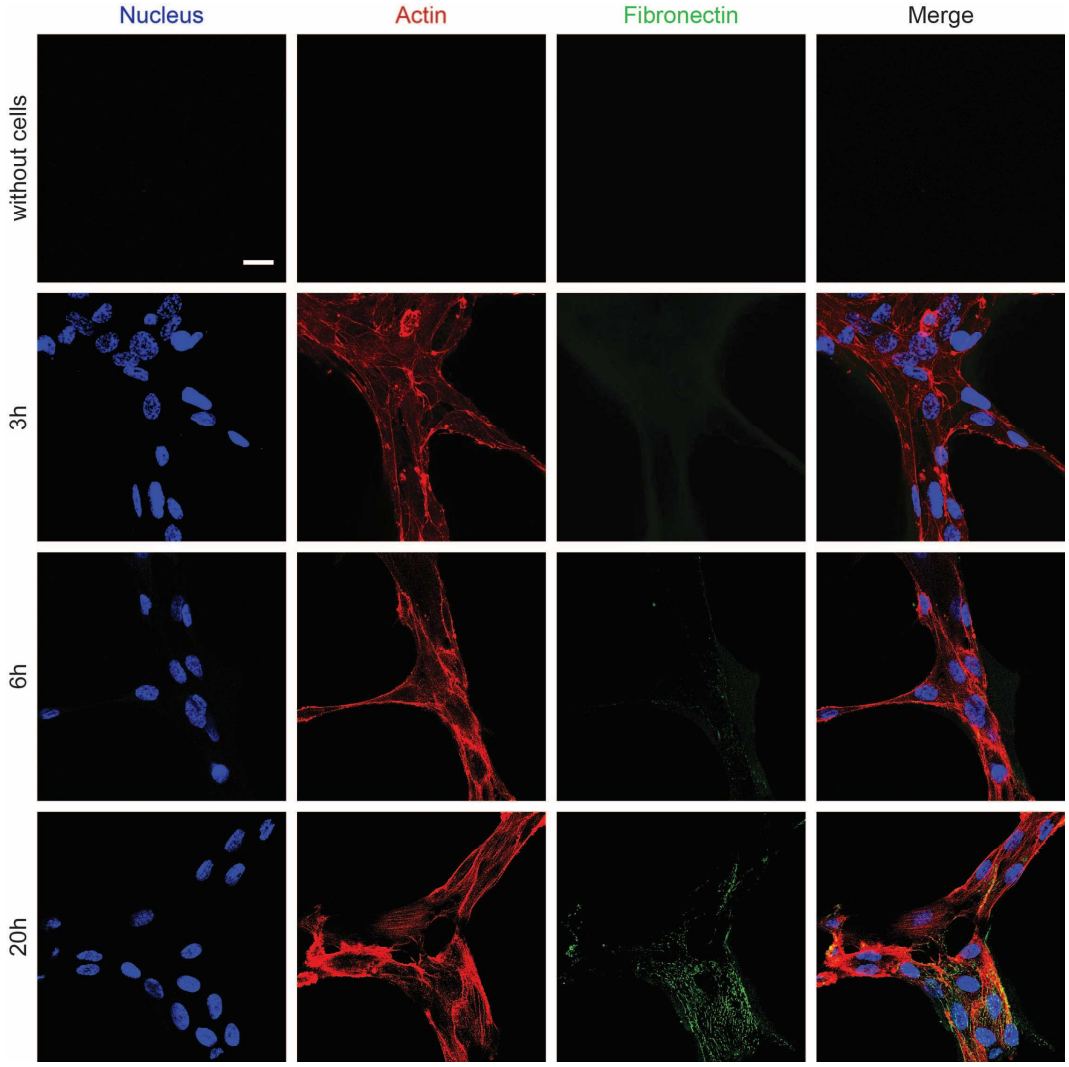

Figure 4-11: Secretion of fibronectin over time.

Immunostaining of fibronectin in Matrigel without (first row) and with cells at different time points. No signal for fibronectin was registered in pure Matrigel. After 3 and 6 h the signal for secreted fibronectin was very weak. The cells only secreted a significant amount of fibronectin after 20 h. Scale bar: 20 µm.

4.3.3 Cell interaction depends on cell contractility and matrix deformation

It can be assumed that the exertion of cell forces on the matrix might be important for a mechanical way of cell communication. To test this, cells were treated with the myosin II ATPase inhibitor blebbistatin (20 µM). This caused a loss in contractility and forces could not be applied on the matrix. The cells survived the treatment, but the initial network formation was dramatically changed (Fig. 4-12A). A more refined network was formed, which led to an increase in the number of tubes and nodes. Next, traction force microscopy experiments were performed to investigate matrix deformation during tube formation (Fig. 4-12B). For that, fluorescent beads were mixed in the Matrigel and the movement of the beads by cellular forces was analyzed (performed by Andriy Goychuk). The analysis of bead displacement for the first 3 h after the cells were seeded showed significant matrix deformation. Matrigel was maximally compressed at distances up to 30 µm from the cell, but the displacement of the beads could be detected at distances of approximately 100 µm (Fig. 4-12B radial displacement and radial strain). This corresponds to the normalized attraction between cells, detected by cell tracking (Fig. 4-2B). With blebbistatin treatment, the deformation was weaker (Fig. 4-12B radial displacement and radial strain) and slower (Fig. 4-12B deformation energy). However, the length scale of substrate compression remained roughly the same. Figure 7-3 shows that the beads were displaced between the cells before the cells had been connected.

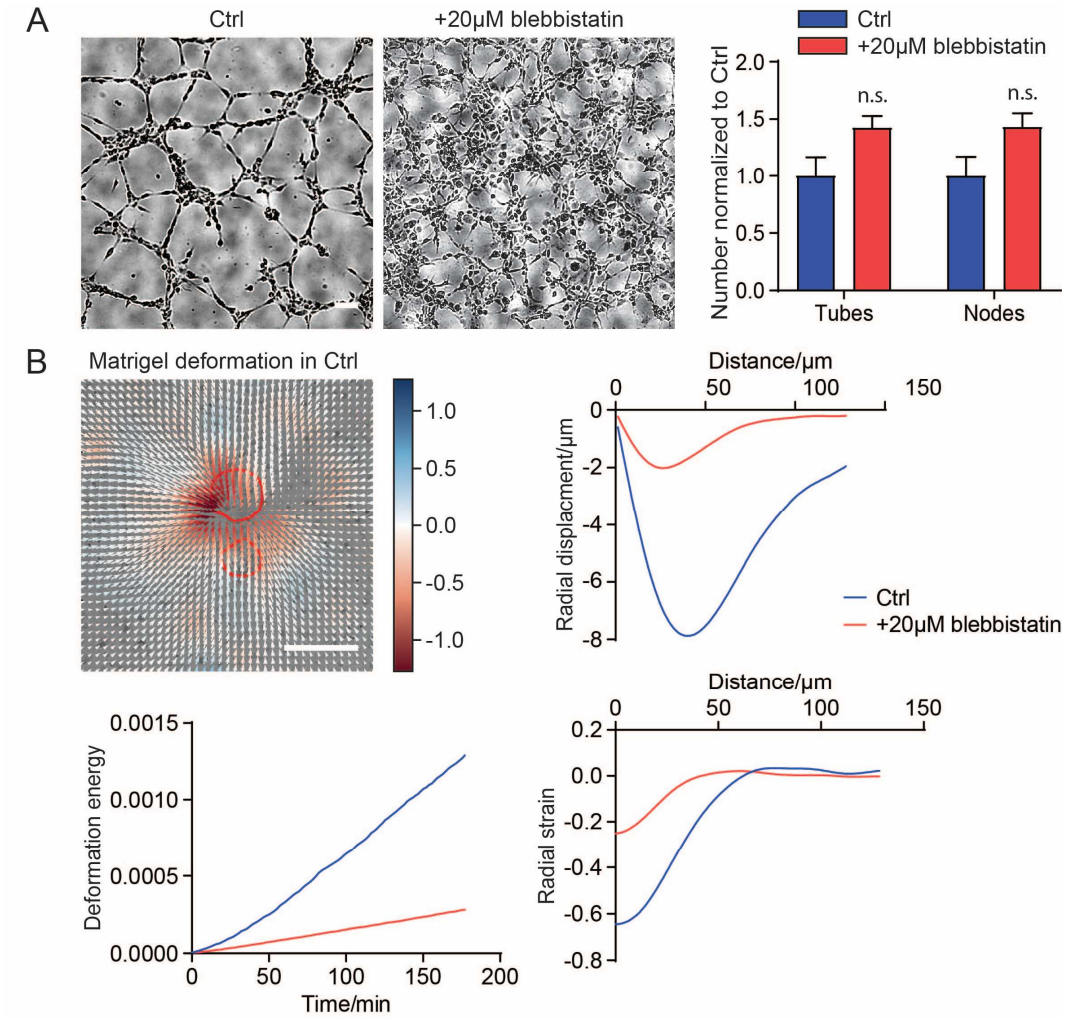

Figure 4-12: Tube formation depends on active matrix deformation.

(A) Inhibition of cell contractility with 20 µM blebbistatin changed the formation of tubular structures to a more refined network. The number of tubes and nodes was increased, compared to the control (Ctrl) (two-tailed unpaired Student's t test with Welch's correction, n.s. ≙ not significant). Images were taken after 6 h. Scale bar: 100 µm **(B)** Upper left: Representative image of bead displacement by cells (red circles) on Matrigel as a dimensionless heatmap. Scale bar: 50 µm. Upper right: An analysis of the bead displacement for the first 3 h after cells were seeded on Matrigel showed that the maxium of the displacement was at a distance of approximately 40 µm. The range of deformation was approximately 100 µm from the cell. Treatment with 20 µM blebbistatin reduced radial displacement, bulk deformation energy (lower left) and radial strain (lower right).

4.3.4 Matrix deformation leads to an irreversible ECM remodeling

The next question was how cellular forces affect the Matrigel structure (Fig. 4-13). Matrigel without cells had a very homogeneous structure of laminin and collagen IV. The untreated cells remodeled the matrix in a short time (30 min-1 h) and created bridges between the cells. The cellular forces created fibers between the cells. The fibers appeared to have clearly emerged from the existing material, because there

were no cells in the area before. However, the structure remained very homogeneous, when the cells were treated with 20µM blebbistatin. The cells could not apply enough forces to rearrange the ECM. The remodeling was a stable and irreversible process (Fig. 4-14A). After 3 h, the cells were treated with 10% DMSO for 1 h to detach the cells. After washing, the Matrigel was incubated at 37 °C with PBS overnight and fixed 20 h after cell detachment. The fiber alignment in the Matrigel by the cells was long term stable. A laminin coating on a PDMS gel with a stiffness for tube formation (1.5kPa) did not induce a tubular network (Fig. 4-14B). The number of tubes and nodes was significantly reduced, compared to Matrigel.

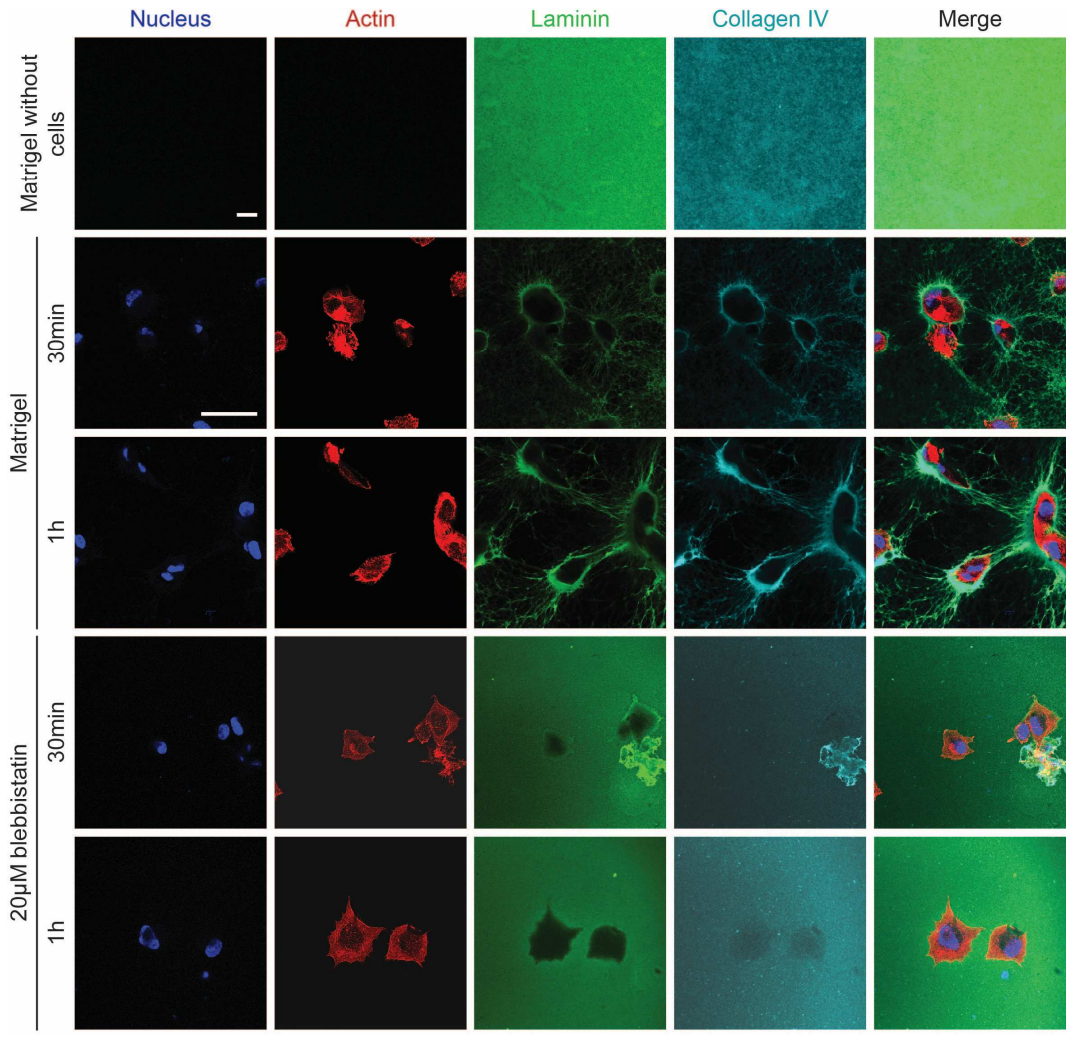

Figure 4-13: Endothelial cells actively remodel ECM during early tube formation.

Immunostaining of laminin and collagen IV in Matrigel without (first row, scale bar: 10 µm) and with cells (scale bar: 50 µm). Cells time-dependently rearranged the matrix proteins in a very early phase of the tube formation so that fibers between cells were formed. The cells used existing material, because there were no cells in the area before. This process depends on cell contractility and is inhibited by 20 µM blebbistatin.

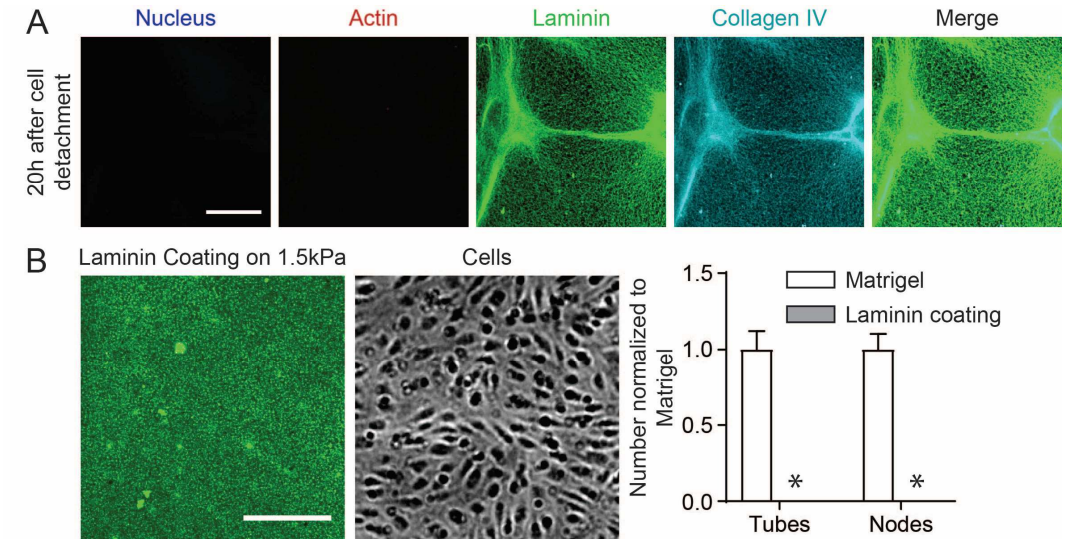

Figure 4-14: Tube formation depends on plastic deformation.

(A) The whole remodeling process was irreversible. After 3 h the cells were detached and the Matrigel was stored in PBS at 37 °C overnight. The Matrigel was fixed and stained 20 h after the cell seeding. The remodeling process by the cells was still visible. Scale bar: 50 µm. **(B)** Tube formation with a laminin coating on 1.5 kPa PDMS led to a cell monolayer and significantly reduced number of tubes and nodes compared to Matrigel (two-tailed unpaired Student's t test with Welch's correction, *P < 0.033). Scale bar: 50 µm.

The matrix remodeling was further shown to be dependents on matrix stiffness: while cells remodeled the matrix at low stiffness values (0.5 and 1.5 kPa), a stiffer gel (4 kPa) remained largely unstructured (Fig. 4-15A). This enables the connection between ECM remodeling and the influence of stiffness on the tube formation. Results show that tube formation only occurs after deformation and restructuring of the matrix. Additionally, tube formation depended on cell contractility and matrix stiffness. No significant structural changes through the cells could be detected on a collagen I gel either, although the stiffness was comparable to Matrigel (Fig. 4-15B). This makes clear that the homogeneous initial structure seems to be a crucial importance.

Laminin showed a very homogenous structure. L:C 6:1 was more like a fiber network, but the mesh size looked slightly smaller than the collagen fiber network. On both gels the remodeling process was observable for a short time scale (1h) (Fig. 4-16). Small fibers were formed between the cells on laminin, while the fibers were stretched long on L:C 6:1 and fiber bundles aligned between the cells. The fiber structure in L:C 6:1 was preserved over a longer period of time and was similar to the remodeling on Matrigel, while the fibers in the laminin gel did not remain stable. The material did not seem to be able to withstand the cell forces and accumulates on the cells. Only residues of the fibers were still visible. This also explains why the cell network on

laminin collapsed over a long period of time. It becomes clear that tube formation is accompanied by a significant structural change, compared to the starting point.

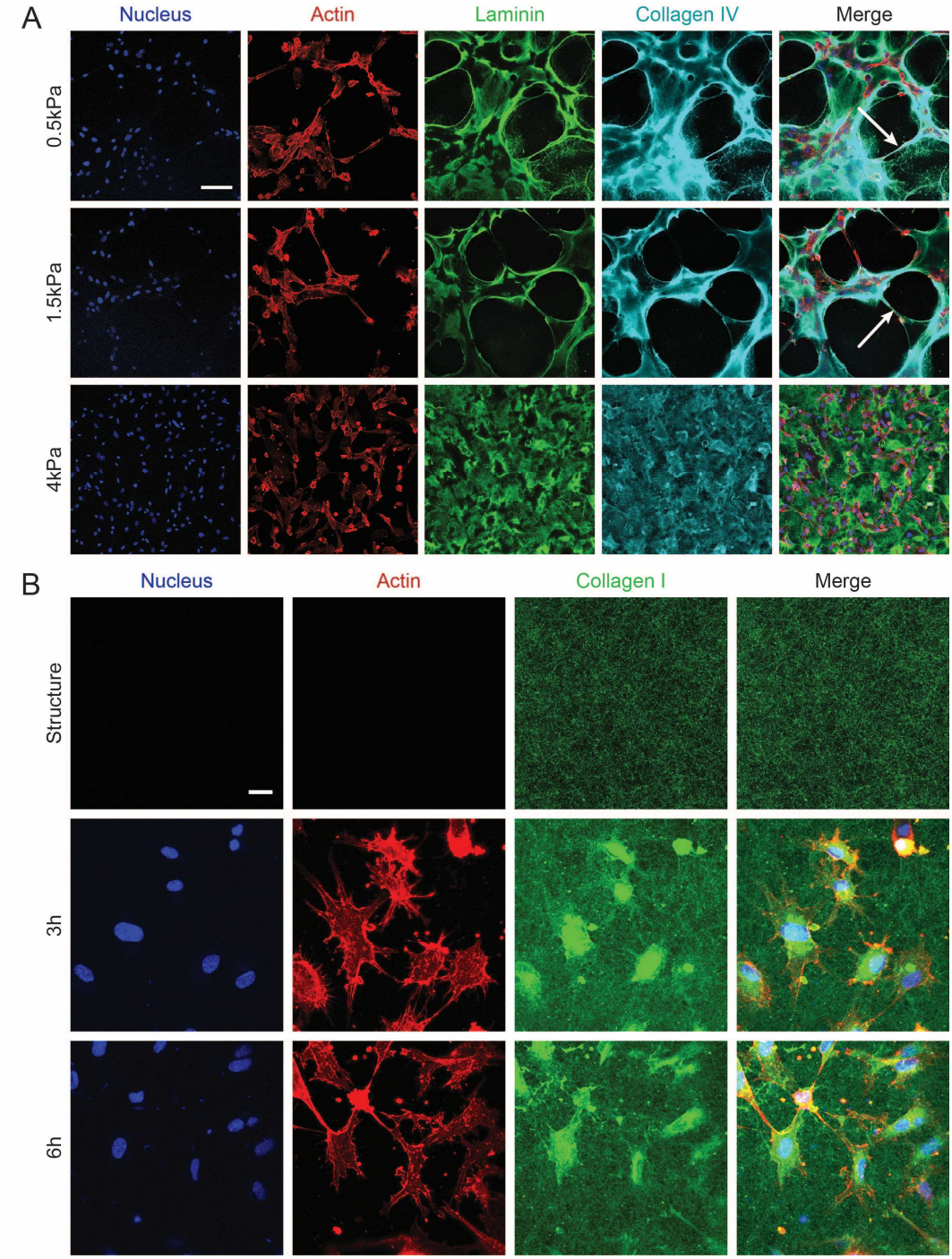

Figure 4-15: Tube formation is prevented by a stiff matrix and an initial fibrous structure.

(A) Immunostaining of HUVECs seeded on Matrigel printed on top of PDMS gels with different stiffnesses. If the stiffness was too high (4 kPa), cells did not form a tubular network but simply spreaded on the surface. At 0.5 and 1.5 kPa cells interacted, and tubes were formed. White arrows indicate the alignment of cells and fibrillary matrix. Scale bar: 100 µm. **(B)** HUVECs seeded on collagen I showed no significant change in fibrous structure after 3 and 6 h. Scale bar: 20 µm

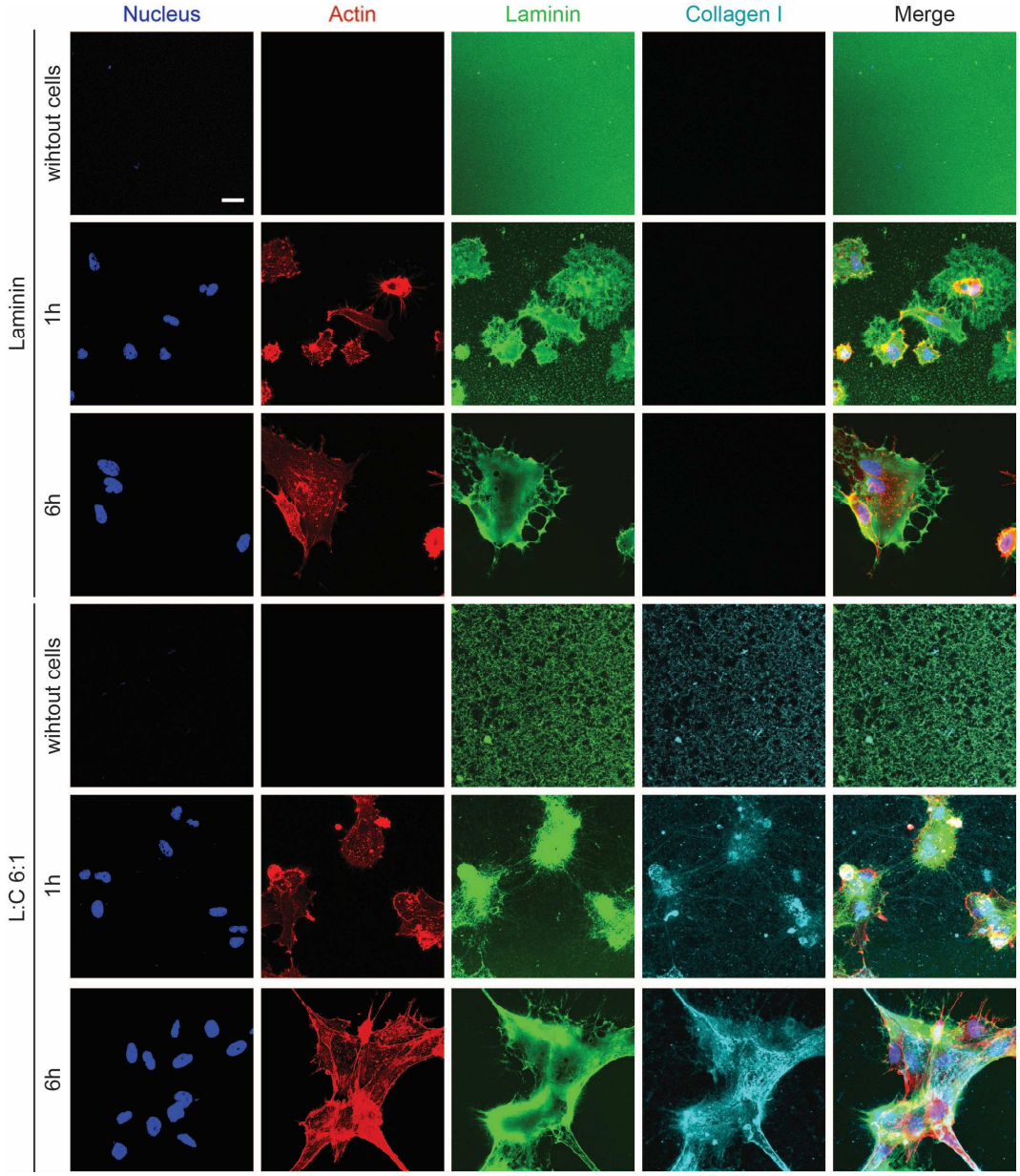

Figure 4-16: Cell finding in the early phase of tube formation is accompanied by fiber formation. Immunostaining of laminin gel and L:C 6:1. Laminin had a homogeneous initial structure and L:C 6:1 showed a small fiber network. After a short time (1 h) the cells remodeled the structure on laminin gels and fibers were formed between the cells. In the L:C 6:1 gel, the fibers became longer and bundles of fibers were aligned between the cells. While on L:C 6:1 the remodeling remained visible (6 h), the laminin gel collapsed.

4.3.5 Strain stiffening guides the cell-cell sensing process

To determine the influence of remodeling on the local matrix stiffness the AFM was used. The stiffness of the areas between two cells was measured. The distance of the cells were below the typical distance of 106 µm, where the cells can sense each other to align (Fig. 4-2B). As a control, an area not affected by cells was also measured. For all cell pairs (n=21), the stiffness of the space between cells increased significantly before cells protruded into this area (Fig. 4-17). After a short period (1-2 h), the cells were connected and formed a small tube. The cells seemed to use the self-created stiff regions by the ECM remodeling as a guidance cue. Figure 7-4 in the appendix shows further examples of the strain stiffening effect and its use for connecting cells.

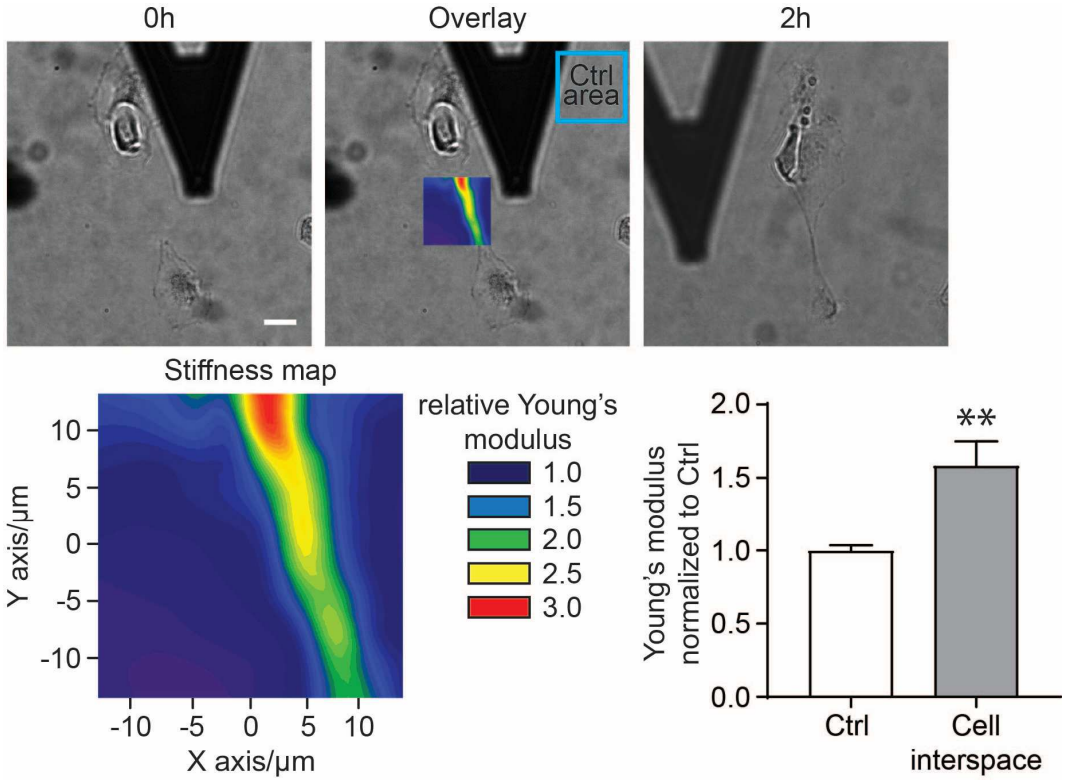

Figure 4-17: Strain stiffening guides the cell connection in the tube formation.

The stiffness of the area between two single cells after adhesion on Matrigel was measured with an AFM and compared to the stiffness of a cell-free part of the gel. The pseudocolored stiffness map shows the relative Young's modulus normalized to the Young's modulus of the control area. An overlay of the microscope image and the stiffness map shows that the cells formed a stiff bridge between them before cell protrusions covered this area. Over all cell pairs (n=21), we detected a significant increase in the Young's modulus of the cell interspace (two-tailed unpaired Student's t test with Welch's correction, *P < 0.033). The cells later used the stiffness bridge for connection. Scale bar: 20 µm.

5 Discussion

5.1 Mechanical communication of endothelial cells

Chemical signals, VEGF in particular, undoubtedly play a decisive role in the communication and organization of endothelial cells in angiogenesis [4, 12]. VEGF determines the direction of migration and coordinates the communication of cells via the Notch/Dll4 signaling pathway [3, 9]. In addition, the communication and organization between cells of different organs and endothelial cells is controlled by the interaction of chemical signals [6, 21]. The tube formation assay has been used for many years as an *in vitro* model to study the behavior of endothelial cells [30, 76]. Thereby, the effect of both pro-angiogenic and anti-angiogenic factors can be investigated and quantified [30, 63, 77, 78]. Using this model assay in the present work, it was possible to exclude chemotactic gradients, whether in soluble or matrix-bound form, as driving forces for the initial structure formation of the cells. VEGF of course can play a role at a later time point [1]. In this study it was also shown that besides chemical communication there is another alternative communication mechanism for endothelial cells – the mechanical communication, which is explained in detail in context with mechanical parameters and cellular processes.

For the mechanical communication, stiffness plays a role [79, 80] and the results show that tube formation is only possible in a certain stiffness range. However, it is not the key factor for angiogenesis, because no tubular network was formed with other hydrogels in the right stiffness range. Furthermore, the structure of the hydrogels plays a role. Whereas the generation of a tubular network was not possible on collagen or other fibrous hydrogels (ECM organ hydrogels), tubes were formed on Matrigel as well as on the L:C 6:1 mixture gel. Only differing in the network structure, hydrogels with a homogenous structure, like Matrigel, or with a less distinctive structure, like the mixture gel, allow and promote tube formation, while the fibrous structure of collagen and the ECM hydrogels prevent tube formation. The tube formation on hydrogels with incomplete homogenous network structures (L:C 6:1), but not on distinct fibrous hydrogels shows the influence of hydrogel structure, but rules this out as a key factor.

The results show that cells have to remodel the matrix, which is always accompanied by an interaction with cells. This is implemented on Matrigel and the L:C 6:1 mixture gel, as well as in the early phase on laminin, whereby a homogeneous structure Matrigel is transformed into fibers. In case of the L:C 6:1 mixture gel fibers from the

existing fine-meshed network are reoriented between the cells. The treatment with blebbistatin shows the importance of cell contraction for the remodeling. In line with this result, Malandrino et al. [39] and other researchers [81, 82] show that remodeling is dependent on the actin machinery and can be inhibited by actin binding compounds (e.g. with Latrunculin B [82]).

The experiments with PDMS and PAA show that the remodeling also depends on the stiffness of the matrix. If the matrix is too stiff, the cell forces are not sufficient for remodeling, whereby different cell types adapt their applied forces to the stiffness [52]. This adjustment is likely to be limited. The results show that the process is independent of proteolytic processes and the secretion of proteins. It is possible that the secretion of fibronectin plays a role in the "maturation phase" for the stabilization of the nodes, as there is a clear deposition after 20 h. Furthermore, fibronectin promotes cell-cell interaction in blood vessels [29] and stabilizes tissue borders [32]. This supports the assumption that fibronectin will stabilize the nodes at a later stage.

The results show that matrix remodeling is accompanied by matrix stiffening. The AFM measurements show a stiffness gradient between the cells, which develops in minutes to hours. This is also confirmed by other studies [39]. The results of this work demonstrate that remodeling and stiffening occur in the same time interval. The increase in matrix stiffness is called strain stiffening [52, 82]. Strain Stiffening is dependent on cell contraction [83] and by increasing the stiffness, the cell contraction is further increased [84], until a maximum stiffness of the gel is achieved [52]. For strain stiffening, nonlinear viscoelastic properties are required in the matrix [85, 86], as shown by computer models [48]. Only natural hydrogels, protein gels and biopolymers exhibit these properties [33, 83, 87], while synthetic gels exhibit linear behavior [52, 88]. This also shows that the nonlinearity is highly relevant for the cell-matrix interaction [83]. The theoretical mechanism is based on two models: the entropic and the enthalpic model [88, 89]. The enthalpic model describes stiffening through the transition from fiber bending to stretching by cell forces [88], while the entropic model assumes that the network deformation occurs in the entire sample, due to the strain of uniformly semi flexible polymers [88]. Only one configuration is perfectly straight and stretches a flexible filament, reducing conformational entropy [89]. The entropic model predicts uniform deformation and the enthalpic model predicts heterogeneous deformation [88]. It is likely that both entropic and enthalpic models contribute to the stiffening [88, 89]. The elongated fibers may also separate from their connecting points and rebind at

another location [36, 86]. With increasing stress, the filaments reorganize themselves more and more and align themselves along the shear direction [88]. This leads to reorientation, restructuring and bundling of the fibers, which is clearly shown in a structural remodeling [36, 85-87]. The process is associated with the applied forces alone and cannot be explained by proteolytic processes or water displacement [36].

Munster et al. show that stretching leads to plastic deformation of the fibers. They retain their length after the force has stopped [86]. In this study it can also be seen that the remodeling of Matrigel is plastic. After removal of the cells, the changed structure is retained for 20 hours. A synthetic gel does not allow plastic deformation [90]. Therefore, in the experiment with the laminin coating on PDMS no plastic deformation is possible. Since the cells do not form tubes, a plastic deformation by the cells is necessary for the mechanical communication.

Strain stiffening depends on the structure of the network and the molecular interaction between monomers or fibers [86]. Increased crosslinking in the network reduces the strain stiffening effect [36, 86, 87]. The synthetic gels have covalent bonds between the monomers, which cannot be broken by cell forces. This prevents stretching and inhibits strain stiffening [86]. Strain stiffening is also important at the physiological level as it limits the amount of deformation of structures in response to a force [33], and ensures tissue integrity [89]. This underlines the importance for the cell level (local) as well as for the tissue level (global) [52, 88].

The AFM experiments conducted in the course of this study show that the cells use the generated stiffness to interact and connect with each other. Each cell attracts the matrix to itself and stiff tracks are generated for migration. The migration along a stiffness gradient is described as durotaxis [91, 92]. Thus, pattern formation can be described as the connection between local strain stiffening and durotaxis [52, 88]. However, it is known that cells follow many different gradients (chemical, mechanical, electrical) [93]. Park et al. also describe the possibility that cells follow a topographic gradient. In contrast to durotaxis and haptotaxis, migration is possible in both directions [93]. In the case of mechanical communication of endothelial cells, topotaxis would explain a migration along the fiber density as a result of remodeling [93, 94]. Topotaxis in combination with other tactic phenomena can provide important information for the understanding and design of tissue structure and function [93]. It is described that cells do not exert durotaxis on laminin [91]. Since laminin is the main component of Matrigel,

another tactic mechanism may play a role. In sum, the cause of the migration cannot be determined exactly and requires further investigation. Since structural compression also leads to stiffening, it is difficult to distinguish between durotaxis and topotaxis.

In the literature, fiber realignment and strain stiffening are also described for fibrous natural hydrogels such as collagen [82, 95, 96], fibrin [39] and fibronectin [24, 97]. The fibrous structure seems unsuitable for endothelial tube formation, but the question concerning the difference in strain stiffening or remodeling between collagen and Matrigel arises. The difference is the degree of the remodeling. In the literature on collagen, fibrin and fibronectin, the fibers are only realigned [24, 39, 82, 95-97]. However, the basic fiber or network structure remains intact. In contrast, the results in this study show that remodeling on Matrigel is much more intensive. The structure is radically transformed from very homogeneous to clear fibers. Also, the modification in L:C 6:1 mixture gel is much more dramatic compared to collagen. A possible hypothesis for the signal for the tube formation is that the signal for the network formation of endothelial cells is a mechanical gradient. This gradient is easier to generate for individual cells, the more mechanical homogeneous the matrix is. Matrigel is therefore very homogeneous, compared to mechanically inhomogeneous collagen. A dramatic structural change is described in the literature as a stronger anisotropy [64, 93]. Since the connection between the different nodes in the tube formation on Matrigel consists of single or few cells, the single cell behavior is probably of greater significance. Korff et al. show that cell spheroids of endothelial cells also interact over a large distance on collagen [17]. This leads to the assumption that collective cells can increase the strain stiffening and thus collagen is mechanically homogeneous over a larger area for a larger cell group. A similar effect can also be observed on fibrin [48, 52]. This means that individual cells cannot produce a significant stiffness gradient on collagen or the structural remodeling / stiffness gradient must occur on a scale visible to single cells. Thus, for the tube formation of endothelial cells, the substrate must provide mechanical homogeneity as a starting condition. It should also be mentioned that other cell types then endothelial cells were used in the literature for remodeling and strain stiffening [24, 39, 82, 95-97]. This work reveals that endothelial cells can also communicate mechanically via remodeling and strain stiffening.

The various experiments in this work with laminin or the manipulation of laminin clearly show that laminin is a key factor in tube formation. Laminin appears to be an essential component of tube formation, as has been demonstrated in several other studies

[37, 59, 76, 98, 99]. This is in good agreement with the *in vivo* observations that vasculogenesis during development [7, 99] or angiogenesis during tissue regeneration [10] are generally laminin-rich. However, the results show that pure laminin does not generate a long term stable tube formation. The soft laminin gel does not appear to be able to withstand the contraction forces of the cells. The L:C 6:1 mixture gel indicates that a proportion of fibrous collagen I, which forms a structural network [57], increases the resistance of breaking without leading to an increase in bulk stiffness. Kubota et al. also show that laminin together with collagen I supports tube formation [76]. However, not all ratios of laminin to collagen are useable for tube formation. More work needs to be done to investigate in which form collagen is supportive in a laminin gel, for example which mechanical properties are changed instead of stiffness. It has also been shown that destruction of the laminin network by netrin-4 [75] leads to inhibition of tube formation. However, netrin-4 and other members of the netrin family can also affect endothelial cell behavior directly, in both pro-angiogenic [100] and anti-angiogenic [101, 102] forms. However, it should be noted that HUVECs are described as having a negative response to netrin-4 [101].

Estrach et al. show that the two communication paths of mechanical and chemical communication are not necessarily separate, since a direct connection can also exist [11]. Binding of VEGF to VEGFR2 can lead to the expression of laminin [11]. Laminin can also influence the Dll4/Notch signaling pathway and enhance differentiation between tip and stalk cells [11, 29]. Laminin is able to bind to integrin $\alpha_6\beta_1$, resulting in direct increase of Dll4 in tip cells and Notch in stalk cells or it can bind to integrin $\alpha_2\beta_1$, which causes an increases of Dll4 via FoxC2 [11]. The connection between the basement membrane and the Dll4/Notch pathway has also been demonstrated *in vivo* [13]. These results also fit very well with the integrin-blocking experiments in this study. Blocking of α_2 and α_6 inhibits tube formation, indicating that laminin acts as a master regulator for endothelial cell function, as described by Kick et al. [26] in the form of a biologically active protein, while other proteins (e.g. fibronectin) are responsible for stability of the tubular network [30]. Both communication modes are linked, but it is also described that the physical stimulus can dominate the chemical one [46].

Different matrix components trigger specific cell processes [99]. Fibronectin [37, 76], collagen I and III [37] can lead to increased cell proliferation, also for microvascular cells [37]. This could also explain why fibronectin only plays a role at a later stage of the tube formation. In angiogenesis, the beginning is marked by the migration and

elongation of tip cells [30]. In a later stage, proliferation of stalk cells plays a role in lumen formation [3]. The migration experiments on collagen shows a stronger and faster cell migration compared to Matrigel and cell alignment to the collagen fibers without interacting with each other. It is also known that cells secrete no proteins during cell migration in collagen I gels [26]. Collagen does not seem to provide the right conditions for mechanical communication, but triggers completely different cell mechanisms. It is assumed that only laminin triggers the right cell mechanisms for endothelial cells. However, it is likely that for other cell types other signals or ECM proteins trigger remodeling and mechanical communication. Similarly, force and frequency vary between different cell types, which implies cell type dependent communication [22].

Besides the connection of the two communication channels, there is also a crucial advantage of mechanical communication in comparison to chemical communication. Communication via signal molecules is dependent on diffusion and is therefore suitable for short distances uniformly in all spatial directions [22]. Mechanical communication depends on the mechanical properties of the ECM [22], but enables communication over longer distances and in a certain direction [48, 52, 80, 94, 103]. As in this study, other works have shown a communication range of round about 100 µm [96]. This explains the results of the dependence of tube formation on cell density. Communication among different cells is only possible over a short range. Wang et al. describe strain stiffening as a requirement for mechanical communication over long distances [104]. Due to the linear elasticity of synthetic gels such as PDMS or PAA, cell communication over large areas is not possible [33, 85]. Because of the small chain diameters, the deformation is only a few µm from the cell boundary and very small in relation to the cell scale [33, 85]. Finally, no communication path can be considered in isolation. Cell communication always occurs via the coupling of different signal pathways, as well as communication modes [22]. The interaction is very coordinated and sensitive, as VEGF can also have a negative influence on endothelial network formation by increasing migration [8].

Figure 5-1 shows a graphical summary of the mechanical communication of endothelial cells. From a single cell point of view, a mechanically homogeneous matrix must be presented as the starting point. Since laminin is an essential protein for tube formation, Matrigel is simply represented by laminin molecules. It has to be possible for the cells to initiate remodeling by contraction. The cells have to apply sufficient force

and the matrix stiffness has to be between 0.5 and 1.5 kPa. The irreversible remodeling creates a mechanical and a protein density gradient at the single cell level. This is used by the cells for migration [105]. Remodeling also plays a key role [15, 48] by acting as cell guidance [64]. The cell contraction results in a positive feedback [79, 80]. The cells pull on the matrix for orientation. As a result the stiffness of the matrix increases and the cell forces also continue to increase [80]. On collagen, the gradient is already there and on single cell level no significant changes occur. The cells start the migration in search of stiffer areas [82] without perceiving other cells.

Endothelial cells sense each other mechanically and angiogenesis can be described as a mechanobiological process in interaction with chemical signals [39]. Vernon and Sage opened up the possibility that the connection of sprouts can be achieved by matrix remodeling [106]. Remodeling from two sides leads to an amplification and the cells can be found by each other. The mechanism can provide both guidance and stability for vessels [79]. All in all it is a complex communication mechanism with many factors [107], which requires an optimal ECM composition for organization [15].

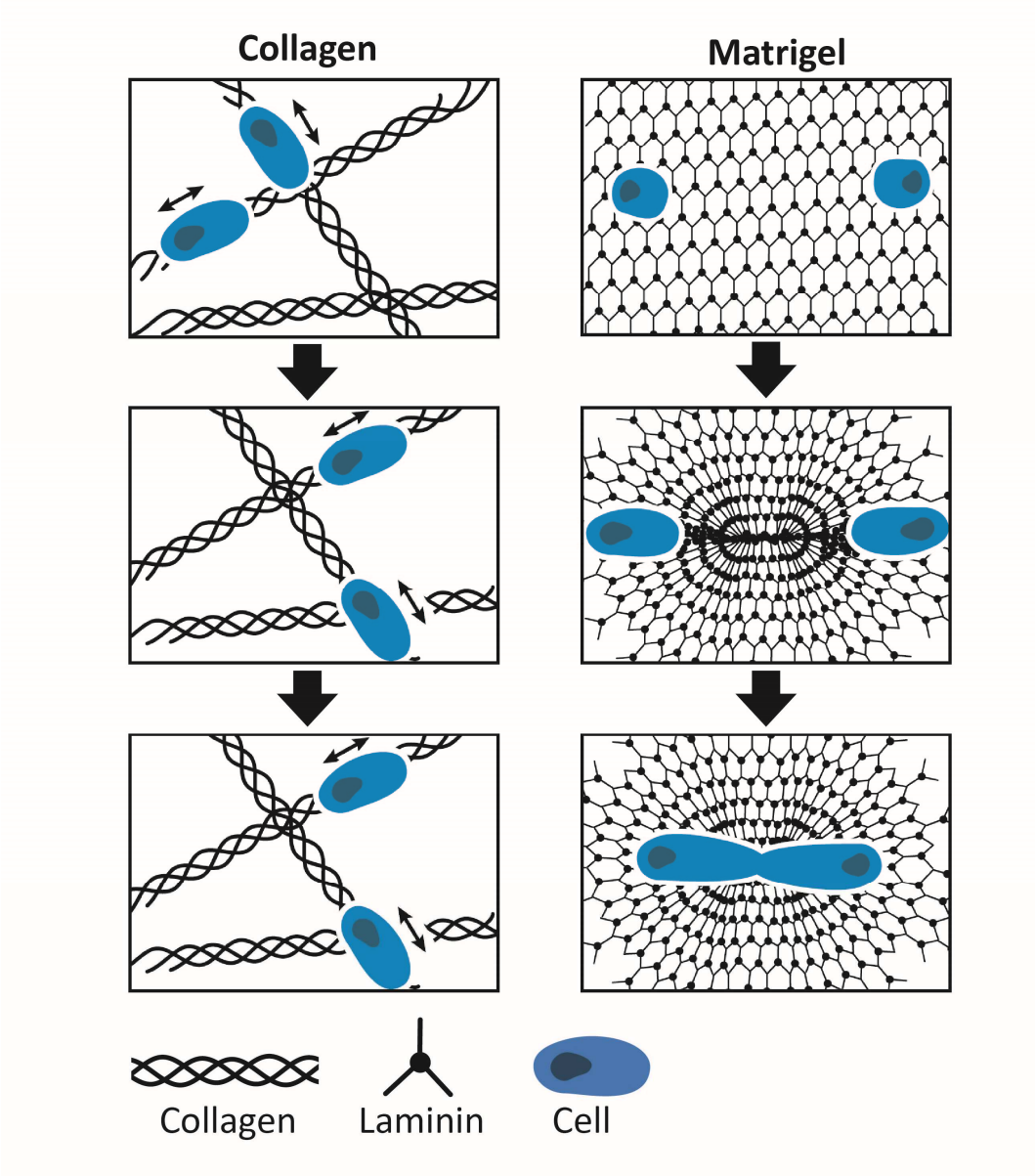

Figure 5-1: Graphical summary of the mechanical endothelial cell communication.

The starting point has to be a mechanical homogeneous matrix with the right stiffness and laminin. Matrix is plastically and irreversibly remodeled by cell contraction. This results in fibers between the cells, which are stiffer than their environment. The cells use the fibers or the stiffness gradient to connect. On collagen, individual cells already have a mechanical gradient and are not able to change it. Therefore, the cells start the migration along the fibers without attention to other cells.

5.2 Critical view on the tube formation assay as an angiogenesis model

Since 1988, the tube formation assay has been used to investigate endothelial cell behavior on the basement membrane [76]. It is suitable for early angiogenesis as it covers many steps such as adhesion, migration, aggregation and elongation [16]. Various substances can be investigated and quantified for their pro- or anti-angiogenic effect [30, 63, 77, 78]. However, this model also has some disadvantages. The most obvious is the cultivation in 2D. Strikingly, the cells feel themselves at distances larger than 100 µm, but they can sense an underlying gel only from 20 µm. This observation was also made in other studies [51, 96]. This indicates that in xy-direction probably a normal cell behavior is observable, while in z-direction there is a discrepancy. Since differences can occur between the cell behavior in 2D and 3D [35, 108], many research areas are moving towards 3D cell cultivation to be closer to the *in vivo* condition [67, 68]. According to Blobel, this holds also true for the investigation of endothelial cells [109], because e.g. endothelial cells show a changed migration behavior in 3D [26, 108]. Different approaches for 3D angiogenesis assays have been developed [110-112]. Network formation in a 3D collagen gel [110] does not necessary contradict the results of this work. Endothelial cells are always surrounded by the basement membrane [3, 9]. Therefore, in a 2D approach, a basement membrane model such as Matrigel [38] may give better results than collagen. However, in the process of angiogenesis, the cells must be able to grow into different ECMs of different tissues. Therefore, it is likely that a kind of network is also created in a 3D collagen gel.

The results indicate an independence of secretion and synthesis for mechanical communication of endothelial cells. However, this is in contrast to *in vivo* angiogenesis. For endothelial cell migration, the basement membrane must be ruptured by proteolytic processes [3, 9, 41]. The secretion of proteins also plays an important role in rebuilding the basement membrane [3, 9]. For example, the synthesis of collagen IV plays a key role in the formation of blood vessels [29] and the secretion of molecular signals (e.g. growth factors) is also important [106]. Proteases [15, 113] and secretion of proteins [26] could only increase in importance in a 3D environment and play a subordinate role in 2D.

It should be mentioned that 2D cultivation is necessary to investigate mechanical communication in connection with stiffening. Only in 2D it is possible to measure matrix

stiffness at a cellular level using AFM [82, 95]. In the clinic, elastography is used to measure tissue stiffness [35, 114]. Like rheological measurements [35] or micro-stretching [115], elastography refers to a macroscopic level. A matrix stiffness can be indirectly calculated by the movement of beads. However, it is very difficult to measure a cell-driven mechanical change. New methods have been developed to image the dynamic remodeling of the ECM (fluorescence resonance energy transfer (FRET), single photon emission computed tomography (SPECT)) or scanning acoustic microscopy (SAM) to measure stiffness at the cellular level [35]. However, AFM remains the most established method for mechanical measurements at the cellular level.

Despite the disadvantages of the model, an additional communication approach for endothelial cells could be shown. It becomes clear that the organization of endothelial cells requires a combination of chemical and mechanical cues. The results are supported by observations of remodeling *in vivo* [7, 10, 13, 99], which is crucial for mechanical communication [15, 48].

5.3 Clinical and pharmacological relevance

In the human body there is a high variability of the ECM, which leads to a highly flexible adapted vascular network. However, the ECM is transformed by diseases such as fibrosis, which also leads to a change in the vessels system [31, 35]. Angiogenesis also belongs to the Hallmarks of cancer [116]. Via VEGF signals, cancer cells cause abnormal growth and function of the blood vessels to supply the tumor with nutrients and thus support the tumor growth. In a later phase, the blood vessels also play a role in metastasis [3, 31, 41, 116]. In 1971, Folkman was the first to address tumor angiogenesis therapeutically [117]. Over the years, various therapeutics have been developed for pro- or anti-angiogenic effects via VEGF [3, 4, 15, 41]. The following targets with drug examples approved by the FDA are available: VEGF-A (e.g. bevacizumab), VEGF-B (e.g. aflibercept), VEGFR2 (e.g. ramucirumab) [118]. However, it is described that addressing VEGF has only a short term effect [41].

Because of the rising importance of the ECM, new therapeutic approaches to influence the ECM, in terms of mechanical properties and the resulting cell behavior or cell adhesion, have been developed [25, 31, 35]. The possibility of mechanical communication of endothelial cells supports the use of this approach against tumor angiogenesis [41]. The matrix stiffening can be manipulated by targeting growth factors (e.g. TGFβ signal effects MMPs), MMPs directly and other proteases or crosslinking enzymes like lysyl oxidase (LOX) [27]. Similarly, the cell response to ECM stiffness can be interrupted by blocking integrins or focal adhesion [27]. The specific generation of ECM fragments by cleavage of the full-length ECM protein can also lead to anti-angiogenic function by blocking integrins [31]. Important for actin dynamics and thus cell contraction is the Rho-GTPase. The statin simvastatin attenuates Rho activity in endothelial cells and thereby reduces cell contraction [27]. Migration as a result of topotaxis is controlled by the interaction of two parallel signaling pathways rho-associated protein kinase (ROCK) and phosphoinositid-3-kinase (PI3K). These two signaling pathways can also be pharmacologically manipulated [93].

For an effective treatment a combination treatment is suitable. This can attack several points of the ECM remodeling [27], the cell-ECM interaction [41] as well as induce cell death of tumor cells with classical chemotherapeutics [25]. In December 2018, the FDA approved atezolizumab, in combination with bevacizumab, paclitaxel, and carboplatin, for the firstline treatment of patients with metastatic, non-squamous non-small cell lung

carcinoma [4]. A disadvantage in the treatment of tumor blood vessels is that the tumor uptake of chemotherapy is reduced [4]. These treatments also induce tumor hypoxia, promoting ECM remodeling by the tumor cells and leading to a revascularization of the tumor [41]. For optimal treatment and avoidance of unwanted side effects, more work is needed with regard to the complex process of angiogenesis and especially in the tumor context.

Tissue engineering, which is considered to have the potential to provide a treatment for many diseases follows a completely different approach [16]. The idea is to remove diseased tissue and replace it with tissue cultivated *ex vivo* using cells from the patient. An important step in tissue engineering is to achieve micro vascularization [16]. Prevascularization allows the engineered tissue to connect better with the host tissue and is supplied with oxygen and nutrients more quickly [16, 57]. No direct connection between blood vessel system from the host tissue and the tissue replacement could lead to an undersupply and necrosis. However, this also depends on the size of the tissue replacement. Mechanoregulation is an important aspect for regenerative medicine [16]. Through the mechanical coordination of endothelial cells, elasticity of the surfaces can influence cell function and be used for scaffold optimization [23]. Thus, a network for endothelial cells can be defined by a specific micro structuring [64]. In this way, the migration of endothelial cells from the host tissue into the replacement tissue can be promoted. Future work will have to be evaluated whether a stiffness gradient is sufficient or whether a natural hydrogel is still required, which the cells can also remodel. However, it also becomes clear that synthetic gels have certain disadvantages as scaffold material due to their lack of nonlinearity [89]. Remodeling due to nonlinearity has a significant contribution to endothelial cell function and should be included. The effective use of tissue engineering and the full replacement of different tissues still requires a lot of work.

5.4 Conclusion and outlook

In conclusion, this thesis provides a mechanical communication mode of endothelial cells, which interacts together with the chemical communication via VEGF. Both contribute to cell coordination in angiogenesis. It has been shown that the cells in the tube formation assay on Matrigel, independent of chemical factors, come together via a mechanical pathway in the first hours. The cell contractions remodel the structure of the matrix on a single cell level plastic and significantly. This results in a density and stiffness gradient, which the cells use for interaction and communication. The conditions for this are a mechanically homogeneous matrices in the stiffness range from 0.5 to 1.5 kPa with nonlinear properties to generate a stiffness gradient and the containing of laminin as a key protein. The advantage of mechanical communication is the long range.

The first approach for further experiments would be to switch to a 3D model together with the use of cell spheroids for collective cell studies. The spheroids can then also consist of a mixture of endothelial cells and mural cells. The complexity can be stepwise increased to improve the angiogenesis model. By using photo-switchable hydrogels (e.g. PhotoCol®), nanostructured environments can be created. With the two photon polymerization a structuring is possible, while the cells are already in the hydrogel. Beside to an endothelial spheroid, a stiffness gradient could be created without influencing the protein density [119] to induce a local formation of vascular sprouts. Based on micro contact printing [120], the Vollmar Lab is working on establishing a sequential patterning. This technique can be used for spatial and temporal control of predefined pathway with different proteins after cell adhesion. The comparison of the migration between the structural and the mechanical pathway could help to distinguish between durotaxis and topotaxis. It would be also helpful to investigate the expression of different tip cell markers, for example with SmartFlare™ reagents [121].

6 References

1. Serini, G., et al., *Modeling the early stages of vascular network assembly.* Embo j, 2003. **22**(8): p. 1771-9.
2. Mutschler, E., H.-G. Schaible, and P. Vaupel, *Anatomie, Phyiologie, Pathophysiologie des Menschen*. Vol. 6. 2007: Wissenschaftliche Verlagsgesellschaft mbH Stuttgart.
3. Potente, M., H. Gerhardt, and P. Carmeliet, *Basic and therapeutic aspects of angiogenesis.* Cell, 2011. **146**(6): p. 873-87.
4. Apte, R.S., D.S. Chen, and N. Ferrara, *VEGF in Signaling and Disease: Beyond Discovery and Development.* Cell, 2019. **176**(6): p. 1248-1264.
5. Vailhe, B., D. Vittet, and J.J. Feige, *In vitro models of vasculogenesis and angiogenesis.* Lab Invest, 2001. **81**(4): p. 439-52.
6. Augustin, H.G. and G.Y. Koh, *Organotypic vasculature: From descriptive heterogeneity to functional pathophysiology.* 2017. **357**(6353).
7. Risau, W. and I. Flamme, *Vasculogenesis.* Annu Rev Cell Dev Biol, 1995. **11**: p. 73-91.
8. Saunders, R.L. and D.A. Hammer, *Assembly of Human Umbilical Vein Endothelial Cells on Compliant Hydrogels.* Cell Mol Bioeng, 2010. **3**(1): p. 60-67.
9. Blanco, R. and H. Gerhardt, *VEGF and Notch in tip and stalk cell selection.* Cold Spring Harb Perspect Med, 2013. **3**(1): p. a006569.
10. Rousselle, P., M. Montmasson, and C. Garnier, *Extracellular matrix contribution to skin wound re-epithelialization.* Matrix Biol, 2019. **75-76**: p. 12-26.
11. Estrach, S., et al., *Laminin-binding integrins induce Dll4 expression and Notch signaling in endothelial cells.* Circ Res, 2011. **109**(2): p. 172-82.
12. Hellstrom, M., L.K. Phng, and H. Gerhardt, *VEGF and Notch signaling: the yin and yang of angiogenic sprouting.* Cell Adh Migr, 2007. **1**(3): p. 133-6.
13. Stenzel, D., et al., *Endothelial basement membrane limits tip cell formation by inducing Dll4/Notch signalling in vivo.* EMBO Rep, 2011. **12**(11): p. 1135-43.
14. Chen, T.T., et al., *Anchorage of VEGF to the extracellular matrix conveys differential signaling responses to endothelial cells.* J Cell Biol, 2010. **188**(4): p. 595-609.
15. Sottile, J., *Regulation of angiogenesis by extracellular matrix.* Biochim Biophys Acta, 2004. **1654**(1): p. 13-22.
16. Sun, J., et al., *Geometric control of capillary architecture via cell-matrix mechanical interactions.* Biomaterials, 2014. **35**(10): p. 3273-80.
17. Korff, T. and H.G. Augustin, *Tensional forces in fibrillar extracellular matrices control directional capillary sprouting.* J Cell Sci, 1999. **112 (Pt 19)**: p. 3249-58.
18. Barkefors, I., et al., *Endothelial cell migration in stable gradients of vascular endothelial growth factor A and fibroblast growth factor 2: effects on chemotaxis and chemokinesis.* J Biol Chem, 2008. **283**(20): p. 13905-12.

19. Astrof, S. and R.O. Hynes, *Fibronectins in vascular morphogenesis.* Angiogenesis, 2009. **12**(2): p. 165-75.

20. Staton, C.A., M.W. Reed, and N.J. Brown, *A critical analysis of current in vitro and in vivo angiogenesis assays.* Int J Exp Pathol, 2009. **90**(3): p. 195-221.

21. Ramasamy, S.K., A.P. Kusumbe, and R.H. Adams, *Regulation of tissue morphogenesis by endothelial cell-derived signals.* Trends Cell Biol, 2015. **25**(3): p. 148-57.

22. Sapir, L. and S. Tzlil, *Talking over the extracellular matrix: How do cells communicate mechanically?* Semin Cell Dev Biol, 2017. **71**: p. 99-105.

23. Jalali, S., et al., *Regulation of Endothelial Cell Adherence and Elastic Modulus by Substrate Stiffness.* Cell Prolif, 2015. **22**(2-6): p. 79-89.

24. DuFort, C.C., M.J. Paszek, and V.M. Weaver, *Balancing forces: architectural control of mechanotransduction.* Nat Rev Mol Cell Biol, 2011. **12**(5): p. 308-19.

25. Pickup, M.W., J.K. Mouw, and V.M. Weaver, *The extracellular matrix modulates the hallmarks of cancer.* EMBO Rep, 2014. **15**(12): p. 1243-53.

26. Kick, K., et al., *New View on Endothelial Cell Migration: Switching Modes of Migration Based on Matrix Composition.* Arterioscler Thromb Vasc Biol, 2016. **36**(12): p. 2346-2357.

27. Lampi, M.C. and C.A. Reinhart-King, *Targeting extracellular matrix stiffness to attenuate disease: From molecular mechanisms to clinical trials.* Sci Transl Med, 2018. **10**(422).

28. Northey, J.J., L. Przybyla, and V.M. Weaver, *Tissue Force Programs Cell Fate and Tumor Aggression.* Cancer Discov, 2017. **7**(11): p. 1224-1237.

29. Marchand, M., et al., *Extracellular matrix scaffolding in angiogenesis and capillary homeostasis.* Semin Cell Dev Biol, 2019. **89**: p. 147-156.

30. Arnaoutova, I., et al., *The endothelial cell tube formation assay on basement membrane turns 20: state of the science and the art.* Angiogenesis, 2009. **12**(3): p. 267-74.

31. Bonnans, C., J. Chou, and Z. Werb, *Remodelling the extracellular matrix in development and disease.* Nat Rev Mol Cell Biol, 2014. **15**(12): p. 786-801.

32. Armstrong, P.B. and M.T. Armstrong, *Intercellular invasion and the organizational stability of tissues: a role for fibronectin.* Biochim Biophys Acta, 2000. **1470**(2): p. O9-20.

33. Miller, R.T., *Mechanical properties of basement membrane in health and disease.* Matrix Biol, 2017. **57-58**: p. 366-373.

34. Pollard, T.D., et al., *Cell Biology 3rd Edition Chapter 29 - Extracellular Matrix Molecules*. 2017, Elsevier.

35. Cox, T.R. and J.T. Erler, *Remodeling and homeostasis of the extracellular matrix: implications for fibrotic diseases and cancer.* Dis Model Mech, 2011. **4**(2): p. 165-78.

36. Nam, S., K.H. Hu, and M.J. Butte, *Strain-enhanced stress relaxation impacts nonlinear elasticity in collagen gels.* 2016. **113**(20): p. 5492-7.

37. Grant, D.S., et al., *Two different laminin domains mediate the differentiation of human endothelial cells into capillary-like structures in vitro.* Cell, 1989. **58**(5): p. 933-43.

38. Kleinman, H.K. and G.R. Martin, *Matrigel: basement membrane matrix with biological activity.* Semin Cancer Biol, 2005. **15**(5): p. 378-86.

39. Malandrino, A., et al., *Non-Elastic Remodeling of the 3D Extracellular Matrix by Cell-Generated Forces.* bioRxiv, 2017: p. 193458.

40. Thorne, J.T., et al., *Dynamic reciprocity between cells and their microenvironment in reproduction.* Biol Reprod, 2015. **92**(1): p. 25.

41. Bordeleau, F., et al., *Matrix stiffening promotes a tumor vasculature phenotype.* Proc Natl Acad Sci U S A, 2017. **114**(3): p. 492-497.

42. Wood, J.A., et al., *The role of substratum compliance of hydrogels on vascular endothelial cell behavior.* Biomaterials, 2011. **32**(22): p. 5056-64.

43. Davidson, C.D., et al., *Cell force-mediated matrix reorganization underlies multicellular network assembly.* Sci Rep, 2019. **9**(1): p. 12.

44. Brownfield, D.G., et al., *Patterned collagen fibers orient branching mammary epithelium through distinct signaling modules.* Curr Biol, 2013. **23**(8): p. 703-9.

45. Mammoto, A., T. Mammoto, and D.E. Ingber, *Mechanosensitive mechanisms in transcriptional regulation.* J Cell Sci, 2012. **125**(Pt 13): p. 3061-73.

46. Paul, C.D., et al., *Probing cellular response to topography in three dimensions.* Biomaterials, 2019. **197**: p. 101-118.

47. Midwood, K.S., et al., *Modulation of cell-fibronectin matrix interactions during tissue repair.* J Investig Dermatol Symp Proc, 2006. **11**(1): p. 73-8.

48. Sopher, R.S., et al., *Nonlinear Elasticity of the ECM Fibers Facilitates Efficient Intercellular Communication.* Biophys J, 2018. **115**(7): p. 1357-1370.

49. Hynes, R.O., *Integrins: bidirectional, allosteric signaling machines.* Cell, 2002. **110**(6): p. 673-87.

50. Huber, F., et al., *Emergent complexity of the cytoskeleton: from single filaments to tissue.* Adv Phys, 2013. **62**(1): p. 1-112.

51. Buxboim, A., et al., *How deeply cells feel: methods for thin gels.* J Phys Condens Matter, 2010. **22**(19): p. 194116.

52. Winer, J.P., S. Oake, and P.A. Janmey, *Non-linear elasticity of extracellular matrices enables contractile cells to communicate local position and orientation.* PLoS One, 2009. **4**(7): p. e6382.

53. Buxboim, A., I.L. Ivanovska, and D.E. Discher, *Matrix elasticity, cytoskeletal forces and physics of the nucleus: how deeply do cells 'feel' outside and in?* J Cell Sci, 2010. **123**(Pt 3): p. 297-308.

54. Gegenfurtner, F.A., et al., *Micropatterning as a tool to identify regulatory triggers and kinetics of actin-mediated endothelial mechanosensing.* J Cell Sci, 2018. **131**(10).

55. Jang, J.M., et al., *Engineering controllable architecture in matrigel for 3D cell alignment.* ACS Appl Mater Interfaces, 2015. **7**(4): p. 2183-8.

56. Gjorevski, N., et al., *Designer matrices for intestinal stem cell and organoid culture.* Nature, 2016. **539**(7630): p. 560-564.

57. Kannan, R.Y., et al., *The roles of tissue engineering and vascularisation in the development of micro-vascular networks: a review.* Biomaterials, 2005. **26**(14): p. 1857-75.

58. Xu, X., M.C. Farach-Carson, and X. Jia, *Three-dimensional in vitro tumor models for cancer research and drug evaluation.* Biotechnol Adv, 2014. **32**(7): p. 1256-68.

59. Schnaper, H.W., H.K. Kleinman, and D.S. Grant, *Role of laminin in endothelial cell recognition and differentiation.* Kidney Int, 1993. **43**(1): p. 20-5.

60. Yurchenco, P.D., Y.S. Cheng, and H. Colognato, *Laminin forms an independent network in basement membranes.* J Cell Biol, 1992. **117**(5): p. 1119-33.

61. Soofi, S.S., et al., *The elastic modulus of Matrigel as determined by atomic force microscopy.* J Struct Biol, 2009. **167**(3): p. 216-9.

62. Abrams, G.A., et al., *Nanoscale topography of the basement membrane underlying the corneal epithelium of the rhesus macaque.* Cell Tissue Res, 2000. **299**(1): p. 39-46.

63. Stryker, Z.I., et al., *Evaluation of Angiogenesis Assays.* Biomedicines, 2019. **7**(2).

64. Barocas, V.H. and R.T. Tranquillo, *An anisotropic biphasic theory of tissue-equivalent mechanics: the interplay among cell traction, fibrillar network deformation, fibril alignment, and cell contact guidance.* J Biomech Eng, 1997. **119**(2): p. 137-45.

65. Chaudhuri, O., et al., *Three-dimensional morphogenesis of MDCK cells induced by cellular contractile forces on a viscous substrate.* Proc Natl Acad Sci U S A, 2015. **5**: p. 14208.

66. Doyle, A.D., *Generation of 3D Collagen Gels with Controlled Diverse Architectures.* Nat Commun, 2016. **72**: p. 10.20.1-10.20.16.

67. Hickman, J.A., et al., *Three-dimensional models of cancer for pharmacology and cancer cell biology: capturing tumor complexity in vitro/ex vivo.* Biotechnol J, 2014. **9**(9): p. 1115-28.

68. Kimlin, L.C., G. Casagrande, and V.M. Virador, *In vitro three-dimensional (3D) models in cancer research: an update.* Mol Carcinog, 2013. **52**(3): p. 167-82.

69. Tinevez, J.Y., et al., *TrackMate: An open and extensible platform for single-particle tracking.* Methods, 2017. **115**: p. 80-90.

70. Arganda-Carreras, I., et al., *Trainable Weka Segmentation: a machine learning tool for microscopy pixel classification.* Bioinformatics, 2017. **33**(15): p. 2424-2426.

71. van der Walt, S., et al., *scikit-image: image processing in Python.* PeerJ, 2014. **2**: p. e453.

72. Farnebäck, G. *Two-Frame Motion Estimation Based on Polynomial Expansion*. 2003. Berlin, Heidelberg: Springer Berlin Heidelberg.

73. Butt, H.J., B. Cappella, and M. Kappl, *Force measurement with atomic force mircroscope: Technique, interpretation and applications.* Surface Science Reports, 2005. **59**(1-6): p. 152.

74. Kick, K., *Artificial Angiogenesis - Characteriztion of endothelial cell migration in three-dimensional model systems*, in *Pharmazeutische Biologie*. 2015, Ludwig-Maximilians-Universität München.

75. Reuten, R., et al., *Structural decoding of netrin-4 reveals a regulatory function towards mature basement membranes.* Nat Commun, 2016. **7**: p. 13515.

76. Kubota, Y., et al., *Role of laminin and basement membrane in the morphological differentiation of human endothelial cells into capillary-like structures.* J Cell Biol, 1988. **107**(4): p. 1589-98.

77. Auerbach, R., et al., *Angiogenesis assays: a critical overview.* Clin Chem, 2003. **49**(1): p. 32-40.

78. Browning, A.C., H.S. Dua, and W.M. Amoaku, *The effects of growth factors on the proliferation and in vitro angiogenesis of human macular inner choroidal endothelial cells.* Br J Ophthalmol, 2008. **92**(7): p. 1003-8.

79. Lesman, A., et al., *Mechanical regulation of vascular network formation in engineered matrices.* Adv Drug Deliv Rev, 2016. **96**: p. 176-82.

80. Hall, M.S., et al., *Fibrous nonlinear elasticity enables positive mechanical feedback between cells and ECMs.* Proc Natl Acad Sci U S A, 2016. **113**(49): p. 14043-14048.

81. Graham, D.M., et al., *Enucleated cells reveal differential roles of the nucleus in cell migration, polarity, and mechanotransduction.* J Cell Biol, 2018.

82. Venugopal, B., et al., *Cell density overrides the effect of substrate stiffness on human mesenchymal stem cells' morphology and proliferation.* Biomater Sci, 2018. **6**(5): p. 1109-1119.

83. Han, Y.L., et al., *Cell contraction induces long-ranged stress stiffening in the extracellular matrix.* Proc Natl Acad Sci U S A, 2018. **115**(16): p. 4075-4080.

84. Ahmadzadeh, H., et al., *Modeling the two-way feedback between contractility and matrix realignment reveals a nonlinear mode of cancer cell invasion.* Proc Natl Acad Sci U S A, 2017. **114**(9): p. E1617-e1626.

85. Rudnicki, M.S., et al., *Nonlinear strain stiffening is not sufficient to explain how far cells can feel on fibrous protein gels.* Biophys J, 2013. **105**(1): p. 11-20.

86. Munster, S., et al., *Strain history dependence of the nonlinear stress response of fibrin and collagen networks.* Proc Natl Acad Sci U S A, 2013. **110**(30): p. 12197-202.

87. Zagar, G., P.R. Onck, and E. van der Giessen, *Two fundamental mechanisms govern the stiffening of cross-linked networks.* Biophys J, 2015. **108**(6): p. 1470-1479.

88. Wen, Q. and P.A. Janmey, *Effects of non-linearity on cell-ECM interactions.* Exp Cell Res, 2013. **319**(16): p. 2481-9.

89. Storm, C., et al., *Nonlinear elasticity in biological gels.* Nature, 2005. **435**(7039): p. 191-4.

90. Nam, S., et al., *Viscoplasticity Enables Mechanical Remodeling of Matrix by Cells.* Biophys J, 2016. **111**(10): p. 2296-2308.

91. Hartman, C.D., et al., *Extracellular matrix type modulates cell migration on mechanical gradients.* Exp Cell Res, 2017. **359**(2): p. 361-366.

92. DuChez, B.J., et al., *Durotaxis by Human Cancer Cells.* Biophys J, 2019. **116**(4): p. 670-683.

93. Park, J., D.H. Kim, and A. Levchenko, *Topotaxis: A New Mechanism of Directed Cell Migration in Topographic ECM Gradients.* Biophys J, 2018. **114**(6): p. 1257-1263.

94. Reinhart-King, C.A., M. Dembo, and D.A. Hammer, *Cell-cell mechanical communication through compliant substrates.* Biophys J, 2008. **95**(12): p. 6044-51.

95. van Helvert, S. and P. Friedl, *Strain Stiffening of Fibrillar Collagen during Individual and Collective Cell Migration Identified by AFM Nanoindentation.* ACS Appl Mater Interfaces, 2016. **8**(34): p. 21946-55.

96. Ma, X., et al., *Fibers in the extracellular matrix enable long-range stress transmission between cells.* Biophys J, 2013. **104**(7): p. 1410-8.

97. Ohashi, T., D.P. Kiehart, and H.P. Erickson, *Dynamics and elasticity of the fibronectin matrix in living cell culture visualized by fibronectin-green fluorescent protein.* Proc Natl Acad Sci U S A, 1999. **96**(5): p. 2153-8.

98. Takizawa, M., et al., *Mechanistic basis for the recognition of laminin-511 by alpha6beta1 integrin.* Sci Adv, 2017. **3**(9): p. e1701497.

99. Rongish, B.J., et al., *Relationship of the extracellular matrix to coronary neovascularization during development.* J Mol Cell Cardiol, 1996. **28**(10): p. 2203-15.

100. Lejmi, E., et al., *Netrin-4 promotes mural cell adhesion and recruitment to endothelial cells.* Vasc Cell, 2014. **6**(1): p. 1.

101. Lejmi, E., et al., *Netrin-4 inhibits angiogenesis via binding to neogenin and recruitment of Unc5B.* Proc Natl Acad Sci U S A, 2008. **105**(34): p. 12491-6.

102. Lu, X., et al., *The netrin receptor UNC5B mediates guidance events controlling morphogenesis of the vascular system.* Nature, 2004. **432**(7014): p. 179-86.

103. van Oers, R.F., et al., *Mechanical cell-matrix feedback explains pairwise and collective endothelial cell behavior in vitro.* PLoS Comput Biol, 2014. **10**(8): p. e1003774.

104. Wang, H., et al., *Long-range force transmission in fibrous matrices enabled by tension-driven alignment of fibers.* Biophys J, 2014. **107**(11): p. 2592-603.

105. Vernon, R.B. and E.H. Sage, *Contraction of fibrillar type I collagen by endothelial cells: a study in vitro.* J Cell Biochem, 1996. **60**(2): p. 185-97.

106. Vernon, R.B. and E.H. Sage, *Between molecules and morphology. Extracellular matrix and creation of vascular form.* Am J Pathol, 1995. **147**(4): p. 873-83.

107. Murray, J.D., *On the mechanochemical theory of biological pattern formation with application to vasculogenesis.* C R Biol, 2003. **326**(2): p. 239-52.

108. Schuster, S.L., et al., *Contractility as a global regulator of cellular morphology, velocity, and directionality in low-adhesive fibrillary micro-environments.* Biomaterials, 2016. **102**: p. 137-47.

109. Blobel, C.P., *3D trumps 2D when studying endothelial cells.* Blood, 2010. **115**(25): p. 5128-30.

110. Sacharidou, A., et al., *Endothelial lumen signaling complexes control 3D matrix-specific tubulogenesis through interdependent Cdc42- and MT1-MMP-mediated events.* Blood, 2010. **115**(25): p. 5259-69.

111. Gagnon, E., et al., *Human vascular endothelial cells with extended life spans: in vitro cell response, protein expression, and angiogenesis.* Angiogenesis, 2002. **5**(1-2): p. 21-33.

112. Galindo-Pumarino, C., et al., *Fibroblast-Derived 3D Matrix System Applicable to Endothelial Tube Formation Assay.* J Vis Exp, 2019(154).

113. Hiraoka, N., et al., *Matrix metalloproteinases regulate neovascularization by acting as pericellular fibrinolysins.* Cell, 1998. **95**(3): p. 365-77.

114. Balleyguier, C., et al., *Breast elasticity: principles, technique, results: an update and overview of commercially available software.* Eur J Radiol, 2013. **82**(3): p. 427-34.

115. Hindman, B., et al., *Non-Muscle Myosin II Isoforms Have Different Functions in Matrix Rearrangement by MDA-MB-231 Cells.* PLoS One, 2015. **10**(7): p. e0131920.

116. Hanahan, D. and R.A. Weinberg, *Hallmarks of cancer: the next generation.* Cell, 2011. **144**(5): p. 646-74.

117. Folkman, J., *Tumor angiogenesis: therapeutic implications.* N Engl J Med, 1971. **285**(21): p. 1182-6.

118. Zirlik, K. and J. Duyster, *Anti-Angiogenics: Current Situation and Future Perspectives.* Oncol Res Treat, 2018. **41**(4): p. 166-171.

119. Gaudet, I.D. and D.I. Shreiber, *Characterization of methacrylated type-I collagen as a dynamic, photoactive hydrogel.* Biointerphases, 2012. **7**(1-4): p. 25.

120. Segerer, F.J., et al., *Versatile method to generate multiple types of micropatterns.* Biointerphases, 2016. **11**(1): p. 011005.

121. McClellan, S., et al., *mRNA detection in living cells: A next generation cancer stem cell identification technique.* Methods, 2015. **82**: p. 47-54.

7 Appendix

7.1 Supplementary figures

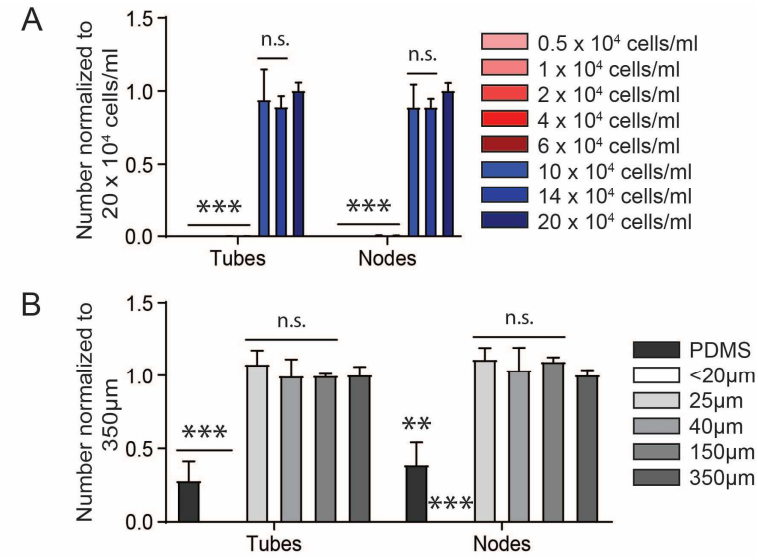

Figure 7-1: Further quantification of the tube formation.

(A) Quantification of the number of tubes and nodes normalized to 20 x 10^4 cells/ml for the different cell concentrations for the tube formation. There was no significant difference between the concentrations for a distinct network. The low concentrations showed a significant reduction (one-way ANOVA with Dunnett's test, compared to 20 x 10^4 cells/ml, n.s. ≙ not significant, ***P < 0.001) **(B)** Quantification of the number of tubes and nodes normalized to 350 µm showed no difference between the thickness of 350 µm, 150 µm, 40 µm and 25 µm. The numbers were significantly decreased on PDMS and with a thickness less than 20 µm (one-way ANOVA with Dunnett's test, compared to 350 µm, n.s. ≙ not significant, **P < 0.002, ***P < 0.001)

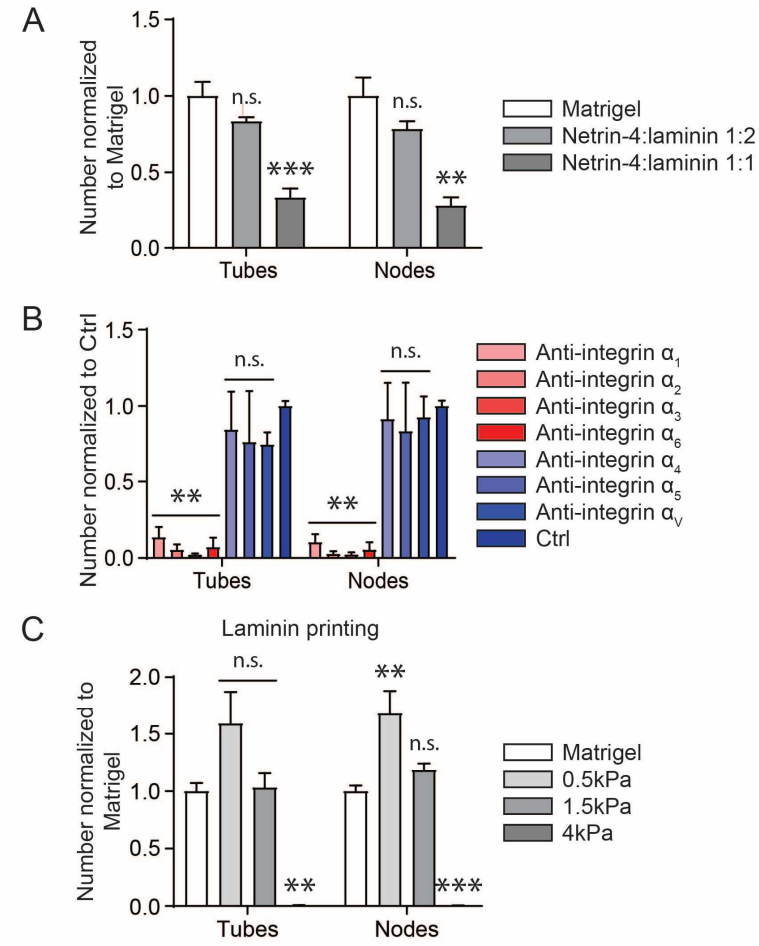

Figure 7-2: Quantification of the tube formation for the laminin influence.

(A) Quantification of the number of tubes and nodes normalized to Matrigel for manipulation of the matrix structure with netrin-4. There was only a slight reduction between Matrigel and netrin-4:laminin 1:2, while a significant decrease was observed compared to netrin-4:laminin 1:1 (one-way ANOVA with Dunnett's test, compared to Matrigel, n.s. ≙ not significant, **P < 0.002, ***P < 0.001) **(B)** Quantification of the number of tubes and nodes normalized to control (Ctrl) for the blocking of different integrins. Integrins favoring binding to fibronectin and other ECM proteins (integrins α_4, α_5 and α_v) showed no significant difference to the control. Integrins against laminin (integrins α_1, α_2, α_3 and α_6) exhibited a significant reduction of tubes and nodes (one-way ANOVA with Dunnett's test, compared to control, n.s. ≙ not significant, **P < 0.002) **(C)** Quantification of the number of tubes and nodes normalized to Matrigel for the laminin printing on different PDMS stiffnesses. Tube formation on 1.5 kPa showed no difference to Matrigel. For a stiffness of 0.5 kPa a significant increase was observed for the number of nodes. On 4 kPa a significant decrease in the number of tubes and nodes was detected (one-way ANOVA with Dunnett's test, compared to Matrigel, n.s. ≙ not significant, **P < 0.002, ***P < 0.001).

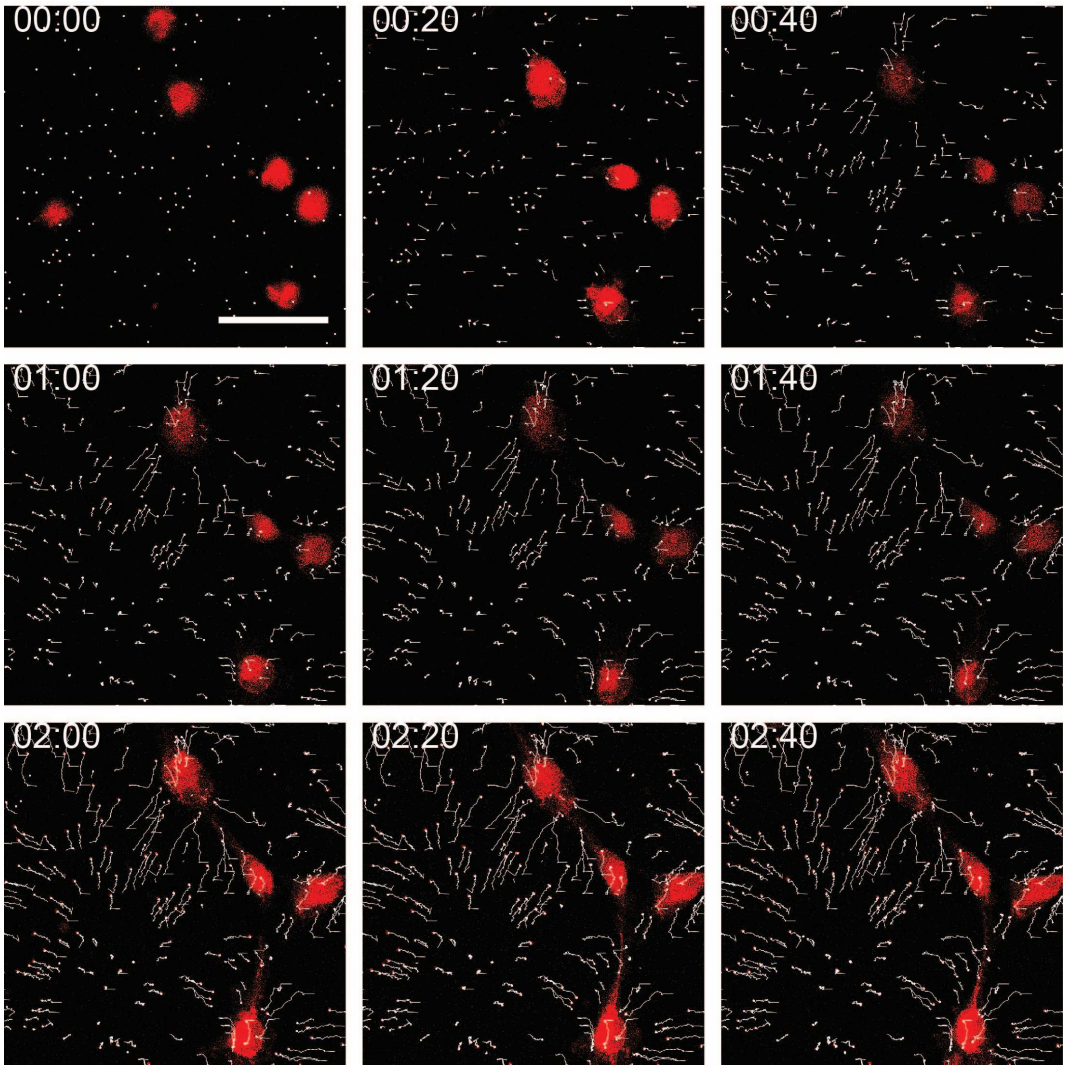

Figure 7-3: Bead displacement during tube formation.

Cells were stained with CellTracker™ Red and Matrigel was mixed with fluorescent beads. In a live cell imaging the displacement of the beads was tracked. Cells are highlighted in red and bead displacement indicated in white lines. First bead movements between the cells can be observed after 40 min. After 2 h the cells start to connect. Scale bar: 100 µm.

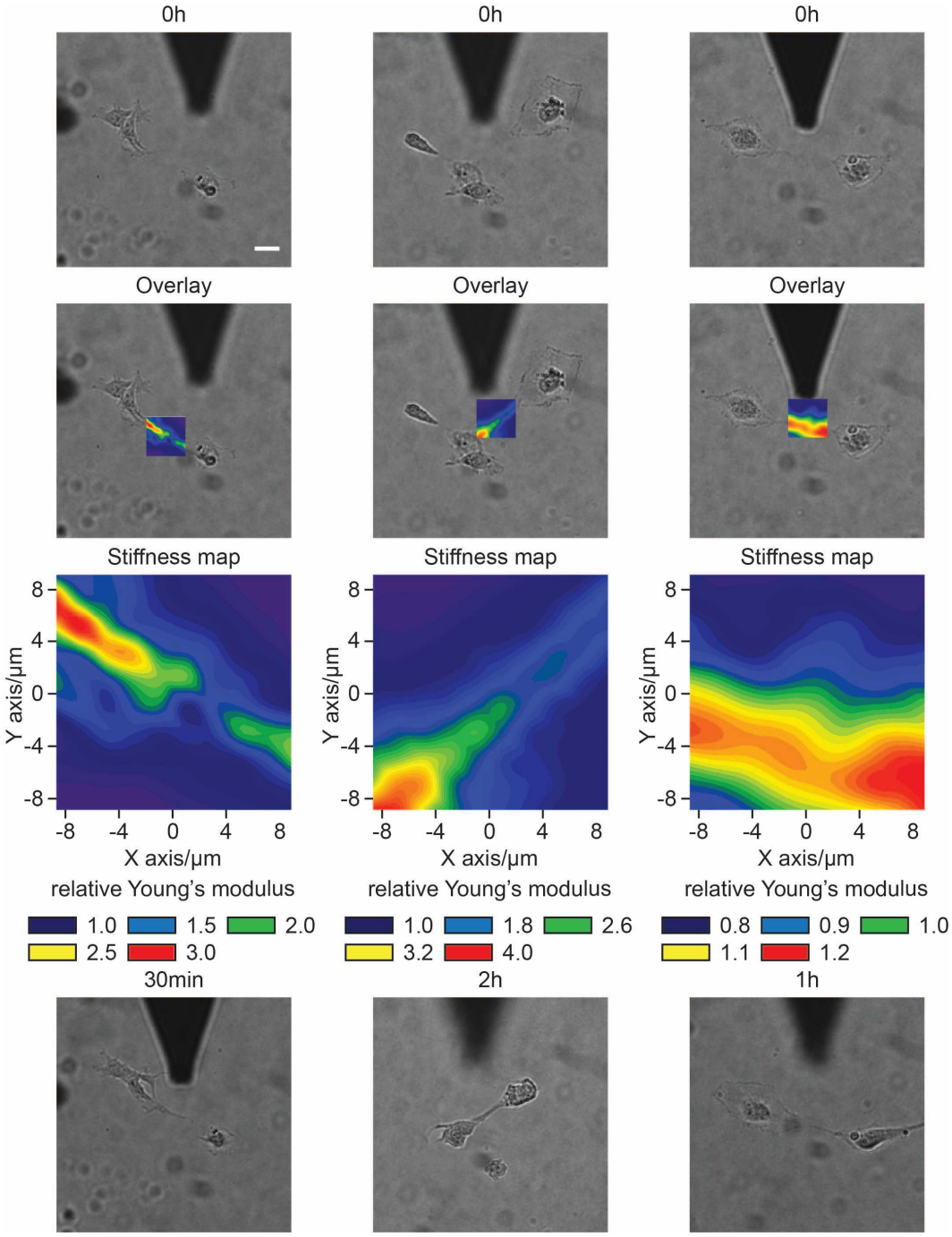

Figure 7-4: Further examples of the strain stiffening effect.

Single cells were seeded on Matrigel, and the stiffness of the gel between the cells was measured with an AFM. As a control, substrate stiffness in a cell-free area was also measured. The pseudocolored stiffness map shows the relative Young's modulus normalized to the Young's modulus of the control area. The overlay of the microscope image and the stiffness map shows that the cells formed a stiff bridge between themselves even before cellular protrusions formed. In the time range from 30 min to 2 h, the cells used the stiff line for locating each other and for making contact. Scale bar: 20 µm.

7.2 List of figures

7.3 List of tables

7.4 List of publications and conference contributions

7.4.1 Article

First authorship:

I. *Cell-based strain stiffening of a nonfibrous matrix as an organizing principle for morphogenesis*

Daniel Rüdiger, Kerstin Kick, Andriy Goychuk, Angelika M. Vollmar, Erwin Frey, Stefan Zahler

In Revision – Cell Reports

Co-authorship:

II. *Persistent inhibition of pore-based cell migration by sub-toxic doses of miuraenamide, an actin filament stabilizer*

Christina Moser, Daniel Rüdiger, Florian Förster, Julia von Blume, Peng Yu, Bernhard Kuster, Uli Kazmaier, Angelika M. Vollmar, Stefan Zahler

Scientific Reports, 2017, 7(1)

III. *Zn2+-triggered self-assembly of Gonadorelin [6-D-Phe] to produce nanostructures and fibrils*

Yordanka Yordanova, Willem Vanderlinden, Raphael Stoll, Daniel Rüdiger, Andreas Tosstorff, Wolfgang Zaremba, Gerhard Winter, Stefan Zahler, Wolfgang Friess

Scientific Reports, 2018, 8(1)

IV. *Fiber stiffness, pore size and adhesion control migratory phenotype of MDA-MB-231 cells in collagen gels*

Florian Geiger, Daniel Rüdiger, Stefan Zahler, Hanna Engelke

PLOS ONE, 2019, 14(11)

V. *Mechanistic studies on protein particle formation during peristaltic pumping - Driving forces for protein film formation and detachment*

Natalie Deiringer, Daniel Rüdiger, Stefan Zahler, Thomas Luxbacher, Wolfgang Frieß

Manuscript in preparation

VI. *Tau release, uptake, and aggregation in small molecule induced neural progenitor cells derived neurons*

Amir Tayaranian Marvian, Tabea Strauss, Sigrid Schwarz, Daniel Rüdiger, Markus Dublinger, Brigitte Nusher, Stefan Zahler Peter Heutink, Wolfgang Wurst, Günter Höglinger

Manuscript in preparation

7.4.2 Oral presentation

Atomic Force Microscope – Measurement device for mechanical properties

Daniel Rüdiger, Stefan Zahler

SFB 1032 Summer School

2017, Herrsching, Germany

Mechanical cell communication and its influence on organization of cellular structures

Daniel Rüdiger, Angelika M. Vollmar, Stefan Zahler

American Society for Matrix Biology (ASMB) Biennial Meeting

2018, Las Vegas, USA

Mechanische Zellkommunikation und ihr Einfluss auf die Organisation zellulärer Strukturen

Daniel Rüdiger, Angelika M. Vollmar, Stefan Zahler

Gastseminar Institut für Bioprozess- und Analysenemesstechnik

2019, Heilbad Heiligenstadt, Germany

7.4.3 Poster presentation

Controlling cellular function by structured surface: “Artificial angiogenesis”

Themistoklis Zissis, Daniel Rüdiger, Stefan Zahler

SFB 1032 Workshop 2017: From Nanoagents to Living Matter

2017, Tutzing, Germany

Mechanical cell communication and its influence on organization of cellular structures

Daniel Rüdiger, Angelika M. Vollmar, Stefan Zahler

American Society for Matrix Biology (ASMB) Biennial Meeting

2018, Las Vegas, USA

Controlling cellular function by structured surface: “Artificial angiogenesis”

Themistoklis Zissis, Daniel Rüdiger, Angelika M. Vollmar, Stefan Zahler

SFB 1032 Workshop 2019

2019, Benediktbeuern, Germany

7.5 Associated bachelor theses

Influence of substrate stiffness on endothelial mechanosensing

Franz Geisslinger, 2017

Influence of mechanical and biological parameters on endothelial cell behavior based on different hydrogels

Franziska Schreiber, 2018

Behaviour of Endothelial Cells under Influence of Translation- and Secretion Inhibitors on Various Matrices

Johanna Streubel, 2019

7.6 Acknowledgements

Mein herzlichster Dank gilt Frau Prof. Dr. Angelika Vollmar und Herrn Prof. Dr. Stefan Zahler für die Möglichkeit meine Promotion in Ihrem Fachbereich Pharmazeutische Biologie durchzuführen. Neben der Begleitung meines wissenschaftlichen Werdegangs danke ich Ihnen auch für Freiheit, die Sie mir im Bezug auf die Gestaltung des Projekts, sowie meiner persönlichen Weiterentwicklung gegeben haben. Außerdem danke ich Ihnen, für das offene Ohr, dass Sie jederzeit bei Fragen oder Problemen für mich hatten.

Der Prüfungskommission bestehend aus Herrn Prof. Dr. Stefan Zahler, Frau Prof. Dr. Angelika Vollmar, Herrn Prof. Dr. Andreas Dendorfer, Frau Prof. Dr. Olivia Merkel, Herrn Prof. Dr. Franz Paintner und Herrn Prof. Dr. Wolfgang Frieß möchte ich für die Bereitschaft zur Bewertung meiner Arbeit und dem damit verbundenen Zeitaufwand danken.

Besonderer Dank gilt Herrn Prof. Dr. Erwin Frey und Andriy Goychuk für die fruchtbare Zusammenarbeit für unser gemeinsames Paper. Ein großer Dank gilt auch Dr. Raphael Reuten für die Bereitstellung von netrin-4 und die hilfreiche Diskussion. Ich möchte mich auch bei allen meinen Kooperationspartnern Dr. Christina Moser, Dr. Yordanka Yordanova, Florian Geiger, Natalie Deiringer und Amir Tayaranian Marvian für die tolle Zusammenarbeit während meiner Promotion bedanken. Herrn Prof. Dr. Joachim Rädler möchte ich für die Leitung des Sonderforschungsbereiches 1032 Nanoagents danken und Marilena Pinto für die Organisation der zahlreichen sehr interessanten Veranstaltungen innerhalb des SFBs. Außerdem möchte ich noch Herrn Prof. Dr. Hauke Clausen-Schaumann und Stefanie Kinderlein für die Hilfe bei allen Fragestellungen rund um das AFM danken.

Ich danke meinen Bachelorstudenten Franz, Franziska und Johanna für ihre geleisteten Arbeiten im Rahmen des Projektes und die vertrauensvolle und freundschaftliche Zusammenarbeit.

Natürlich geht auch ein großer Dank an den gesamten AK Vollmar, aktuelle wie ehemalige Mitarbeiter. Es war nicht nur eine wunderschöne Zeit im Labor auch die Aktivitäten außerhalb des Laborbetriebs waren einfach unvergesslich. Die sportlichen Aktivitäten (Basketball + Frisbee), Biertasting, Filmabend, Besuch des Starkbierfests oder auch unsere Wiesn-Ausflug waren Events, die das Miteinander gestärkt und den Alltag aufgelockert haben. Besonders hervorheben möchte ich Jana. Vielen Dank für

deine unermüdliche Unterstützung und Hilfsbereitschaft bei allen Fragen. Ich möchte mich auch bei Martina, Themis und Maibritt für unsere tolle Zeit im Labor bedanken. Bei Caro, Chrissi und Martin möchte ich mich für die unzähligen gemeinsamen Essenspausen bedanken. Es war immer sehr unterhaltsam und ich danke euch, dass ich mit jedem Problem, ob beruflich oder privat zu euch kommen konnte. Außerdem möchte ich mich bei Conny, Maibritt, Katrin und Flo für die Korrektur und Verbesserungsvorschläge für meine Arbeit bedanken. Zu guter Letzt möchte ich bei den beiden wichtigsten Personen im Arbeitskreis bedanken. Flo, du hast mir den Eintritt am AK Vollmar sehr erleichtert, warst bei allen Problemen und Fragen immer für mich da und ich danke dir für all die Diskussionen (auch um das Thema Fussball). Und natürlich auch dir Conny danke ich für die unvergessliche Zeit. Du warst in allen Situationen immer für mich da und hast mir immer mit Rat und Tat zu Seite gestanden und warst nebenbei ein treuer Essenbegleiter/-lieferant.

Natürlich gilt auch ein großer Dank an meine Familie und all meinen Freunde. Ihr habt mich nicht nur während der Promotion begleitet, sondern tut das eigentlich schon mein ganzes Leben, dafür danke ich euch sehr. Ohne euch wäre ich weder so weit gekommen, noch wäre ich der, der ich heute bin.

Zum Schluss möchte natürlich der wichtigsten Person in meinem Leben danken: vielen Dank, Marissa! Ohne dich wäre ich heute nicht hier. Du warst immer ein großer Rückhalt für mich, besonders auch in schwierigen Situationen. Ich bin mir sicher ohne dich hätte ich das alles nicht schaffen können. Ich kann meine Dankbarkeit und Liebe nicht in Worte ausdrücken. Manche Menschen machen das Leben besonders, einfach weil sie da sind.